Diss. ETH No. 16372

SUPERCONDUCTIVITY IN CRYSTALS WITHOUT AN INVERSION CENTER

A dissertation submitted to the

SWISS FEDERAL INSTITUTE OF TECHNOLOGY ZÜRICH
(ETH ZÜRICH)

for the degree of
Doctor of Natural Sciences

presented by

PAOLO ANTONIO FRIGERI

Dipl. Phys. ETHZ
born 14.11.1973
citizen of Lamone (TI-CH) and Italian nationality

accepted on the recommendation of
Prof. Dr. M. Sigrist, examiner
Prof. Dr. E. Bauer, co-examiner
PD. Dr. D. Manske, co-examiner

2005

Seite Leer /
Blank leaf

Seite Leer /
Blank leaf

Seite Leer /
Blank leaf

Riassunto

Questa tesi tratta differenti aspetti della superconduttivitá in materiali senza un centro d'inversione. Questo studio mira a chiarire varie proprietá non convenzionali osservate recentemente nello stato superconduttore del materiale $CePt_3Si$.

Dopo un accenno all'evoluzione storica della superconduttivitá, si discutono i principali risultati sperimentali riguardanti il composto $CePt_3Si$. Vengono quindi presentati i "Teoremi di Anderson", che dettano le simmetrie necessarie per l'accoppiamento di tipo spin-singoletto e spin-tripletto.

Si affronta poi il tema del formalismo matematico utilizzato dalla teoria BCS nella descrizione dello stato superconduttore in termini di coppie di Copper di tipo spin-singoletto e spin-tripletto. Si dimostra che, in materiali con un'interazione spin-orbita e una struttura cristallina senza un centro d'inversione, la simmetria d'inversione nello spazio dei vettori d'onda $\boldsymbol{k}$ è assente a causa della presenza di una parte anti-simmetrica nell'interazione spin-orbita (ASOC). Contrariamente a quanto solitamente pensato, l'accoppiamento di tipo spin-tripletto non è completamente escluso in questo tipo di materiali. Il limite paramagnetico e la suscettibilità statica e uniforme degli spin sono analizzati per entrambi i tipi di accoppiamento: spin-singoletto e spin-tripletto. Questi risultati sono applicati ai materiali MnSi e $CePt_3Si$.

La teoria dei gruppi puntuali viene utilizzata per classificare lo stato superconduttore in materiali caratterizzati da una forte ASOC. In questo caso, la superconduttività non può essere semplicemente classificata in termini di spin-singoletto o spin-tripletto. Il parametro d'ordine dello stato superconduttore è generalmente una sovrapposizione di queste due componenti. Le

funzioni utilizzate per la descrizione dello stato superconduttore dei diversi sistemi cristallini vengono classificate e catalogate. Si fornisce inoltre un elenco di materiali superconduttori senza un centro di inversione. La forma generale dell'interazione d'accoppiamento include, oltre al potenziale di tipo spin-singoletto e spin-tripletto, un termine misto - del quale spieghiamo lorigine microscopica - che descrive la diffusione tra le coppie di Cooper con differenti spin.

In materiali con una forte ASOC è conveniente e interessante descrivere lo stato normale del sistema attraverso le due bande non degenerate create dalla presenza dell'ASOC. Utilizzando come esempio $CePt_3Si$ si effettua l'analisi strutturale del parametro d'ordine dello stato superconduttore più simmetrico, chiamato stato "s-wave", in funzione dell'interazione d'accoppiamento e della densità degli stati nelle due bande non degenerate. Si discute inoltre la presenza di linee nodali nel *gap* delle quasi-particelle. Questi nodi sono essenziali per spiegare le recenti misure effettuate a basse temperature riguardanti il tasso di rilassamento degli spin, la profondità di penetrazione di London e la conduttività termica. La dipendenza della posizione dei nodi dalla temperatura viene anchessa analizzata e discussa.

Infine viene indagato l'effetto del disordine sullo stato superconduttore "s-wave", con particolare attenzione allo studio della dipendenza della temperatura critica e della suscettibilità degli spin dalla concentrazione di impurità non magnetiche.

Abstract

This thesis deals with different aspects of superconductivity in materials without an inversion center. Our study aims at clarifying various non-conventional properties observed in the recently discovered heavy Fermion superconductor $CePt_3Si$.

After a brief historical introduction on the phenomenon of superconductivity, we discuss the main experimental data characterizing superconductivity in $CePt_3Si$. Then, we introduce "Anderson's theorems", which show the necessary symmetries required for spin-singlet and spin-triplet pairing.

We explain the BCS formalism, which is used to describe superconductivity in terms of spin-singlet and spin-triplet Cooper pairs. Then, we show that in materials with significant spin-orbit coupling and without an inversion center, the inversion symmetry in $\boldsymbol{k}$-space is lifted by antisymmetric spin-orbit coupling (ASOC). We show that, in contrast to the common belief, spin-triplet pairing is not entirely excluded in such systems. The paramagnetic limiting and static uniform spin susceptibility are analyzed for both spin-singlet and spin-triplet pairing. We apply the results to the cases of MnSi and $CePt_3Si$.

We use the point group theory to classify the superconducting states in materials with large ASOC. In this case superconductivity cannot be classified in terms of the spin-singlet or the spin-triplet. The superconducting order parameter is, in general, a mixture of these two components. Thus, we list the basis functions relevant for the classification of this type of superconductivity for the different crystal systems. In addition, for each crystal system, we provide a list of superconducting materials without an inversion center. The general form of the pairing interaction includes, in addition to the spin-

singlet and spin-triplet pairing potential, a mixing term which describes the scattering of Cooper pairs with different total spin. The micriscopic origin of this last term is explained.

In materials with large ASOC, it is convenient to describe the normal state through the two non-degenerate bands generated by the presence of the ASOC. Using the example of $CePt_3Si$, we determine the structure of the order parameter for the most symmetric pairing state, the so-called "s-wave" state, as a function of the pairing interaction and the distribution of the density of states in the two non-degenerate bands. Moreover, we explore the possibility of the presence of accidental line nodes in the quasiparticle gap. Such nodes are essential for the explanation of the recent low-temperature measurement of NMR-T_1^{-1}, London penetration depth and heat conductance. We also show that the position of these line nodes will, in general, depend on temperature.

Finally, we investigate the effect of disorder for the "s-wave" pairing state. In particular, we study the dependence of the critical temperature and static uniform spin susceptibility on the impurity concentration.

Contents

Chapter 1

Introduction

The complete disappearance of DC electric resistivity of a material at sufficiently low temperatures was first observed in 1911 by H. Kamerlingh Onnes. This phenomenon took the name of superconductivity. Only after more than thirty years, in 1957, three theorists, J. Bardeen, L. Cooper, and J. Schrieffer, found a satisfactory theoretical picture of this phenomenon [1]. This theory, commonly called the BCS theory, is based on Cooper's theorem, which shows the instability of the ground state of an electron gas in the presence of an arbitrarily small attractive interaction against the formation of bound electron states, called Cooper pairs.

In most superconductors, the attraction between electrons is due to the mediation of the electron-electron interaction by the vibrational modes of the crystal: the phonons. In this case, the attractive interaction is almost isotropic, so that the Cooper pairs are formed in a state with zero orbital momentum, $L = 0$, and zero total spin, $S_{tot} = 0$, the so-called spin-singlet s-wave pairing. This type of superconductivity is called *conventional*.

The same theoretical approach was applied with success to explain the complete disappearance of viscosity in the Fermionic liquid ^{3}He [2]. However, the mechanism inducing superfluidity in ^{3}He is quite different. The Cooper pairing is due to the interaction between nuclear spins of helium-3 atoms mediated by the fluctuation of the liquid magnetization: the paramagnon. In this case, the interaction is essentially anisotropic and leads to the formation of Cooper pairs with orbital momentum $L = 1$ and total spin $S_{tot} = 1$, the

so-called spin-triplet p-wave pairing.

These two examples belong to the body of the most well-understood quantum many-body problems in physics. However, at the end of the 70s, superconductivity once again became a problem full of questions with the discovery of superconductivity in heavy fermion materials, first in $CeCu_2Si_2$, then in UBe_{13} and UPt_3. In 1986, the field attracted additional attention when Bednorz and Müller opened the era of high-T_c superconductors with the discovery of superconductivity in $(La,Sr)_2CuO_4$. These superconductors show unconventional properties, those of the heavy fermions much more significantly than those of the high-T_c.

Heavy fermions are compounds containing rare earth or actinide ions whose f-shell electrons are strongly correlated. These f electrons determine the properties of quasiparticles at the Fermi level, giving rise to a large effective mass. In these compounds, the strong electron-electron correlation is considered responsible for superconductivity. But, up until now, the microscopic origin of pairing in these materials has remained obscure.

In 1984, Ott *et al.* observed the T^3 law in the specific heat of UBe_{13} [3]. Consequently, such power laws have been measured in other quantities, such as ultrasonic attenuation, NMR relation rate, thermal conductivity and London penetration depth. The generalization of the BCS theory to anisotropic pairing state led to the understanding of such power laws as a consequence of gapless excitations in the particle spectrum. The term *unconventional* superconductivity was introduced to indicate the deviation from the ordinary s-wave BCS state. Moreover, the development of phenomenological theories of unconventional superconductivity [4, 5] led to the understanding of many physical properties characterising this class of superconductors, and in some cases permitted the identification of the pairing symmetry.

The aim of this thesis is to extend the BCS theory to the case of materials without an inversion center and to calculate some basic properties of the superconducting state in $CePt_3Si$, which is a Ce-based heavy Fermion superconductor whose crystal structure lacks inversion symmetry.

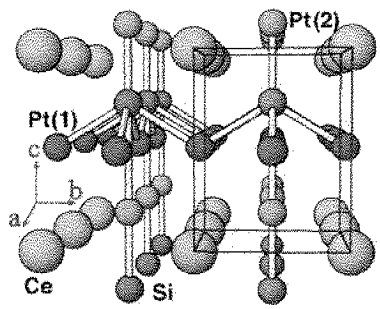

Figure 1.1: Crystal structure of $CePt_3Si$.

1.1 Superconductivity in $CePt_3Si$

In 2004, the group of E. Bauer reported the discovery of superconductivity in the heavy fermion compound $CePt_3Si$ [6]. Its crystal structure is tetragonal, space group P4mm, with a generating point group C_{4v}. The material has no inversion center due to the lack of the mirror plane perpendicular to the c-axis, see Fig. 1.1. $CePt_3Si$ exhibits an antiferromagnetic transition at $T_N \approx 2.2K$ followed by a transition into a heavy fermion superconducting state at $T_c \approx 0.75K$. The magnetic structure of the antiferromagnetic order has been determined by Neutron scattering. The magnetic moments are ordered ferromagnetically in the ab-plane, and are stacked antiferromagnetically along the c-axis [7]. The Muon-Spin Rotation (μSR) seems to indicate the microscopic coexistence of magnetism and superconductivity [8]. Superconductivity and antiferromagnetism are suppressed by hydrostatic pressure on the order of the GPa [9, 10]. Whether or not the superconductivity is constrained within the magnetic phase is still unknown. The location of the superconducting dome close to the antiferromagnetic quantum phase transition indicates that Cooper pairing may be mediated by magnetic fluctuation. $CePt_3Si$ attracted wide interest because of a surprisingly high upper critical field H_{c2}. Its value at $T = 0$ was first determined on a polycrystalline sample by the group of E. Bauer [6], $H_{c2}(0) = 5T$, and then measured in a monocrystal by the group of T. Yasuda, $H_{c2}(0) = 2.7 - 3.2T$ [11], see Fig.

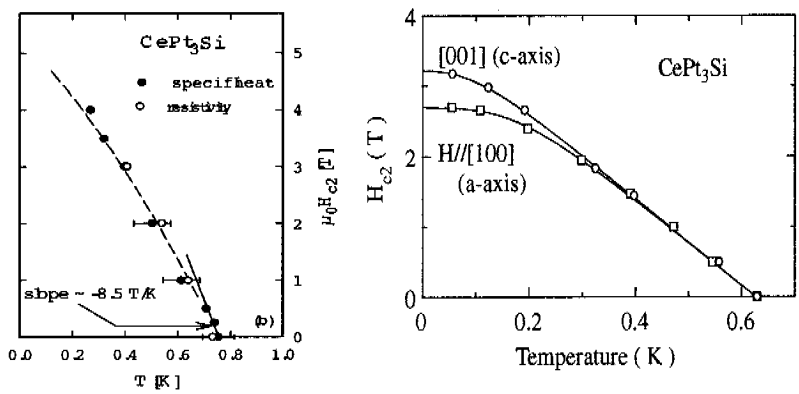

Figure 1.2: The upper critical temperature H_{c2} measured in $CePt_3Si$ as a function of temperature. The left plot shows the result for a polycrystalline sample, from [6]. The right plot shows the result for a monocrystal, from [11].

1.2. In both cases $H_{c2}(0)$ exceeds the paramagnetic limiting field H_P, which can be estimated using the standard BCS relation [5]

$$H_P = \frac{\Delta_0}{\sqrt{2}\mu_B} \approx \frac{1.25 k_B T_c}{\mu_B} \approx 1T < H_{c2}. \tag{1.1}$$

In a superconductor with an inversion center, spin-singlet pairing is energetically unfavorable in the field higher than H_P. The high H_{c2} can be interpreted as a signal of spin-triplet superconductivity.

In Chaper 2, we show that the presence of strong spin-orbit coupling associated with the absence of an inversion center in the material induces a drastic reduction of the paramagnetic limiting in the case of spin-singlet pairing [12–16]. We also show that, under such conditions, all except one class of spin-triplet pairing channels are suppressed [12].

The absence of the inversion symmetry leads to a breakdown of the strict classification into even-parity spin-singlet and odd-parity spin-triplet; these states are mixed, resulting in a state containing both components [17–20]. The classification of the possible superconducting states using point group analysis is the subject of Chapter 3.

The analysis of the results concerning the nuclear magnetic relaxation rate

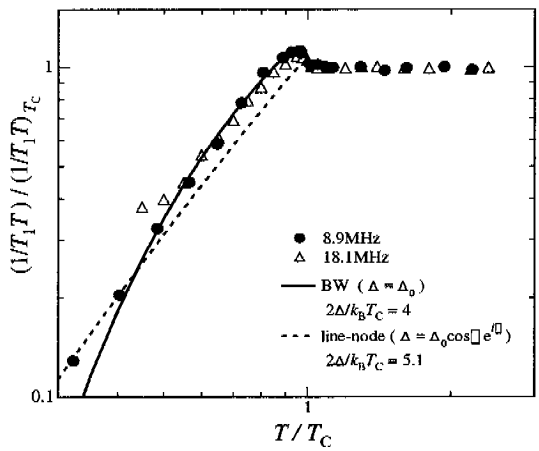

Figure 1.3: Temperature dependence of the nuclear spin lattice relaxation rate $1/T_1T$, from M. Yogi *et al.* [21]. The solid line is a tentative fit calculated assuming an isotropic spin-triplet state. The dashed line indicates a fit by line-node gap.

$1/T_1T$, obtained by Pt-NMR [21,22], the London penetration depth [23] and thermal conductivity [24] can serve to identify the possible pairing symmetry. All measurements give evidence of the possible presence of line nodes in the quasiparticle gap. Moreover, the magnetic relaxation rate exhibits a peak just below T_c, indicating the presence of an isotropic component, see Fig. 1.3. In Chapter 4, we study the structure of the most symmetric pairing state, termed "s-wave". It turns out that if the "s-wave" pairing is mostly spin-triplet, then there are line nodes in the quasiparticle gap [17]. Recent numerical calculations of $1/T_1T$ confirm the compatibility of this state with experiments [25]. In the last part of this work, Chapter 5, we analyze the effect of disorder on the "s-wave" pairing state.

1.2 Cooper pairs and Anderson's theorem

In the context of the BCS theory, it is possible to show that the ability of the attractive electron-electron interaction $V_{s_1 s_2, s_2' s_1'}(\boldsymbol{k}, \boldsymbol{k}')$ to form Cooper pairs with zero momentum relies on the degeneracy of the eigenstates, $|\boldsymbol{k}', s_1'\rangle$ and $|-\boldsymbol{k}', s_2'\rangle$, of the single particle Hamiltonian $\mathcal{H}_{\mathcal{T}}$.

In his famous paper of 1959, Anderson showed that the spin-singlet pairing between the state $|\boldsymbol{k}, \uparrow\rangle$ and $|-\boldsymbol{k}, \downarrow\rangle$ is possible if their energies $\mathcal{H}_{\mathcal{T}}|\boldsymbol{k}, \uparrow\rangle = E_{\boldsymbol{k},\uparrow}|\boldsymbol{k}, \uparrow\rangle$ and $\mathcal{H}_{\mathcal{T}}|-\boldsymbol{k}, \downarrow\rangle = E_{-\boldsymbol{k},\downarrow}|-\boldsymbol{k}, \downarrow\rangle$ are the same $E_{\boldsymbol{k},\uparrow} = E_{-\boldsymbol{k},\downarrow}$ [26]. Since those two states are connected by time reversal symmetry $\mathcal{K}$

$$\mathcal{K}|\boldsymbol{k}, \uparrow\rangle = |-\boldsymbol{k}, \downarrow\rangle, \tag{1.2}$$

the symmetry necessary to form Cooper pairs with zero total momentum is the time reversal symmetry $\mathcal{K}$, i.e $\mathcal{K}\,\mathcal{H}_{\mathcal{T}}\,\mathcal{K}^{-1} = \mathcal{H}_{\mathcal{T}}$.

In 1984, Anderson extended this type of analysis to spin-triplet superconductors [27]. He showed that, in addition to the time reversal symmetry $\mathcal{K}$, the inversion symmetry $\mathcal{I}$ is necessary to guarantee the degeneracy among the four different states: $|\boldsymbol{k}, \uparrow\rangle$, $|-\boldsymbol{k}, \uparrow\rangle$, $|\boldsymbol{k}, \downarrow\rangle$ and $|-\boldsymbol{k}, \uparrow\rangle$. In fact, $\mathcal{I}$ reverses only $\boldsymbol{k}$. Thus,

$$\begin{aligned} \mathcal{K}|\boldsymbol{k}, \uparrow\rangle &= |-\boldsymbol{k}, \downarrow\rangle, \\ \mathcal{I}|\boldsymbol{k}, \uparrow\rangle &= |-\boldsymbol{k}, \uparrow\rangle, \\ \mathcal{I}\mathcal{K}|\boldsymbol{k}, \uparrow\rangle &= |\boldsymbol{k}, \downarrow\rangle. \end{aligned}$$

This led to the belief that the spin-triplet superconductivity would be indiscriminately suppressed in the absence of the inversion symmetry. The discovery of $CePt_3Si$ seems, however, to contradict this conclusion.

Chapter 2

First consequences of the lack of an inversion center

2.1 BCS formalism, Gork'ov equations

Consider the effective Hamiltonian in momentum space given by

$$\begin{aligned}\mathcal{H} &= \sum_{\boldsymbol{k},s_1,s_2} \langle \boldsymbol{k},s_1|\mathcal{H}_T|\boldsymbol{k},s_2\rangle\, c^{\dagger}_{\boldsymbol{k},s_1} c_{\boldsymbol{k},s_2} \\ &+ \frac{1}{2}\sum_{\boldsymbol{k},\boldsymbol{k},s_i} V_{s_1s_2,s_2's_1'}(\boldsymbol{k},\boldsymbol{k}')\, c^{\dagger}_{\boldsymbol{k},s_1} c^{\dagger}_{-\boldsymbol{k},s_2} c_{-\boldsymbol{k}',s_2'} c_{\boldsymbol{k}',s_1'} \end{aligned} \tag{2.1}$$

where $c^{\dagger}_{\boldsymbol{k}s}$ ($c_{\boldsymbol{k}s}$) creates (annihilates) an electron with momentum $\boldsymbol{k}$ and spin s. $\mathcal{H}_T$ is the term describing the normal state of the system, while $V_{s_1s_2,s_2's_1'}(\boldsymbol{k},\boldsymbol{k}')$ denotes the matrix element $\langle \boldsymbol{k},s_1;-\boldsymbol{k},s_2|\mathcal{V}|-\boldsymbol{k}',s_2';\boldsymbol{k}',s_1'\rangle$ which acts on the Cooper channel. The operator $\mathcal{V}$ is a general effective electron-electron interaction which is attractive over a small range close to the Fermi surface. The pairing potential has the following symmetries

$$\begin{aligned} V_{s_1s_2,s_2's_1'}(\boldsymbol{k},\boldsymbol{k}') &= -V_{s_2s_1,s_2's_1'}(-\boldsymbol{k},\boldsymbol{k}') \\ &= -V_{s_1s_2,s_1's_2'}(\boldsymbol{k},-\boldsymbol{k}') = V^{*}_{s_1's_2',s_2s_1}(\boldsymbol{k}',\boldsymbol{k}) \end{aligned} \tag{2.2}$$

to ensure that the Fermion sign and the time reversal symmetry ($\mathcal{K}$) be preserved. The BCS solution of the Hamiltonian, Eq. (2.1), is obtained by

mean-field approximation. We define the mean field potential by

$$\Delta_{s_1',s_2'}(\boldsymbol{k}) = -\sum_{\boldsymbol{k}',s_2,s_1} V_{s_1 s_2,s_2' s_1'}(\boldsymbol{k},\boldsymbol{k}')\langle c_{-\boldsymbol{k}',s_2'} c_{\boldsymbol{k}',s_1'}\rangle$$
$$\Delta^*_{s_1,s_2}(-\boldsymbol{k}) = -\sum_{\boldsymbol{k}',s_2',s_1'} V_{s_1 s_2,s_2' s_1'}(\boldsymbol{k},\boldsymbol{k}')\langle c^\dagger_{\boldsymbol{k},s_1} c^\dagger_{-\boldsymbol{k},s_2}\rangle. \qquad (2.3)$$

The brackets $\langle A\rangle$ denote the expectation value $\mathrm{Tr}[\exp(-\beta\mathcal{H})A]/\mathrm{Tr}[\exp(-\beta\mathcal{H})]$. The amplitude of the mean field potential is the order parameter of the superconducting phase. If the fluctuations $\langle(c^\dagger c^\dagger - \langle c^\dagger c^\dagger\rangle)^2\rangle << \langle c^\dagger c^\dagger\rangle^2$ are small, the many-body problem of Eq. (2.1) is reduced to the one particle Hamiltonian

$$\begin{aligned}\mathcal{H} &= \sum_{\boldsymbol{k},s_1,s_2} \langle \boldsymbol{k},s_1|\hat{H}_0|\boldsymbol{k},s_2\rangle\, c^\dagger_{\boldsymbol{k},s_1} c_{\boldsymbol{k},s_2} \\ &+ \frac{1}{2}\sum_{\boldsymbol{k}}\sum_{s_1,s_2}\left[\Delta_{s_1,s_2}(\boldsymbol{k})\, c^\dagger_{\boldsymbol{k},s_1} c^\dagger_{-\boldsymbol{k},s_2} - \Delta^*_{s_1,s_2}(-\boldsymbol{k})\, c_{-\boldsymbol{k},s_1} c_{\boldsymbol{k},s_2}\right]. \qquad (2.4)\end{aligned}$$

Here, we omitted the term containing only the mean field but not the operators as it only gives a contribution to the ground state energy. From Eq. (2.2) and Eq. (2.3), it is clear that the order parameter has the following symmetry

$$\hat{\Delta}(\boldsymbol{k}) = -\hat{\Delta}^\top(-\boldsymbol{k}). \qquad (2.5)$$

In superconductors with an inversion center, the order parameter $\hat{\Delta}(\boldsymbol{k})$ has the symmetry of the Cooper pairing wave function in $\boldsymbol{k}$-space. In this case, the Kramer's degeneracy (due to the time reversal symmetry) allows the classification of the Cooper pairs in terms of their *pseudo spin*. The term spin and pseudo spin will be used synonymously in the following text. In the case of spin-singlet pairing, $\hat{\Delta}(\boldsymbol{k})$ is an antisymmetric matrix which can be described by a single even function $\psi(\boldsymbol{k}) = \psi(-\boldsymbol{k})$,

$$\hat{\Delta}(\boldsymbol{k}) = \psi(\boldsymbol{k}) i\hat{\sigma}_y = \begin{pmatrix} 0 & \psi(\boldsymbol{k}) \\ -\psi(\boldsymbol{k}) & 0 \end{pmatrix} = \psi(\boldsymbol{k})(|\uparrow\downarrow\rangle - |\downarrow\uparrow\rangle). \qquad (2.6)$$

In the case of spin-triplet pairing, the spin component of the wave function corresponding to the three different spin projections on the quantization axis

can be written as,

$$S_z = \begin{cases} 1 & |\uparrow\uparrow\rangle = \begin{pmatrix} 1 & 0 \\ 0 & 0 \end{pmatrix} \\ 0 & |\uparrow\downarrow\rangle + |\downarrow\uparrow\rangle = \begin{pmatrix} 0 & 1 \\ 1 & 0 \end{pmatrix} \\ -1 & |\downarrow\downarrow\rangle = \begin{pmatrix} 0 & 0 \\ 0 & 1 \end{pmatrix} \end{cases} \tag{2.7}$$

Thus, in general, the orbital part has three different components. The formalism used in this case involves an odd vectorial function $\boldsymbol{d}(\boldsymbol{k}) = -\boldsymbol{d}(\boldsymbol{k})$ and the Pauli matrices $\hat{\boldsymbol{\sigma}} = (\hat{\sigma}_x, \hat{\sigma}_y, \hat{\sigma}_z)$

$$\begin{aligned} \hat{\Delta}(\boldsymbol{k}) &= (\boldsymbol{d}\cdot\hat{\boldsymbol{\sigma}})i\hat{\sigma}_y = \begin{pmatrix} -d_x(\boldsymbol{k}) + id_y(\boldsymbol{k}) & d_z(\boldsymbol{k}) \\ d_z(\boldsymbol{k}) & d_x(\boldsymbol{k}) + id_y(\boldsymbol{k}) \end{pmatrix} \\ &= (-d_x(\boldsymbol{k}) + id_y(\boldsymbol{k}))|\uparrow\uparrow\rangle + d_z(\boldsymbol{k})(|\uparrow\downarrow\rangle + |\downarrow\uparrow\rangle) + (d_x(\boldsymbol{k}) + id_y(\boldsymbol{k}))|\downarrow\downarrow\rangle. \end{aligned} \tag{2.8}$$

The functions $\psi(\boldsymbol{k})$ and $\boldsymbol{d}(\boldsymbol{k})$ are classified using basis functions belonging to the irreducible representation of the point groups of the crystal. This type of pairing function is often called s-, p-, or d-wave, etc., according to its $\boldsymbol{k}$-symmetry

$$\alpha^L\hat{\Delta}(\boldsymbol{k}) = \hat{\Delta}(\alpha\boldsymbol{k}) \text{ with } L = 0, 1, 2, \cdots \text{respectively.} \tag{2.9}$$

In our work, we will study superconductivity using the quantum field approach [28]. The formulation of the theory in terms of Green's function allows one to solve a wide range of problems. For example, to study the effect of disorder, see Chapter 5. We introduce, for this purpose, two different Green's functions. The regular Green's function

$$G_{\lambda\mu}(\boldsymbol{k},\tau) = -\langle T_\tau\{c_{\boldsymbol{k},\lambda}(\tau)c^\dagger_{\boldsymbol{k},\mu}(0)\}\rangle \tag{2.10}$$

and the so called anomalous Green's functions

$$\begin{aligned} F_{\lambda\mu}(\boldsymbol{k},\tau) &= \langle T_\tau\{c_{\boldsymbol{k},\lambda}(\tau)c_{-\boldsymbol{k},\mu}(0)\}\rangle \\ F^\dagger_{\lambda\mu}(\boldsymbol{k},\tau) &= \langle T_\tau\{c^\dagger_{-\boldsymbol{k},\lambda}(\tau)c^\dagger_{\boldsymbol{k},\mu}(0)\}\rangle \end{aligned} \tag{2.11}$$

where $c_{\boldsymbol{k},\lambda}(\tau) = \exp(\tau\mathcal{H})c_{\boldsymbol{k},\lambda}\exp(-\tau\mathcal{H})$ are fermion operators in the Matsubara representation, and T_τ is the time ordering operator with respect to the imaginary time τ. The functions $\hat{G}$ and $\hat{F}$ satisfy a system of differential equations which are commonly called Gork'ov equations. Taking the derivative with respect to τ,

$$\begin{aligned}\frac{\partial G_{\lambda\mu}(\boldsymbol{k},\tau)}{\partial\tau} &= -\delta_{\lambda,\mu}\delta(\tau) - \left\langle T_\tau \left\{ \frac{\partial c_{\boldsymbol{k},\lambda}(\tau)}{\partial\tau} c^\dagger_{\boldsymbol{k},\mu}(0) \right\} \right\rangle \\ &= -\delta_{\lambda,\mu}\delta(\tau) \\ &+ \sum_{s_2} \left[-\langle \boldsymbol{k},\lambda|\mathcal{H}_T|\boldsymbol{k},s_2\rangle\, G_{s_2\mu}(\boldsymbol{k},\tau) + \Delta_{\lambda,s_2}(\boldsymbol{k})\; F^\dagger_{s_2\mu}(\boldsymbol{k},\tau) \right],\end{aligned}$$

where we used

$$\begin{aligned}\frac{\partial c_{\boldsymbol{k}',s'}(\tau)}{\partial\tau} &= e^{\mathcal{H}\tau}\left[\mathcal{H}, c_{\boldsymbol{k}',s'}\right] e^{-\mathcal{H}\tau} \\ &= -\sum_{s_2}\Big[\langle \boldsymbol{k}',s'|\mathcal{H}_T|\boldsymbol{k}',s_2\rangle\, c_{\boldsymbol{k},s_2}(\tau) \\ &+ \frac{1}{2}\left[\Delta_{s',s_2}(\boldsymbol{k}') - \Delta_{s_2,s'}(-\boldsymbol{k}')\right] c^\dagger_{-\boldsymbol{k}',s_2}(\tau)\Big],\end{aligned}$$

and going to the Matsubara momentum-frequency representation

$$G_{\lambda\mu}(\boldsymbol{k},i\omega_n) = \frac{1}{\beta}\sum_n e^{-i\omega_n\tau} G_{\lambda\mu}(\boldsymbol{k},\tau) \text{ etc.},$$

where $\omega_n = \pi k_B T(2n+1)$ is the fermion Matsubara frequency, we find the Gor'kov equations, which read

$$\hat{G}_0^{-1}(\boldsymbol{k},i\omega_n)\hat{G}(\boldsymbol{k},i\omega_n) + \hat{\Delta}(\boldsymbol{k})\hat{F}^\dagger(\boldsymbol{k},i\omega_n) = \hat{\sigma}_0 \qquad (2.12)$$

$$\hat{G}_0^{-1^\top}(-\boldsymbol{k},-i\omega_n)\hat{F}^\dagger(\boldsymbol{k},i\omega_n) - \hat{\Delta}^\dagger(\boldsymbol{k})\hat{G}(\boldsymbol{k},i\omega_n) = 0 \qquad (2.13)$$

$$\hat{G}_0^{-1}(\boldsymbol{k},i\omega_n)\hat{F}(\boldsymbol{k},i\omega_n) - \hat{\Delta}(\boldsymbol{k})\hat{G}^\top(-\boldsymbol{k},-i\omega_n) = 0, \qquad (2.14)$$

where $\hat{G}_0^{-1}(\boldsymbol{k},i\omega_n) = (i\omega_n\hat{\sigma}_0 - \langle\boldsymbol{k}|\hat{\mathcal{H}}_T|\boldsymbol{k}\rangle)$. Together with the gap equation

$$\Delta_{s_1',s_2'}(\boldsymbol{k}) = -\sum_{\boldsymbol{k}',s_2,s_1}\sum_n V_{s_1s_2,s_2's_1'}(\boldsymbol{k},\boldsymbol{k}')F_{s_2's_1'}(\boldsymbol{k},i\omega_n) \qquad (2.15)$$

the Gork'ov equations Eqs (2.12), (2.13) and (2.14) determine $\hat{G}$ and $\hat{F}$. The knowledge of $\hat{G}$ and $\hat{F}$ allows one to evaluate different physical quantities characterizing the superconducting phase.

2.2 Antisymmetric spin-orbit coupling

The model used in this work to describe the normal state of the material without an inversion center has the following single-particle Hamiltonian:

$$\mathcal{H}_T = \mathcal{H}_0 + \mathcal{H}', \tag{2.16}$$

with

$$\mathcal{H}_0 = \sum_{\boldsymbol{k},s} \xi_{\boldsymbol{k}}\ c^\dagger_{\boldsymbol{k}s} c_{\boldsymbol{k}s}, \tag{2.17}$$

$$\mathcal{H}' = \alpha \sum_{\boldsymbol{k},s,s'} (\boldsymbol{g}_{\boldsymbol{k}} \cdot \boldsymbol{\sigma}_{ss'})\ c^\dagger_{\boldsymbol{k}s} c_{\boldsymbol{k}s'}. \tag{2.18}$$

The band energy $\xi_{\boldsymbol{k}} = \epsilon_{\boldsymbol{k}} - \mu$ is measured relative to the chemical potential μ, and $\alpha \boldsymbol{g}_{\boldsymbol{k}} \cdot \boldsymbol{\sigma}$ introduces the antisymmetric spin-orbit coupling (ASOC) with α as a coupling constant (we set $\langle \boldsymbol{g}^2_{\boldsymbol{k}} \rangle_{\boldsymbol{k}} = 1$ where $\langle\rangle_{\boldsymbol{k}}$ denotes the integral over the Fermi surface $\int \frac{d\Omega_{\boldsymbol{k}}}{4\pi}$).

Here follows a brief discussion on the origin and some basic properties of this Hamiltonian. In a crystal lattice, the electrons move in a periodic potential $U(\boldsymbol{r})$. In the absence of inversion symmetry, there is no symmetry point in the unit cell relative to which $U(\boldsymbol{r}) = U(-\boldsymbol{r})$ is satisfied. This also implies that the Bloch function does not have the property $u_{\boldsymbol{k}}(\boldsymbol{r}) = u_{-\boldsymbol{k}}(-\boldsymbol{r})$. Ignoring, for the moment, relativistic effects, the potential yields the following contribution to the single-particle Hamiltonian:

$$\begin{aligned} \mathcal{H}_p &= \sum_{\boldsymbol{k},s} \int_{u.c.} d^3r\, u^*_{\boldsymbol{k}}(\boldsymbol{r}) U(\boldsymbol{r}) u_{\boldsymbol{k}}(\boldsymbol{r})\, c^\dagger_{\boldsymbol{k}s} c_{\boldsymbol{k}s} \\ &= \sum_{\boldsymbol{k},s} \int_{u.c.} d^3r\, u_{-\boldsymbol{k}}(\boldsymbol{r}) U(\boldsymbol{r}) u_{\boldsymbol{k}}(\boldsymbol{r})\, c^\dagger_{\boldsymbol{k}s} c_{\boldsymbol{k}s} = \sum_{\boldsymbol{k},s} \tilde{U}(\boldsymbol{k})\, c^\dagger_{\boldsymbol{k}s} c_{\boldsymbol{k}s}\,. \end{aligned} \tag{2.19}$$

The integral runs over the unit cell of the lattice. The resulting potential $\tilde{U}(\boldsymbol{k})$ is even in $\boldsymbol{k}$, i.e. $\tilde{U}(\boldsymbol{k}) = \tilde{U}(-\boldsymbol{k})$. On this (non-relativistic) level, the lack of inversion symmetry does not affect the band structure, which remains symmetric under the operation $\boldsymbol{k} \to -\boldsymbol{k}$ due to time reversal symmetry, i.e. the fact that $u^*_{\boldsymbol{k}}(\boldsymbol{r}) = u_{-\boldsymbol{k}}(\boldsymbol{r})$.

Now, we include the spin-orbit coupling (SOC). The symmetric SOC of each ion couples different atomic orbitals and requires a multi-orbital description. In this way, the spins would be converted into pseudo spins, which

can be handled formally in the same way as the original spins. For our purpose, the most important influence of this would be an anisotropic g-tensor which could be straightforwardly introduced into the following discussion and would affect the susceptibility of the normal and superconducting phase in the same way. For the sake of simplicity, however, we will keep the g-tensor isotropic here. The effect of spin-orbit coupling on the pairing interaction is ignored here, but it will be discussed later in Chapter 4.

For a lattice without inversion symmetry, SOC already appears at the level of a single-band model yielding the ASOC term $\mathcal{H}'$, Eq. (2.18) [29]. The vector function $\alpha \boldsymbol{g}_{\boldsymbol{k}}$ is derived from the relativistic correction $\frac{e}{2mc^2}[\boldsymbol{v} \times \boldsymbol{\nabla}_{\boldsymbol{r}} U(\boldsymbol{r})] \cdot \boldsymbol{S}$, which yields

$$\alpha \boldsymbol{g}_{\boldsymbol{k}} = -\frac{e}{2mc^2} \int_{u.c.} d^3r \, \{\boldsymbol{J}_{\boldsymbol{k}}(\boldsymbol{r}) \times \boldsymbol{\nabla}_{\boldsymbol{r}} U(\boldsymbol{r})\} \tag{2.20}$$

with

$$\boldsymbol{J}_{\boldsymbol{k}}(\boldsymbol{r}) = \frac{\hbar}{2mi} \left[u^*_{\boldsymbol{k}}(\boldsymbol{r})(i\boldsymbol{k} + \boldsymbol{\nabla}_{\boldsymbol{r}}) u_{\boldsymbol{k}}(\boldsymbol{r}) + u_{\boldsymbol{k}}(\boldsymbol{r})(i\boldsymbol{k} - \boldsymbol{\nabla}_{\boldsymbol{r}}) u^*_{\boldsymbol{k}}(\boldsymbol{r}) \right] . \tag{2.21}$$

It is easy to verify that $\alpha \boldsymbol{g}_{\boldsymbol{k}} = 0$, if $U(\boldsymbol{r}) = U(-\boldsymbol{r})$ and $u_{\boldsymbol{k}}(-\boldsymbol{r}) = u_{-\boldsymbol{k}}(\boldsymbol{r})$. In the absence of inversion symmetry, however, $\boldsymbol{g}_{\boldsymbol{k}}$ is finite and satisfies $\boldsymbol{g}_{\boldsymbol{k}} = -\boldsymbol{g}_{-\boldsymbol{k}}$, since $\boldsymbol{J}_{-\boldsymbol{k}}(\boldsymbol{r}) = -\boldsymbol{J}_{\boldsymbol{k}}(\boldsymbol{r})$ (note if $\boldsymbol{g}_{\boldsymbol{k}} = \boldsymbol{g}_{-\boldsymbol{k}}$ this implies time reversal symmetry is broken). With these properties, it is now clear that the Hamiltonian $\mathcal{H}_T$ is invariant under time reversal $\mathcal{K}$ but not under inversion operation $\mathcal{I}$, because

$$\alpha \boldsymbol{g}_{\boldsymbol{k}} \cdot \hat{\boldsymbol{\sigma}} \xrightarrow{\mathcal{I}} \alpha \boldsymbol{g}_{-\boldsymbol{k}} \cdot \hat{\boldsymbol{\sigma}} = -\alpha \boldsymbol{g}_{\boldsymbol{k}} \cdot \hat{\boldsymbol{\sigma}}$$

and

$$\alpha \boldsymbol{g}_{\boldsymbol{k}} \cdot \hat{\boldsymbol{\sigma}} \xrightarrow{\mathcal{K}} -\alpha \boldsymbol{g}_{-\boldsymbol{k}} \cdot \hat{\boldsymbol{\sigma}} = \alpha \boldsymbol{g}_{\boldsymbol{k}} \cdot \hat{\boldsymbol{\sigma}}.$$

The ASOC yields a modified band structure. We parameterize the normal state Green's function by

$$\hat{G}_0(\boldsymbol{k}, i\omega_n) = G^0_+(\boldsymbol{k}, i\omega_n)\hat{\sigma}_0 + (\hat{\boldsymbol{g}}_{\boldsymbol{k}} \cdot \hat{\boldsymbol{\sigma}}) G^0_-(\boldsymbol{k}, i\omega_n) \tag{2.22}$$

where

$$G_\pm(\boldsymbol{k}, i\omega_n) = \frac{1}{2}\left[\frac{1}{i\omega_n - \xi_{\boldsymbol{k}} - \alpha|\boldsymbol{g}_{\boldsymbol{k}}|} \pm \frac{1}{i\omega_n - \xi_{\boldsymbol{k}} + \alpha|\boldsymbol{g}_{\boldsymbol{k}}|} \right] \tag{2.23}$$

and $\hat{\boldsymbol{g}}_{\boldsymbol{k}} = \boldsymbol{g}_{\boldsymbol{k}}/|\boldsymbol{g}_{\boldsymbol{k}}|$ ($|\boldsymbol{g}| = \sqrt{\boldsymbol{g}^2}$). The band splits into two spin dependent parts with energies $\xi_{1,2} = \xi \pm \alpha|\boldsymbol{g}|$. The spinor is twisted on the two bands in a way that is described by the antisymmetric part of the Green's function, $(\hat{\boldsymbol{g}}_{\boldsymbol{k}} \cdot \hat{\boldsymbol{\sigma}})G^0_-(\boldsymbol{k}, i\omega_n)$.

2.3 Selection of the superconducting state

Now we turn to the superconducting phase and introduce the general pairing interaction

$$\mathcal{H}_{pair} = \frac{1}{2} \sum_{\boldsymbol{k},\boldsymbol{k},s_i} V_{s_1 s_2, s_2' s_1'}(\boldsymbol{k}, \boldsymbol{k}')\, c^\dagger_{\boldsymbol{k},s_1} c^\dagger_{-\boldsymbol{k},s_2} c_{-\boldsymbol{k}',s_2'} c_{\boldsymbol{k}',s_1'}. \tag{2.24}$$

The pairing potential can be written in the form

$$\begin{aligned} V_{s_1 s_2, s_2' s_1'}(\boldsymbol{k}, \boldsymbol{k}') &= \sum_a v_a\, \psi_a(\boldsymbol{k})\psi_a(\boldsymbol{k}')\hat{\tau}_{s_1 s_2}\hat{\tau}^\dagger_{s_2' s_1'} \\ &+ \sum_b v_b\, (\boldsymbol{d}_b(\boldsymbol{k}) \cdot \hat{\boldsymbol{\tau}})_{s_1 s_2} (\boldsymbol{d}_b(\boldsymbol{k}') \cdot \hat{\boldsymbol{\tau}})^\dagger_{s_2' s_1'} \end{aligned} \tag{2.25}$$

where $\hat{\tau}_{s_1 s_2} = (i\hat{\sigma}^y)_{s_1 s_2}$, and, $\hat{\boldsymbol{\tau}}_{s_1 s_2} = (i\boldsymbol{\sigma}\hat{\sigma}^y)_{s_1 s_2}$. We use the BCS decoupling scheme and determine the linearized gap equation in order to calculate the transition temperature T_c:

$$\Delta_{ss'}(\boldsymbol{k}) = -k_B T \sum_{n,\boldsymbol{k}'} \sum_{s_1,s_2} V_{\boldsymbol{k},\boldsymbol{k}'} G^0_{ss_1}(\boldsymbol{k}', i\omega_n)\Delta_{s_1,s_2}(\boldsymbol{k}')G^0_{s's_2}(-\boldsymbol{k}', -i\omega_n) \tag{2.26}$$

where $V_{\boldsymbol{k},\boldsymbol{k}'} = \sum_a v_a\, \psi_a(\boldsymbol{k})\psi_a(\boldsymbol{k}') + \sum_b v_b\, \boldsymbol{d}_b(\boldsymbol{k})\boldsymbol{d}_b(\boldsymbol{k}')$. The gap function is decomposed into a spin-singlet $[\psi(\boldsymbol{k})]$ and a triplet $[\boldsymbol{d}(\boldsymbol{k})]$ part, $\hat{\Delta}(\boldsymbol{k}) = \{\psi(\boldsymbol{k})\hat{\sigma}_0 + \boldsymbol{d}(\boldsymbol{k}) \cdot \hat{\boldsymbol{\sigma}}\}i\sigma_y$. For simplicity, we assume that the gap functions have the same magnitude on both Fermi surface sheets. Replacing (2.22) in Eq. (2.26) allows us to write the linearized gap equations as

$$\psi(\boldsymbol{k}) = -k_B T \sum_{n,\boldsymbol{k}'} V_{\boldsymbol{k},\boldsymbol{k}'} \Big\{ [G_+G_+ + G_-G_-]\psi(\boldsymbol{k}') + [G_+G_- + G_-G_+]\hat{\boldsymbol{g}}_{\boldsymbol{k}'} \cdot \boldsymbol{d}(\boldsymbol{k}') \Big\} \tag{2.27}$$

and

$$\begin{aligned} \boldsymbol{d}(\boldsymbol{k}) &= -k_B T \sum_{n,\boldsymbol{k}'} V_{\boldsymbol{k},\boldsymbol{k}'} \{[G_+ G_+ + G_- G_-]\boldsymbol{d}(\boldsymbol{k}') \\ &+ 2G_- G_- [\hat{\boldsymbol{g}}_{\boldsymbol{k}'}(\hat{\boldsymbol{g}}_{\boldsymbol{k}'} \cdot \boldsymbol{d}(\boldsymbol{k}')) - \boldsymbol{d}(\boldsymbol{k}')] + [G_+ G_- + G_- G_+]\hat{\boldsymbol{g}}_{\boldsymbol{k}'}\psi(\boldsymbol{k}') \} \end{aligned} \tag{2.28}$$

where we have used the short notation: $G_a G_b = G_a(\boldsymbol{k}, i\omega_n)G_b(-\boldsymbol{k}, -i\omega_n)$ with $a, b = \pm$. For finite α, the spin-singlet and triplet pairing channel are coupled. However, this coupling

$$k_B T \sum_{n,\boldsymbol{k}'} [G_+ G_- + G_- G_+] \;\propto\; \alpha \frac{N_0'}{N_0}$$

depends on the degree of particle-hole asymmetry N_0' or the difference of the density of states on the two Fermi surface sheets. The effect of this term is considered in detail in Chapter 4. Here we consider $N_0' = 0$. In this particular case, the "singlet" and "triplet" pairing channels can be considered separately. However, as we will see in Section 2.5, independent of the particle-hole asymmetry, the Cooper pairs result in a mixture of spin-singlet and spin-triplet pairs [19].

For spin-singlet pairing, it is convenient to perform the sum over the Matsubara frequency ω_n first

$$\begin{aligned} k_B T \sum_n [G_+ G_+ + G_- G_-] &= \frac{k_B T}{2} \sum_n \left\{ \frac{1}{\omega_n^2 + \xi_1^2} + \frac{1}{\omega_n^2 + \xi_2^2} \right\} \\ &= \frac{1}{4} \left\{ \frac{1}{\xi_1} \tanh\left(\frac{\xi_1}{2k_B T}\right) + \frac{1}{\xi_2} \tanh\left(\frac{\xi_2}{2k_B T}\right) \right\}. \end{aligned}$$

In the weak coupling approach, we replace the sum over $\boldsymbol{k}$ by $\sum_{\boldsymbol{k}} \to N_0 \int \frac{d\Omega}{4\pi} \int d\xi$, where the integral over the band energy ξ is bounded by the cutoff energy ϵ_c

$$k_B T \int_{-\epsilon_c}^{+\epsilon_c} d\xi \, N_0 \sum_n [G_+ G_+ + G_- G_-] =$$

$$N_0 \left\{ \ln\left(\frac{2\gamma\epsilon_c}{\pi k_B T}\right) + \frac{1}{2} \ln\left(1 - \frac{\alpha^2 |\boldsymbol{g}_{\boldsymbol{k}}|^2}{\epsilon_c^2}\right) \right\}.$$

Here $2\gamma/\pi \approx 1.14$, where $\ln\gamma = C \approx 0.577$ is called the Euler constant. We find in this way that the transition temperature (T_c) is given by

$$\ln\left(\frac{T_c}{T_{cs}}\right) = O\left(\frac{\alpha^2}{\epsilon_c^2}\right) . \tag{2.29}$$

The transition temperature remains essentially unchanged from $k_B T_{cs} = 1.14\epsilon_c \exp(-1/N_0 v_s)$. Here T_{cs} is T_c for $\alpha = 0$, and v_s is given by $v_s\psi(\boldsymbol{k}) = \langle V_{\boldsymbol{k},\boldsymbol{k}'}\psi(\boldsymbol{k}')\rangle_{\boldsymbol{k}'}$.

For triplet pairing, the equation for T_c is obtained by permuting the order between the energy integration and the Matsubara sum. First we perform the unbounded integration

$$\int_{-\infty}^{\infty} d\xi \, [G_\uparrow G_\downarrow - G_- G_-] \;=\; \frac{1}{2k_B T_c}\left\{\frac{1}{|2n+1| + i\rho_{\boldsymbol{k}}} + \frac{1}{|2n+1| - i\rho_{\boldsymbol{k}}}\right\}. \tag{2.30}$$

with $\rho_{\boldsymbol{k}} = \alpha|\boldsymbol{g}_{\boldsymbol{k}}|/\pi k_B T_c$. The Matsubara sum of the expression (2.30) is clearly divergent. But summing and subtracting $1/|\omega_n|$

$$\sum_n \int_{-\infty}^{\infty} d\xi \, [G_+ G_+ - G_- G_-] \;=\; \pi \sum_n \frac{1}{|\omega_n|} + Re \sum_{n-1}^{\infty} \frac{2}{k_B T}\left\{\frac{1}{2n-1+i\rho_{\boldsymbol{k}}} - \frac{1}{2n-1}\right\}.$$

the logarithmic divergency of the first term is cutoff at the boundary frequency ϵ_c

$$\pi k_B T \sum_n^{|\omega_n|<\epsilon_c} \frac{1}{|\omega_n|} \;=\; \ln\left(\frac{2\gamma\epsilon_c}{\pi k_B T}\right).$$

In this way, it is easy to find the expression for the transition temperature

$$\ln\left(\frac{T_c}{T_{ct}}\right) = \langle\{|\boldsymbol{d}(\boldsymbol{k})|^2 - |\hat{\boldsymbol{g}}_{\boldsymbol{k}} \cdot \boldsymbol{d}(\boldsymbol{k})|^2\} f(\rho_{\boldsymbol{k}})\rangle_{\boldsymbol{k}} + O\left(\frac{\alpha^2}{\epsilon_F^2}\right) \tag{2.31}$$

where $k_B T_{ct} = \epsilon_c \exp(-1/N_0 v_t)$ with $v_t \boldsymbol{d}(\boldsymbol{k}) = \langle V_{\boldsymbol{k},\boldsymbol{k}'}\boldsymbol{d}(\boldsymbol{k}')\rangle_{\boldsymbol{k}'}$ and $\rho_{\boldsymbol{k}} = \alpha|\boldsymbol{g}_{\boldsymbol{k}}|/\pi k_B T_c$. We use the normalized gap function with $\langle|\boldsymbol{d}(\boldsymbol{k})|^2\rangle_{\boldsymbol{k}} = 1$ in all numerical calculations. The function $f(\rho)$ is defined as

$$f(\rho) = Re\left\{\Psi\left(\frac{-1}{2}\right) - \Psi\left(\frac{i\rho - 1}{2}\right)\right\}. \tag{2.32}$$

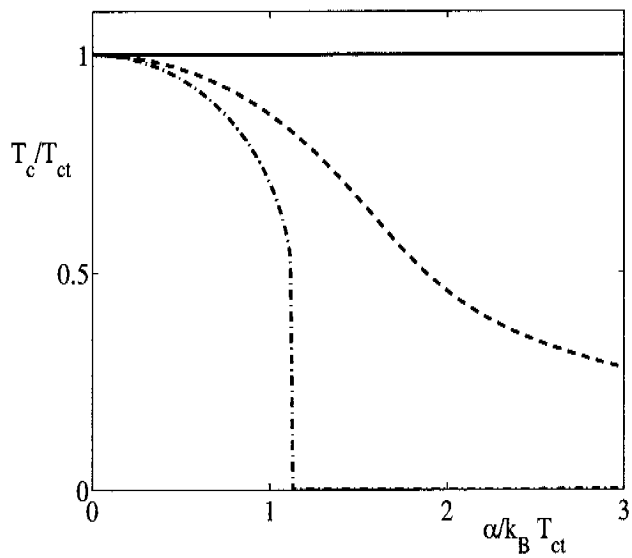

Figure 2.1: Transition temperature as a function of α for $\boldsymbol{g_k} = (-k_y, k_x, 0)$. The curves from top to bottom correspond to $\boldsymbol{d} = \hat{\boldsymbol{y}}k_x - \hat{\boldsymbol{x}}k_y$, $\boldsymbol{d} = \hat{\boldsymbol{y}}k_x + \hat{\boldsymbol{x}}k_y$, and $\boldsymbol{d} = \hat{\boldsymbol{x}}k_x + \hat{\boldsymbol{y}}k_y + \hat{\boldsymbol{z}}k_z$, respectively.

Here we have introduced the digamma function $\Psi(z)$ defined by $\Psi(z) \equiv d/dz \ln(z!)$.

The correction term in Eq. (2.31) suppresses T_c in general. For a spherical Fermi surface and $\alpha = 0$, all gap functions with a given relative angular momentum ℓ have the same T_c. Eq.(2.32) determines how this degeneracy is lifted by the broken inversion symmetry. The highest T_c is obtained for a state with $\boldsymbol{d}(\boldsymbol{k}) \parallel \boldsymbol{g_k}$, for which the right-hand side of Eq.(2.31) vanishes and $T_c = T_{ct}$. Hence, we conclude that spin-triplet pairing is not indiscriminately suppressed in the absence of an inversion center. In principle, there may be spin-triplet pairing states which are completely unaffected by the lack of inversion symmetry, taking advantage of the spinor structure induced by $\boldsymbol{g_k}$.

$\alpha \boldsymbol{g_k} \cdot \boldsymbol{\sigma}$ can be derived microscopically, as described in the previous sec-

tion [14, 29]. However, for qualitative studies, it is sufficient to deduce the structure of the $\boldsymbol{g}$-vector from symmetry arguments, as shown in detail in Chapter 3. Here we consider the form of $\boldsymbol{g_k}$ for two examples: MnSi and $CePt_3Si$. We start with the space group that corresponds to the basic "point group" symmetry G. Due to the lack of inversion symmetry, this group is reduced to a subgroup G'. The correction term $\boldsymbol{g_k} \cdot \boldsymbol{\sigma}$ is invariant under all transformations of G', but not of G. MnSi has the cubic space group $P2_13$. The point group is only the tetrahedral group $T \subset O_h$. The symmetry breaking terms satisfying the above conditions correspond to the irreducible representations A_{2u} and A_{1u} of O_h which map to A_1 of T. The expansion in $\boldsymbol{k}$ leads to (we assume a spherical Fermi surface for simplicity)

$$\boldsymbol{g_k} = \alpha_1[k_x, k_y, k_z] + \alpha_2[k_x(k_y^2 - k_z^2), k_y(k_z^2 - k_x^2), k_z(k_x^2 - k_y^2)]. \qquad (2.33)$$

The $\boldsymbol{d}$-vector, which remains unaffected by the lack of inversion symmetry, is parallel to $\boldsymbol{g_k}$. Consequently, there are stringent conditions for triplet superconductivity in MnSi. However how strict these conditions are depend on the relative size of α_1/α_2 and on the strength of the ASOC. Up to now, there are no numerical estimations of α_1 and α_2.

$CePt_3Si$ is a tetragonal system with space group P4mm. Here, the removal of the inversion center leads to the point group $C_{4v} \subset D_{4h}$, which corresponds to the loss of the basal plane as a mirror plane ($z \to -z$). One finds that $\boldsymbol{g_k} \cdot \boldsymbol{\sigma} = k_x\sigma_y - k_y\sigma_x$, which is a basis function of A_{2u} of D_{4h}. This term has the form of the well-known Rashba spin-orbit coupling [30]. The $\boldsymbol{g}$-vector has only two nodes lying along the [001]-direction. In Fig. 2.1, we show the reduction of various spin-triplet pairing states with this $\boldsymbol{g}$-vector. The favored pairing state of the p-wave type is: $\boldsymbol{d}(\boldsymbol{k}) = \hat{\boldsymbol{x}}k_y - \hat{\boldsymbol{y}}k_x$ in A_{2u} of D_{4h}, while other p-wave pairing states are severely suppressed for $\alpha > k_BT_c$.

Let us consider the situation of a system with an unbiased spin-triplet pairing interaction $V_{\boldsymbol{k},\boldsymbol{k}'} = v_b\ \boldsymbol{k} \cdot \boldsymbol{k}'$. In the absence of antisymmetric spin-orbit coupling, the critical temperatures of the different p-wave states are degenerate. In the weak coupling limit, the Balian-Werthamer state $\boldsymbol{d}(\boldsymbol{k}) = \hat{\boldsymbol{x}}k_x + \hat{\boldsymbol{y}}k_y + \hat{\boldsymbol{z}}k_z$ is the most stable state for a spherical surface. This is because its nodeless structure provides the largest condensation energy. However, with the increment of the ASOC strength α, its critical temperature quickly

decreases. We have, in this case, a first transition to the protected spin-triplet state and if α is small enough ($\alpha < k_B T_{ct}$), we will observe a second transition to the Balian-Werthamer state at lower temperature. This is not the case for $CePt_3Si$, since band structure calculations show $\alpha >> k_B T_c$ [31].

2.4 Paramagnetic limiting field

Lifting the degeneracy of the spins is detrimental to spin-singlet superconductivity, an effect known as paramagnetic limiting. Spin-triplet pairing is less vulnerable in this respect. In the absence of inversion symmetry, however, this effect of pair breaking is modified. It is well known that impurity spin-orbit scattering reduces the effect of paramagnetic limiting [32–34]. We will show that an analogous effect occurs in systems with broken inversion symmetry. For simplicity, we ignore the effect of orbital pair breaking and include the magnetic field only through its coupling to the spin. Our aim is to demonstrate the effect of finite α on the paramagnetic limiting and a discussion for the upper critical field H_{c2} is given in [35]. We replace $\alpha \boldsymbol{g}_{\boldsymbol{k}} \rightarrow \boldsymbol{g}^-_{\boldsymbol{k}} = \alpha \boldsymbol{g}_{\boldsymbol{k}} - \boldsymbol{h}$ with $\boldsymbol{h} = \mu_B \boldsymbol{H}$. The linear gap equation yields the transition temperatures for a continuous onset of superconductivity. We first consider a spin-singlet pairing ($\psi(\boldsymbol{k})$). In this case, Eq. (2.27) becomes

$$\begin{aligned}
\psi(\boldsymbol{k}) &= -k_B T \sum_{n,\boldsymbol{k}'} V_{\boldsymbol{k},\boldsymbol{k}'} \Big\{ [G_+ G_+ + \hat{\boldsymbol{g}}^+_{\boldsymbol{k}'} \cdot \hat{\boldsymbol{g}}^-_{\boldsymbol{k}'} G_- G_-] \psi(\boldsymbol{k}') \Big\} \\
&= -\frac{k_B T}{2} \sum_{n,\boldsymbol{k}'} V_{\boldsymbol{k},\boldsymbol{k}'} \Big\{ [(\hat{F}^1_+ + \hat{F}^1_-) + \hat{\boldsymbol{g}}^+_{\boldsymbol{k}'} \cdot \hat{\boldsymbol{g}}^-_{\boldsymbol{k}'} (\hat{F}^1_- - \hat{F}^1_+)] \psi(\boldsymbol{k}') \Big\} ,
\end{aligned}$$

where we introduce $\boldsymbol{g}^\pm_{\boldsymbol{k}} = \alpha \boldsymbol{g}_{\boldsymbol{k}} \pm \boldsymbol{h}$, $\hat{\boldsymbol{g}}^\pm_{\boldsymbol{k}} = \boldsymbol{g}^\pm_{\boldsymbol{k}} / |\boldsymbol{g}^\pm_{\boldsymbol{k}}|$, and,

$$\begin{aligned}
F^1_\pm(\boldsymbol{k}', i\omega_n) &= \frac{1}{2} \Bigg[\frac{1}{[\omega_n + \frac{i}{2}(|\boldsymbol{g}^+_{\boldsymbol{k}'}| \pm |\boldsymbol{g}^-_{\boldsymbol{k}'}|)]^2 + [\xi_{\boldsymbol{k}'} + \frac{1}{2}(|\boldsymbol{g}^-_{\boldsymbol{k}'}| \mp |\boldsymbol{g}^+_{\boldsymbol{k}'}|)]^2} \\
&\quad + \frac{1}{[\omega_n - \frac{i}{2}(|\boldsymbol{g}^+_{\boldsymbol{k}'}| \pm |\boldsymbol{g}^-_{\boldsymbol{k}'}|)]^2 + [\xi_{\boldsymbol{k}'} - \frac{1}{2}(|\boldsymbol{g}^-_{\boldsymbol{k}'}| \mp |\boldsymbol{g}^+_{\boldsymbol{k}'}|)]^2} \Bigg] .
\end{aligned}$$

Evaluating the sum over $\boldsymbol{k}'$ first and then the Matsubara sum, as done previously to obtain Eq. (2.31), we derive the equation determining T_c

$$\ln\left(\frac{T_c}{T_{cs}}\right) = \left\langle \frac{|\psi(\boldsymbol{k})|^2}{2}\left\{\left[f(\rho_{\boldsymbol{k}}^-)+f(\rho_{\boldsymbol{k}}^+)\right] + \frac{\alpha^2\boldsymbol{g}_{\boldsymbol{k}}^2-\boldsymbol{h}^2}{[(\alpha\boldsymbol{g}_{\boldsymbol{k}}+\boldsymbol{h})^2(\alpha\boldsymbol{g}_{\boldsymbol{k}}-\boldsymbol{h})^2]^{1/2}}\left[f(\rho_{\boldsymbol{k}}^-)-f(\rho_{\boldsymbol{k}}^+)\right]\right\}\right\rangle_{\boldsymbol{k}} \quad (2.34)$$

with $\rho_{\boldsymbol{k}}^{\pm} = |\alpha\boldsymbol{g}_{\boldsymbol{k}}+\boldsymbol{h}|/2\pi k_B T_c \pm |\alpha\boldsymbol{g}_{\boldsymbol{k}}-\boldsymbol{h}|/2\pi k_B T_c$. If it is possible to choose $\boldsymbol{h} \perp \boldsymbol{g}_{\boldsymbol{k}}$ for all $\boldsymbol{k}$ (as it is for $CePt_3Si$), then in the small $T_c(h)/T_{cs}$ limit, the paramagnetic limiting field obeys $h'^2 \ln h' = -\alpha^2 \ln(T_c/T_{cs})$; with $h' = |\boldsymbol{h}|/\pi k_B T_{cs}$. In particular, the paramagnetic limiting field *diverges* as $T \to 0$ (Fig. 2.2).

For the spin-triplet channel, we obtain analogously from Eq. (2.28)

$$\begin{aligned}\boldsymbol{d}(\boldsymbol{k}) &= -k_B T \sum_{n,\boldsymbol{k}'} V_{\boldsymbol{k},\boldsymbol{k}'}\Big\{[G_+G_+ - \hat{\boldsymbol{g}}_{\boldsymbol{k}'}^{\dagger}\cdot\hat{\boldsymbol{g}}_{\boldsymbol{k}'}^{-}G_-G_-]\boldsymbol{d}(\boldsymbol{k}') \\ &- G_-G_-[\hat{\boldsymbol{g}}_{\boldsymbol{k}'}^{\dagger}(\hat{\boldsymbol{g}}_{\boldsymbol{k}'}^{-}\cdot\boldsymbol{d}(\boldsymbol{k}')) + \hat{\boldsymbol{g}}_{\boldsymbol{k}'}^{-}(\hat{\boldsymbol{g}}_{\boldsymbol{k}'}^{+}\cdot\boldsymbol{d}(\boldsymbol{k}'))]\Big\} \\ &= -\frac{k_B T}{2}\sum_{n,\boldsymbol{k}'} V_{\boldsymbol{k},\boldsymbol{k}'}\Big\{(\hat{F}_+^1+\hat{F}_-^{\dagger 1})\boldsymbol{d}(\boldsymbol{k}') \\ &+ (\hat{F}_+^1-\hat{F}_-^{\dagger 1})[\hat{\boldsymbol{g}}_{\boldsymbol{k}'}^{+}(\hat{\boldsymbol{g}}_{\boldsymbol{k}'}^{-}\cdot\boldsymbol{d}(\boldsymbol{k}')) + \hat{\boldsymbol{g}}_{\boldsymbol{k}'}^{-}(\hat{\boldsymbol{g}}_{\boldsymbol{k}'}^{+}\cdot\boldsymbol{d}(\boldsymbol{k}')) + (\hat{\boldsymbol{g}}_{\boldsymbol{k}'}^{+}\cdot\hat{\boldsymbol{g}}_{\boldsymbol{k}'}^{-})\boldsymbol{d}(\boldsymbol{k}')]\Big\},\end{aligned}$$

The corresponding equation governing T_c reads

$$\begin{aligned}\ln\left(\frac{T_c}{T_{ct}}\right) = &\left\langle \frac{|\boldsymbol{d}(\boldsymbol{k})|^2}{2}\left\{\left[f(\rho_{\boldsymbol{k}}^+)+f(\rho_{\boldsymbol{k}}^-)\right] + \frac{\alpha^2\boldsymbol{g}_{\boldsymbol{k}}^2-\boldsymbol{h}^2}{[(\alpha\boldsymbol{g}_{\boldsymbol{k}}+\boldsymbol{h})^2(\alpha\boldsymbol{g}_{\boldsymbol{k}}-\boldsymbol{h})^2]^{1/2}}\left[f(\rho_{\boldsymbol{k}}^{\dagger})-f(\rho_{\boldsymbol{k}}^-)\right]\right\}\right\rangle_{\boldsymbol{k}} \\ &+\left\langle\left[f(\rho_{\boldsymbol{k}}^+)-f(\rho_{\boldsymbol{k}}^-)\right]\frac{|\boldsymbol{h}\cdot\boldsymbol{d}(\boldsymbol{k})|^2-\alpha^2|\boldsymbol{g}_{\boldsymbol{k}}\cdot\boldsymbol{d}(\boldsymbol{k})|^2}{[(\alpha\boldsymbol{g}_{\boldsymbol{k}}+\boldsymbol{h})^2(\alpha\boldsymbol{g}_{\boldsymbol{k}}-\boldsymbol{h})^2]^{1/2}}\right\rangle_{\boldsymbol{k}} \quad (2.35)\end{aligned}$$

For $\alpha = 0$ there is no paramagnetic limiting, provided $\boldsymbol{d}(\boldsymbol{k})\cdot\boldsymbol{h} \neq 0$ can be found for all $\boldsymbol{k}$. According to Eq.(2.35), paramagnetic limiting is absent if $\boldsymbol{h} \perp \boldsymbol{d}(\boldsymbol{k})$ for all $\boldsymbol{k}$ and $\boldsymbol{d}(\boldsymbol{k}) \parallel \boldsymbol{g}_{\boldsymbol{k}}$. Fig. 2.2 shows the paramagnetic limiting field for a singlet state as a function of α obtained by Eq. (2.34), with $\boldsymbol{g}_{\boldsymbol{k}} = (-k_y, k_x, 0)$, as for $CePt_3Si$. For the field along the z-axis, (top

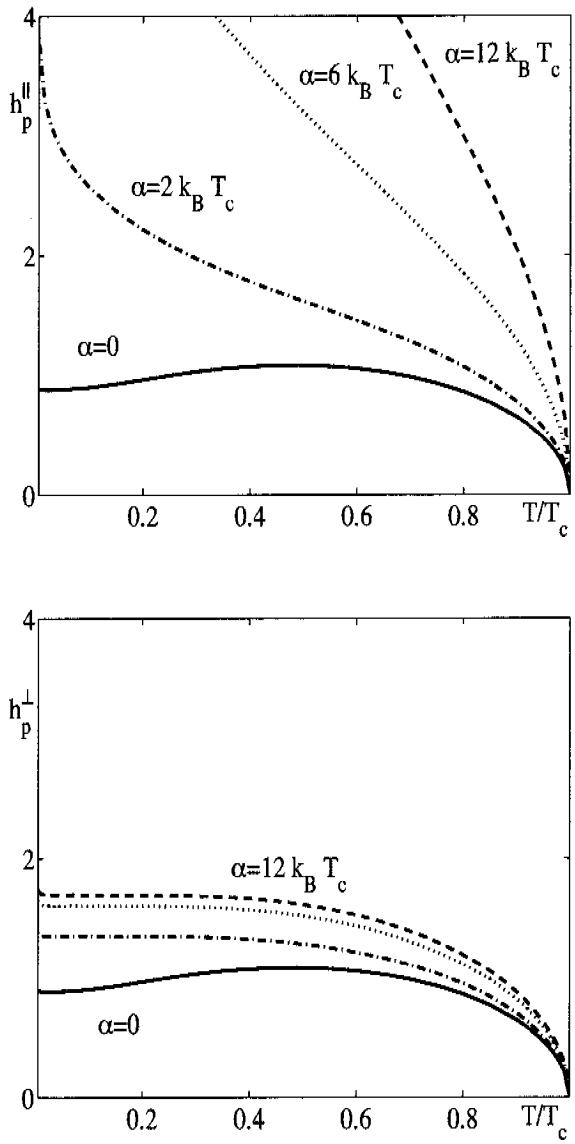

Figure 2.2: The paramagnetic limiting field h_p in units of $k_B T_c$ for $CePt_3Si$ in the case of the s-wave spin-singlet order parameter for different α values. The top plot shows h_p when the field is applied along the z-axis. The botton plot shows the case with the field in the xy-plane.

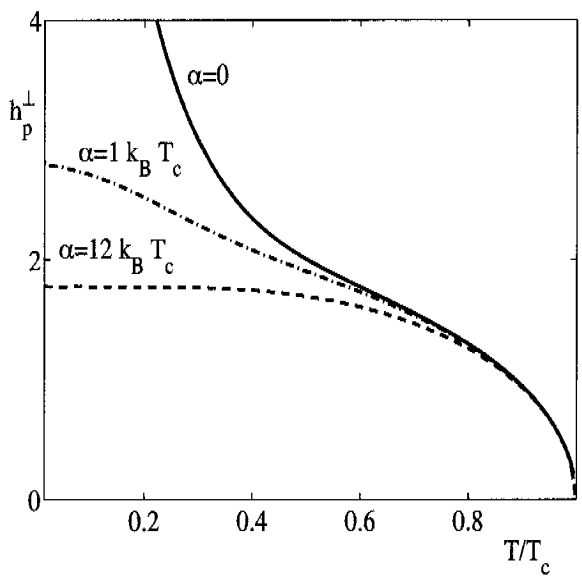

Figure 2.3: The paramagnetic limiting field h_p for fields in the xy-plane in units of $k_B T_c$ for $CePt_3Si$ in the case of the protected spin-triplet order parameter $\boldsymbol{d} = \hat{\boldsymbol{x}} k_y - \hat{\boldsymbol{y}} k_x$ for different α values.

plot), the figure illustrates the divergent paramagnetic limiting field at low temperatures described earlier. In this case, we could argue that paramagnetic limiting for a singlet state is rendered less effective by the presence of spin-orbit coupling. However, for the field in the xy-plane, (bottom plot), the paramagnetic limiting field doesn't diverge at low temperature, and its dependence on the spin-orbit coupling is small.

For the protected spin-triplet state $\boldsymbol{d}(\boldsymbol{k}) = \hat{\boldsymbol{x}}k_y - \hat{\boldsymbol{y}}k_x$, relevant for $CePt_3Si$, there is no paramagnetic limiting for fields along the z-axis. Its paramagnetic limiting for fields in the xy-plane, shown by Fig. 2.3, becomes very similar to that obtained for the singlet state at large α values.

It is important to study this system for single crystals, since for both the spin-singlet and spin-triplet cases a large anisotropy in the paramagnetic limiting field is predicted. The experiments seem to shown that this anisotropy is much smaller than expected [11]. Kaur *et al.* were able to show that this anisotropy reduction is possibly induced by the presence of a finite $\boldsymbol{q}$ helical phase [35].

However, the main result, for which, at large spin-orbit coupling $\alpha >> k_B T_c$, the paramagnetic limiting field for spin-singlet states becomes similar to that characterizing the protected spin-triplet state, still holds. Moreover, as we will show in the next section, the Knight shift shows related effects of the spin-orbit coupling.

2.5 Static uniform spin-susceptibility

For the following calculations, it is advantageous to discuss the superconducting phase by means of Green's functions defined by Eqs. (2.10) and (2.11). These Green's functions have to satisfy the Gor'kov equations introduced in Eqs. (2.12), (2.13) and (2.14), which can be written in the following form

$$\left[\hat{G}_0^{-1}(\boldsymbol{k}, i\omega_n) + \hat{\Delta}(\boldsymbol{k})\hat{G}_0^{\top}(-\boldsymbol{k}, -i\omega_n)\hat{\Delta}^{\dagger}(\boldsymbol{k})\right]\hat{G}(\boldsymbol{k}, i\omega_n) = \hat{\sigma}_0. \tag{2.36}$$

$$\hat{F}(\boldsymbol{k}, i\omega_n) = \hat{G}_0(\boldsymbol{k}, i\omega_n)\hat{\Delta}(\boldsymbol{k})\hat{G}^{\top}(-\boldsymbol{k}, -i\omega_n). \tag{2.37}$$

$$\hat{F}^{\dagger}(\boldsymbol{k}, i\omega_n) = \hat{G}_0^{\top}(-\boldsymbol{k}, -i\omega_n)\hat{\Delta}^{\dagger}(\boldsymbol{k})\hat{G}(\boldsymbol{k}, i\omega_n) \tag{2.38}$$

We assume that $k_B T_c < \alpha << \epsilon_F$ and solve the equations (2.36, 2.37, 2.38) in sequence. The solutions are formally the same for both spin-singlet, $\hat{\Delta}(\boldsymbol{k}) = i\{\psi(\boldsymbol{k})\}\hat{\sigma}_y$, and protected spin-triplet, $\hat{\Delta}(\boldsymbol{k}) = i\{\boldsymbol{d}(\boldsymbol{k})\cdot\hat{\boldsymbol{\sigma}}\}\hat{\sigma}_y$, with $\boldsymbol{d}(\boldsymbol{k})||\boldsymbol{g}(\boldsymbol{k})$ pairing. We find

$$\begin{aligned} \hat{G}(\boldsymbol{k}, i\omega_n) &= G_+(\boldsymbol{k}, \omega_n)\hat{\sigma}_0 + (\hat{\boldsymbol{g}}_{\boldsymbol{k}}\cdot\hat{\boldsymbol{\sigma}})G_-(\boldsymbol{k}, i\omega_n) \\ G_\pm(i\omega_n) &= -\frac{1}{2}\left[\frac{i\omega_n + \xi_1}{(\omega_n^2 + |\Delta|^2 + \xi_1^2)} \pm \frac{i\omega_n + \xi_2}{(\omega_n^2 + |\Delta|^2 + \xi_2^2)}\right], \end{aligned} \quad (2.39)$$

and

$$\begin{aligned} \hat{F}(\boldsymbol{k}, i\omega_n) &= [F_\mathrm{I}(\boldsymbol{k}, i\omega_n)\hat{\sigma}_0 + (\hat{\boldsymbol{g}}_{\boldsymbol{k}}\cdot\hat{\boldsymbol{\sigma}})F_-(\boldsymbol{k}, i\omega_n)]\hat{\Delta}(\boldsymbol{k}), \\ \hat{F}^\dagger(\boldsymbol{k}, i\omega_n) &= \hat{\Delta}^\dagger(\boldsymbol{k})[F_+(\boldsymbol{k}, i\omega_n)\hat{\sigma}_0 + (\hat{\boldsymbol{g}}_{\boldsymbol{k}}\cdot\hat{\boldsymbol{\sigma}})F_-(\boldsymbol{k}, i\omega_n)] \\ F_\pm(\boldsymbol{k}, i\omega_n) &= \frac{1}{2}\left[\frac{1}{(\omega_n^2 + |\Delta|^2 + \xi_1^2)} \pm \frac{1}{(\omega_n^2 + |\Delta|^2 + \xi_2^2)}\right]. \end{aligned} \quad (2.40)$$

Note that the anomalous Green's function has less symmetry than the gap function. In particular, $\Delta(\boldsymbol{k})$ is either symmetric (singlet) or antisymmetric (triplet) with respect to $\boldsymbol{k} \to -\boldsymbol{k}$, while the resulting anomalous Green's function has both a symmetric and an antisymmetric component. This leads to the mixing of the spin-singlet and spin-triplet Cooper pairs and has been discussed by Gor'kov and Rashba in the case of 2D metals [19]. However, F_- is an odd function in ξ and doesn't contribute to the gap equation in its weak coupling formulation. In this way, the magnitude of the gap $\psi = \psi(\boldsymbol{k})$ for the singlet s-wave order parameter can be approximated by the standard and universal BCS gap equation,

$$\ln(\psi) = -\int_{-\infty}^{\infty} dx \frac{1}{\sqrt{\psi^2 + x^2}} \frac{1}{\exp\left(\frac{\pi}{\gamma}\frac{\sqrt{\psi^2+x^2}}{k_B T}\right) + 1}, \quad (2.41)$$

where T is expressed in units of T_c, ψ in units of $\psi(T=0)$, where $\psi(T = 0)/k_B T_c = \pi/\gamma$ and $C = \ln(\gamma) = 0.577$ correspond to the Euler constant. The deviation will be on the order $(\alpha/\epsilon_c)^2$, with ϵ_c the cutoff energy of the attractive interaction, which is small in our case. For the protected spin-triplet state $\boldsymbol{d}(\boldsymbol{k}) = \sqrt{2/3}\Delta_0\boldsymbol{g}(\boldsymbol{k})$, we have

$$\Delta_0 = \frac{3vN_0}{4}\pi k_B T \sum_n \frac{\Delta_0}{|\Delta_0|}\left[\left(1 - \frac{\omega_n^2}{\Delta_0^2}\right)\mathrm{atan}\left(\frac{|\Delta_0|}{|\omega_n|}\right) + \frac{|\omega_n|}{|\Delta_0|}\right] \quad (2.42)$$

corresponding to the gap equation obtained for the ABM state [4].

In materials with a spatial inversion center, the measurement of the Knight shift in the resonance frequency ($\delta\omega$) by nuclear magnetic resonance (NMR) is an important experimental tool in determining the nature of the superconducting state. In particular, it allows the determination of the spin structure of the Cooper pairs. The measurement of the temperature dependence of the ratio $\delta\omega_s/\delta\omega_n = \chi_s/\chi_n$ is a direct measurement of the behavior of the spin susceptibility of the superconducting state (χ_s) (χ_n is the spin-susceptibility of the normal state). For spin-singlet superconductors, it is known that the paramagnetic susceptibility depends on the density of normal electrons, which vanishes at zero temperature. In the spin-triplet case, the spin of the Cooper pairs can contribute to the susceptibility. In particular, if the external field ($\boldsymbol{H}$) is parallel to the spin of the Cooper pair ($\boldsymbol{H} \perp \boldsymbol{d}$), then the susceptibility coincides with that of the Fermi-liquid normal state. This property was used to confirm spin-triplet superconductivity experimentally, for example, in Sr_2RuO_4 [36].

In principle, for materials with strong spin-orbit coupling, the total magnetic susceptibility cannot be split into separate orbital and spin parts. However, if $\alpha << \epsilon_F$, it is possible to isolate the two components [37]. As shown in Ref. [38], the spin susceptibility tensor χ_{ij} in the superconducting state can be expressed as

$$\chi_{ij} = -\mu_B^2 k_B T \sum_{\boldsymbol{k}} \sum_{\omega_n} \mathrm{Tr}\{\hat{\sigma}_i \hat{G}(\boldsymbol{k},\omega_n)\hat{\sigma}_j \hat{G}(\boldsymbol{k},\omega_n) - \hat{\sigma}_i \hat{F}(\boldsymbol{k},\omega_n)\hat{\sigma}_j^{\top} \hat{F}^{\dagger}(\boldsymbol{k},\omega_n)\}. \tag{2.43}$$

We first evaluate the trace over the spin

$$\mathrm{Tr}\{\hat{\sigma}_i \hat{G}(i\omega_n)\hat{\sigma}_j \hat{G}(i\omega_n)\} = 2\delta_{i,j}[G_+^2(i\omega_n) - G_-^2(i\omega_n)] + 4\delta_{i,j}\hat{g}_i^2 G_-^2(i\omega_n)$$

and

$$\mathrm{Tr}\{\hat{\sigma}_i \hat{F}(i\omega_n)\hat{\sigma}_j^{\top} \hat{F}^{\dagger}(i\omega_n)\} = \begin{cases} -|\psi|^2\delta_{i,j}\{2[F_+^2(i\omega_n) - F_-^2(i\omega_n)] \\ +4\hat{g}_i^2 F_-^2(i\omega_n)\} \quad \text{for the singlet.} \\ \\ |\boldsymbol{d}|^2\delta_{i,j}\{2[F_+^2(i\omega_n) - F_-^2(i\omega_n)] \\ -4\hat{g}_i^2 F_+^2(i\omega_n)\} \quad \text{for the triplet.} \end{cases}$$

If we assume a constant density of states $N(\xi)$ close to the Fermi surface, then we can also replace here the sum over $\boldsymbol{k}$ by $\sum_{\boldsymbol{k}} \to N_0 \int \frac{d\Omega}{4\pi} \int d\xi$. In the normal state, the integral over $d\xi$ cannot be carried out before the sum over ω_n, because the regular Green's function will be formally divergent [28]. Doing the sum first, we find that the normal state spin susceptibility

$$\begin{aligned}\chi_n &= -\mu_B^2 k_B T \sum_{\boldsymbol{k}} \sum_{\omega_n} 2\delta_{i,j}[G_{0,+}^2(i\omega_n) - G_{0,-}^2(i\omega_n)] + 4\delta_{i,j}\hat{g}_i^2 G_{0,-}^2(i\omega_n) \\ &= \mu_B^2 \delta_{i,j} \sum_{\boldsymbol{k}} \left\{ \frac{n_F(\xi_1) - n_F(\xi_2)}{\alpha|\boldsymbol{g}_{\boldsymbol{k}}|}(1-\hat{g}_i^2) + \left(\frac{\partial n_F(\xi_1)}{\partial \xi_1} + \frac{\partial n_F(\xi_2)}{\partial \xi_2} \right) \hat{g}_i^2 \right\}\end{aligned}$$

corresponds to the Pauli susceptibility $\chi_n = 2\mu_B^2 N_0$. Here we introduced the Fermi distribution $n_F(\xi) = (e^{\xi/k_B T} + 1)^{-1}$ and $\xi_{1,2} = \xi \pm \alpha|\boldsymbol{g}|$. We have to note that, without the assumption of constant density of state $N(\xi) = N_0$, the normal state susceptibility is anisotropic, see Section 4.4.

To avoid carrying out analytically the summation over ω_n in the superconducting state, we follow Abrikosov *et al.* and sum and subtract the expression corresponding to the normal state [28]. The integral of the difference between the integrands rapidly converges in this case. Consequently, the order of summation of ω_n and $\boldsymbol{k}$ can be interchanged.

Carrying out the summation over $\boldsymbol{k}$ first, we found that the contribution of the regular Green's function in Eq. (4.50) is the same for spin-singlet and protected spin-triplet states

$$\begin{aligned}- \mu_B^2 k_B T \sum_{\omega_n} \sum_{\boldsymbol{k}} \mathrm{Tr}\{\hat{\sigma}_i \hat{G}(\boldsymbol{k},\omega_n) \hat{\sigma}_i \hat{G}(\boldsymbol{k},\omega_n)\} = \\ \chi_n \Bigg\{ 1 - \frac{k_B T \pi}{2} \sum_{\omega_n} \Bigg\langle \frac{1 - \hat{g}_{\boldsymbol{k},i}^2}{(\omega_n^2 + |\Delta(\boldsymbol{k})|^2 + \alpha^2 |\boldsymbol{g}_{\boldsymbol{k}}|^2)} \frac{|\Delta(\boldsymbol{k})|^2}{\sqrt{\omega_n^2 + |\Delta(\boldsymbol{k})|^2}} \\ + \hat{g}_{\boldsymbol{k},i}^2 \frac{|\Delta(\boldsymbol{k})|^2}{(\omega_n^2 + |\Delta(\boldsymbol{k})|^2)^{3/2}} \Bigg\rangle_{\boldsymbol{k}} \Bigg\}.\end{aligned}$$

On the contrary, the contribution of the anomalous Green's function depends

on the parity of the order parameter

$$\mu_B^2 k_B T \sum_{\omega_n} \sum_{\boldsymbol{k}} tr\{\hat{\sigma}_i \hat{\Gamma}(\boldsymbol{k},\omega_n)\hat{\sigma}_i^{\top}\hat{F}^{\dagger}(\boldsymbol{k},\omega_n)\}_{s,t} =$$
$$\chi_n \frac{k_B T \pi}{2} \sum_{\omega_n} \left\{ \left\langle \frac{\mp(1-\hat{g}_{\boldsymbol{k},i}^2)}{(\omega_n^2 + |\psi(\boldsymbol{k})|^2 + \alpha^2|\boldsymbol{g}_{\boldsymbol{k}}|^2)} \frac{|\psi(\boldsymbol{k})|^2}{\sqrt{\omega_n^2 + |\psi(\boldsymbol{k})|^2}} \right.\right.$$
$$\left.\left. -\hat{g}_{\boldsymbol{k},i}^2 \frac{|\psi(\boldsymbol{k})|^2}{(\omega_n^2 + |\psi(\boldsymbol{k})|^2)^{3/2}} \right\rangle_{\boldsymbol{k}} \right\}.$$

For a singlet gap function, we find a generalization of the result obtained by Gork'ov and Rashba [19] and Bulaevskii *et al.* [13]

$$\chi_{ii} = \chi_n \left\{ 1 - k_B T \pi \sum_{\omega_n} \left\langle \frac{1-\hat{g}_{\boldsymbol{k},i}^2}{(\omega_n^2 + |\psi(\boldsymbol{k})|^2 + \alpha^2|\boldsymbol{g}_{\boldsymbol{k}}|^2)} \cdot \frac{|\psi(\boldsymbol{k})|^2}{\sqrt{\omega_n^2 + |\psi(\boldsymbol{k})|^2}} \right.\right.$$
$$\left.\left. +\hat{g}_{\boldsymbol{k},i}^2 \frac{|\psi(\boldsymbol{k})|^2}{(\omega_n^2 + |\psi(\boldsymbol{k})|^2)^{3/2}} \right\rangle_{\boldsymbol{k}} \right\}. \tag{2.44}$$

For the triplet gap function (with $\boldsymbol{d}(\boldsymbol{k})||\boldsymbol{g}_{\boldsymbol{k}}$), the susceptibility is independent of α

$$\chi_{ii} = \chi_n \left\{ 1 - k_B T \pi \sum_{\omega_n} \left\langle \hat{g}_{\boldsymbol{k},i}^2 \frac{|\boldsymbol{d}(\boldsymbol{k})|^2}{(\omega_n^2 + |\boldsymbol{d}(\boldsymbol{k})|^2)^{3/2}} \right\rangle_{\boldsymbol{k}} \right\}. \tag{2.45}$$

More precisely, the contribution due to α from the regular Green's function is cancelled out by the contribution of the anomalous Green's function.

We now apply the results to $CePt_3Si$; this means $\boldsymbol{g}_{\boldsymbol{k}} \propto (-k_y, k_x, 0)$. The spin-susceptibility for the singlet s-wave gap function is shown in Fig. 2.4. The top plot shows the corresponding behavior of the susceptibility for the field along the z-axis ($\chi_{\parallel} = \chi_{z,z}$). The bottom plot shows the spin susceptibility for the field in the xy-plane ($\chi_{\perp} = \chi_{x,x} = \chi_{y,y}$) as a function of the temperature for three different values of the spin-orbit coupling (α). For $\alpha \gg k_B T_c$ the $\chi_{\parallel}$ approaches χ_n and $\chi_{\perp} = \chi_n/2$. We remark that the susceptibility increases with the spin-orbit coupling strength. For very large α values the resulting susceptibility looks very similar to that obtained for the triplet p-wave gap function shown in Fig. 2.5. The similar properties of the spin susceptibilities make it difficult to distinguish between a spin-triplet

and a spin-singlet order parameter through NMR measurements in the strong SOC limit. Due to the complicated band structure of $CePt_3Si$ [31] and the coexistence of superconductivity with antiferromagnetism [39], our theory does not provide a quantitative description for the spin susceptibility for $CePt_3Si$.

However, our approach illustrates the behavior expected at a qualitative level. More precisely, the susceptibility, independent of the kind of pairing and of the strength of the SOC, is more strongly suppressed in the xy-plane than along the z-axis. This angle dependence of the static uniform susceptibility should be confirmed by NMR-Knight-shift measurements. Moreover, our discussion supports the result obtained for the paramagnetic limiting field h_p, that the spin-singlet pairing state acquires a certain robustness against pair breaking due to spin polarization [12]. A rough estimate of the zero-temperature limiting field is obtained by comparison of superconducting condensation and spin polarization energy, leading to

$$H_p \approx \frac{k_B T_c}{\mu_B \sqrt{1 - \chi^s(T=0)/\chi_n}} \,. \tag{2.46}$$

In principle, this can become very large for fields along the z-axis and roughly 1- 2 Tesla for fields in the basal plane.

2.6 Discussion and conclusion

We start the discussion focusing on $CePt_3Si$. We may adopt two different points of view. First, there is a protected p-wave spin-triplet pairing state ($\boldsymbol{d}(\boldsymbol{k}) = \hat{\boldsymbol{x}} k_y - \hat{\boldsymbol{y}} k_x$). This may indeed explain the apparent absence of paramagnetic limiting observed in polycrystaline samples [6]. On the other hand, it is important to notice that superconductivity appears here in the background of antiferromagnetic order ($T_N \approx 2K$), and it seems more natural to assume a spin-singlet type of pairing. In this case, we could argue that paramagnetic limiting for a singlet state is rendered less effective by the presence of spin-orbit coupling. This conclusion is also supported by the results concerning the static uniform spin-susceptibility, which increase with the strength of the spin-orbit coupling constant.

However, the limiting case of large spin-orbit coupling relative to T_c shows what could happen in materials like $CePt_3Si$. For this limit, the paramagnetic limiting field and the spin susceptibility have similar behavior for both spin-singlet or protected spin-triplet states. In fact, the paramagnetic limiting field of the uniform superconducting state has the same expression in the limit of $\alpha \to \infty$

$$\ln\left(\frac{T_c}{T_{cst}}\right) = \left\langle 2|\Delta(\boldsymbol{k})|^2 f\left(\frac{\hat{\boldsymbol{g}}_{\boldsymbol{k}} \cdot \boldsymbol{h}}{\pi k_B T_c}\right)\right\rangle_{\boldsymbol{k}}$$

independent of the parity of the order parameter $\Delta(\boldsymbol{k})$. This last can be either spin-singlet $\Delta(\boldsymbol{k}) = \psi(\boldsymbol{k})$ or $\Delta(\boldsymbol{k}) = \boldsymbol{d}(\boldsymbol{k})$ spin-triplet, respectively, with the restriction to belong to the protected class of states, i.e $\boldsymbol{d}(\boldsymbol{k}) \parallel \boldsymbol{g}_{\boldsymbol{k}}$. For the uniform spin susceptibility, we also obtain in this limit also a unified expression

$$\chi_{ii} = \chi_n \left\{ 1 - k_B T \pi \sum_{\omega_n} \left\langle \hat{g}^2_{\boldsymbol{k},i} \frac{|\Delta(\boldsymbol{k})|^2}{(\omega_n^2 + |\Delta(\boldsymbol{k})|^2)^{3/2}} \right\rangle_{\boldsymbol{k}} \right\}.$$

As we will see in the next chapter the similarity between spin-singlet and protected spin-triplet states lies in the fundamental relationship between these states. In particular, we will see that the spin singlet-state described by $\Delta(\boldsymbol{k}) = \psi(\boldsymbol{k})$ belongs to the same irreducible representation as the protected spin-triplet state characterized by $\Delta(\boldsymbol{k}) = \psi(\boldsymbol{k})\boldsymbol{g}_{\boldsymbol{k}}$.

Now we address the selection of the superconducting state on MnSi, which does not show superconductivity in the vicinity of the quantum critical point of a ferromagnetic state. Given our result that spin-triplet pairing is not suppressed completely by broken inversion symmetry, it is useful to reexamine the reason for why spin-triplet superconductivity is not observed. As one would expect, the lack of inversion symmetry in this compound with (cubic) B20-structure is perhaps crucial. For MnSi, we found

$$\boldsymbol{g}_{\boldsymbol{k}} = \alpha_1[k_x, k_y, k_z] + \alpha_2[k_x(k_y^2 - k_z^2), k_y(k_z^2 - k_x^2), k_z(k_x^2 - k_y^2)]$$

According to our analysis, if $\alpha_2 > \alpha_1$, the pairing should occur in the f-wave channel in order to survive the spin-orbit coupling effect. The fact that the strongly anisotropic f-wave state is more difficult to obtain by spin fluctuation than the p-wave pairing state might explain the absence of superconductivity in MnSi.

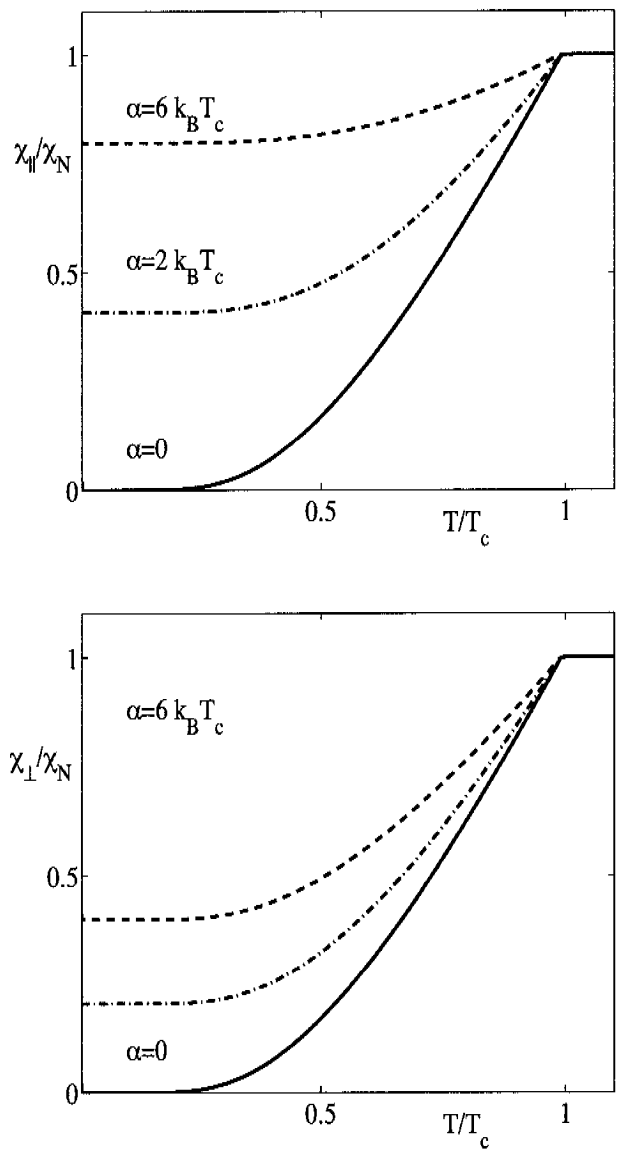

Figure 2.4: The static uniform spin susceptibility for the case of the singlet s-wave gap function for $\boldsymbol{g_k} \propto (-k_y, k_x, 0)$ ($CePt_3Si$). The spin susceptibility in the xy-plane $\chi_\perp$ and along the z-axis $\chi_\parallel$ as a function of T for three different values of the spin orbit coupling α. The susceptibility in the superconducting state ($T/T_c < 1$) increases with the spin-orbit coupling strength. The susceptibility is more strongly suppressed in the xy-plane than along the z-axis. At $T = 0$, we have $\chi_\perp = \chi_\parallel/2$.

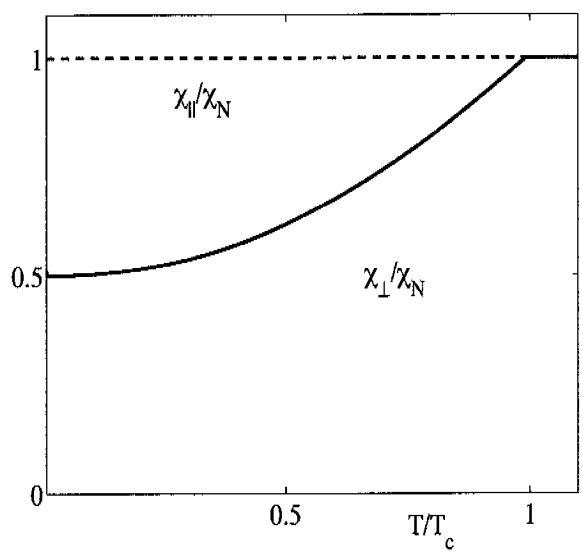

Figure 2.5: The static uniform spin susceptibility for a spin-triplet p-wave gap function $\boldsymbol{d}(\boldsymbol{k}) \parallel \boldsymbol{g}_{\boldsymbol{k}} \propto (-k_y, k_x, 0)$ ($CePt_3Si$). The spin susceptibility in the xy-plane $\chi_\perp$ and along the z-axis $\chi_\parallel$ as function of T. The susceptibility is, in this case, independent of the spin orbit coupling α. In the superconducting state, the susceptibility in the xy-plane coincides with that of the normal state.

Chapter 3

Characterization of the problem by symmetry arguments

3.1 Symmetry classification of the g_k-vector

In the previous chapter, we briefly discussed the microscopic origin of the ASOC term. Here, we want to deduce the structure of the $\boldsymbol{g_k}$-vector characterizing the ASOC using only symmetry arguments. Group theory gives us this opportunity.

Let us consider a crystal with a space group generating by one of the twenty one point groups with no inversion transformation. We call this point group G'. In the absence of SOC, the electrons moving in this material can be described by a single-particle Hamiltonian $\mathcal{H}_0 = \sum_{\boldsymbol{k},s} \xi_{\boldsymbol{k}}\ c^\dagger_{\boldsymbol{k}s} c_{\boldsymbol{k}s}$, Eq. (2.17). Since $\mathcal{H}_0$ is supposed to be invariant under time reversal $\mathcal{K}$,

$$\xi_{\boldsymbol{k}} \xrightarrow{\mathcal{K}} \xi_{-\boldsymbol{k}} \qquad \text{so that} \qquad \xi_{\boldsymbol{k}} = \xi_{-\boldsymbol{k}},$$

then $\mathcal{H}_0$ is also invariant under the inversion operation $\mathcal{I}$ in $\boldsymbol{k}$-space, because both operations take $\xi_{\boldsymbol{k}}$ to $\xi_{-\boldsymbol{k}}$. This means that, at the level of point symmetry, $\mathcal{H}_0$ is more symmetric than the crystal. $\mathcal{H}_0$ is invariant under the operations of the symmetry group $\mathcal{G} = G \times \mathcal{K} \times U(1)$, with $G = G' \times C_i$,

where the group C_i consists of the identity and the inversion $\mathcal{I}$. Then G and G' belong to the same Laue class [1].

We now include the SOC: Its effect already appears at the level of the single band model through the ASOC term $\mathcal{H}' = \alpha \sum_{\boldsymbol{k},s,s'} \left(\boldsymbol{g}_{\boldsymbol{k}} \cdot \boldsymbol{\sigma}_{ss'}\right) c^{\dagger}_{\boldsymbol{k}s} c_{\boldsymbol{k}s'}$, Eq. (2.18). The presence of this term, as already shown in the previous chapter, breaks the inversion symmetry, but not the time reversal symmetry. The symmetry group of the ASOC term is $\mathcal{G}' = G' \times \mathcal{K} \times U(1)$. The ASOC acts as an inversion symmetry breaking term. The point symmetry of the Hamiltonian $\mathcal{H}_T = \mathcal{H}_0 + \mathcal{H}'$ is reduced to that of the crystal, with point-group G'. To find a basis function for the ASOC, we use the fact that G' is an invariant subgroup of G. This means that there are non-trivial irreducible representations $\Gamma(G)$ of the basic point-group G which map to the trivial representation A_1 of G'. The ASOC term belongs to this non-trivial representation of G. To simplify the presentation of the results, we use the same basic group G inside the same crystal system in order to classify the different symmetry breaking terms. Consequently, for some point groups G', G does not belong to the same Laue class of G', contrary to what we stated above. However, the results concerning $\boldsymbol{g}_{\boldsymbol{k}}$ are not affected by this choice, because G is chosen such that all point groups G' of the same crystal system are invariant subgroups of G.

The results for the seven different crystal systems are presented in Appendix A. For each crystal system, we first show the three-dimensional representation of the different point groups without inversion symmetry. Then we show the corresponding basis function for the $\boldsymbol{g}_{\boldsymbol{k}}$-vector obtained by the symmetry analysis. We express this function using the different components of $\boldsymbol{k}$. However, in case we have to deal with realistic bands, it is convenient to replace $\boldsymbol{k}$ by $\boldsymbol{v}_F(\boldsymbol{k})$, which is the Fermi velocity of the unperturbed system $\hbar \boldsymbol{v}_F(\boldsymbol{k}) = \boldsymbol{\nabla}_{\boldsymbol{k}} \xi_{\boldsymbol{k}}$. In addition, we give a list of superconductors without inversion symmetry which we took from Ref. [40]. We found more than thirty different superconducting compounds with a crystal structure without an

[1] the Laue class includes all point groups which cannot be distinguished by methods which are not sensitive to the presence of a center of symmetry. Example: The five trigonal point groups $(C_3, C_{3i}, D_3, C_{3v}, D_{3d})$ can be separated into two Laue classes because $C_3 \times C_i = C_{3i}$ and $D_3 \times C_i = C_{3v} \times C_i = D_{3d}$

inversion center.

3.2 Structure of the superconducting state

The classification of the superconducting state in accordance with the irreducible representations of the symmetry group in the normal state is well known for crystals with inversion symmetry. The superconducting state with the highest critical temperature is described by the basis function of an irreducible representation Γ of dimensionality d_Γ of the crystallographic point group G. The superconducting order parameter is frequently expessed by the 2 x 2 matrix $\hat{\Delta}(\boldsymbol{k})$, which takes the form of $\hat{\Delta}(\boldsymbol{k}) = \sum_{i=1}^{d_\Gamma} \psi_i^{\Gamma_g}(\boldsymbol{k}) i\sigma_y$ for spin-singlet pairing (g $\equiv$ even representation) or $\hat{\Delta}(\boldsymbol{k}) = \sum_{i=1}^{d_\Gamma} (\boldsymbol{d}_i^{\Gamma_u}(\boldsymbol{k}) \cdot \hat{\boldsymbol{\sigma}}) i\sigma_y$ for spin-triplet pairing (u $\equiv$ odd representation) with strong-spin orbit coupling.

In crystals without inversion symmetry, the presence of the ASOC is indeed detrimental for most spin-triplet pairing, as noted by Anderson [27]. As shown above all, except one family of spin-triplet states are suppressed by sufficiently strong ASOC, i.e $\alpha >> k_B T_c$ (we will always suppose in our study that this is the case). It was found that triplet states whose $\boldsymbol{d}$-vector lies parallel to $\boldsymbol{g_k}$ would be stable [12]. For that reason, this class of spin-triplet states have been called protected. It contains all triplet states characterized by $\boldsymbol{d}$-vectors with $\boldsymbol{d}(\boldsymbol{k}) = \chi(\boldsymbol{k})\boldsymbol{g_k}$ where $\chi(\boldsymbol{k})$ is an even function. The simplest protected spin-triplet state is given by $\chi(\boldsymbol{k}) = d$, where d is a constant, and belongs to the trivial representation A_1 of the point group G' of the solid. Such a spin-triplet state has the full symmetry of the crystal point group; we will therefore call it the S-triplet state from now on. For this reason, this "high-symmetry" state mixes with the s-wave spin-singlet state characterized by $\psi(\boldsymbol{k}) = \psi$. We will call this combined phase, characterized by

$$\hat{\Delta}_s(\boldsymbol{k}) = \left[\psi + d(\boldsymbol{g_k} \cdot \hat{\boldsymbol{\sigma}})\right] i\sigma_y, \tag{3.1}$$

the "s-wave" state, where the ratio between the spin-triplet and the spin-singlet components is given by d/ψ. The generalized expression for the order-parameter follows straightforwardly

$$\hat{\Delta}_\Gamma(\boldsymbol{k}) = \sum_{i=1}^{d_\Gamma} \chi_i^\Gamma(\boldsymbol{k}) \hat{\Delta}_s(\boldsymbol{k}). \tag{3.2}$$

The function $\chi_i^\Gamma(\boldsymbol{k})$ is an even function which transforms according to the irreducible representations of the point group G' without inversion symmetry. Examples of even basis functions $\chi_i^\Gamma(\boldsymbol{k})$ for the irreducible representations of the twenty one point groups without inversion operations are given in Tables A.3-A.20 in Appendix A. From these tables, we see that the basis functions for $\chi_i^\Gamma(\boldsymbol{k})$ are identical inside the same Laue class. However, the form of the order parameter $\hat{\Delta}_\Gamma(\boldsymbol{k})$ is different for every point group.

The presence of ASOC leads to a splitting of the electron bands by lifting the spin degeneracy. Thus, the discussion of the superconductivity is in some sense a two-band problem in this case. However, as we will see in the next chapter, the order parameter $\hat{\Delta}_\Gamma(\boldsymbol{k})$ defined by Eq. (3.2) is sufficient to define the gaps

$$\hat{\Delta}_\gamma^\Gamma(\boldsymbol{k}) = \Delta_\gamma^\Gamma(\boldsymbol{k})\{\hat{\sigma}_\gamma(\boldsymbol{k})i\hat{\sigma}_y\} \tag{3.3}$$

on the two non-degenerate bands, which are labeled here by $\gamma = \{1, 2\}$. The amplitude of the gaps

$$\Delta_{1,2}^\Gamma(\boldsymbol{k}) = \sum_{i=1}^{d_\Gamma} \chi_i^\Gamma(\boldsymbol{k})(\psi \pm d|\boldsymbol{g_k}|) \tag{3.4}$$

depends on the ratio between the spin-singlet ψ and the spin-triplet d component of the order paramenter. This is in contrast to the spin mixing of the pairs which is only related to the form of the ASOC

$$\hat{\sigma}_{1,2}(\boldsymbol{k})i\hat{\sigma}_y = 1/2(\hat{\sigma}_0 \pm (\hat{\boldsymbol{g}}_{\boldsymbol{k}} \cdot \hat{\boldsymbol{\sigma}}))i\hat{\sigma}_y. \tag{3.5}$$

Various groups [31, 41, 42] have already determined the basis function $\chi_i^\Gamma(\boldsymbol{k})$ for irreducible representations of point groups C_{4v} and C_2 assuming that superconductivity is restricted to a single non-degenerate band. Unfortunately those studies did not include the spin structure of the gap function. In that case, one finds that the gap function is given by $\Delta^\Gamma(\boldsymbol{k}) = \sum_{i=1}^{d_\Gamma} \chi_i^\Gamma(\boldsymbol{k})t(\boldsymbol{k})$, where the odd function $t(\boldsymbol{k}) = -t(-\boldsymbol{k})$ can be defined as a phase shift $t(\boldsymbol{k}) = i\exp(-i\phi_{\boldsymbol{k}})$ which involves the function $\phi_{\boldsymbol{k}}$ defined through $\boldsymbol{g_k} = |\boldsymbol{g_k}|(\sin\theta_{\boldsymbol{k}}\cos\phi_{\boldsymbol{k}}, \sin\theta_{\boldsymbol{k}}\sin\phi_{\boldsymbol{k}}, \cos\theta_{\boldsymbol{k}})$. This phase shift is absorbed here by the spin structure.

In addition to the symmetry dictated nodes which are determined by the zeros of the function $\sum_{i-1}^{d_\Gamma} \chi_i^\Gamma(\boldsymbol{k})$, Eq. (3.4) shows the possibility, for

particular symmetry, of having additional accidental nodes induced by the mixing of the spin-singlet and spin-triplet component of the order parameter, i.e. in correspondence to the zeros of $(\psi \pm d|\boldsymbol{g}_{\boldsymbol{k}}|)$. It is clear that this mixing depends mainly on the form of the pairing potential, which is the subject of the next section. However, as we will see in the next chapter, the distribution on the density of state in the two bands also plays a role.

3.3 Structure of the pairing-potential

In unconventional superconductors, the state of knowledge on the nature of the pairing potential is rather limited. However, in the context of the BCS theory, we can deduce the form of the attractive interaction using symmetry arguments. More precisely, it is possible to build up the effective pairing potential starting from the form of the order parameter under investigation.

This approach has already been used with success for crystals with inversion symmetry. In this case, parity is a good quantum number. Thus, the Cooper pairing states can be classified by their total spin. The effective interaction can always be decomposed in spin-singlet and spin-triplet channels. The phenomenological interaction proposed in Chapter 2 is of that kind. The pairing potential with the symmetry properties given by Eq. (2.2) can be factorized in two identical parts which have exactly the same structure as the order parameter. We have $V_{s_1s_2,s_2's_1'}(\boldsymbol{k},\boldsymbol{k}') = v_a \sum_{i=1}^{d_\Gamma} \psi_i^{\Gamma_g}(\boldsymbol{k})\psi_i^{\Gamma_g}(\boldsymbol{k}')\hat{\tau}_{s_1s_2}\hat{\tau}^\dagger_{s_2's_1'}$ for spin-singlet channels and $V_{s_1s_2,s_2's_1'}(\boldsymbol{k},\boldsymbol{k}') = v_b \sum_{i=1}^{d_\Gamma} (\boldsymbol{d}_i^{\Gamma_u}(\boldsymbol{k})\cdot\hat{\boldsymbol{\tau}})_{s_1s_2}(\boldsymbol{d}_i^{\Gamma_u}(\boldsymbol{k}')\cdot\hat{\boldsymbol{\tau}})^\dagger_{s_2's_1'}$ for spin-triplet pairing with strong SOC. The pseudo-spin dependence of the interaction potential is expressed through the matrices $\hat{\tau}_{s_1s_2} = (i\hat{\sigma}_y)_{s_1s_2}$, and, $\hat{\boldsymbol{\tau}}_{s_1s_2} = (i\boldsymbol{\sigma}\hat{\sigma}_y)_{s_1s_2}$ which are antisymmetric and symmetric under permutation of indices s_1s_2, respectively, since the $\boldsymbol{k}$ dependent part $\psi_i^{\Gamma_g}(\boldsymbol{k})$ and $\boldsymbol{d}_i^{\Gamma_u}(\boldsymbol{k})$ are even and odd functions, respectively.

The same approach can be extended to systems with large ASOC. In this case, parity can no longer be used to classify the order parameter. The even basis function $\chi_i^\Gamma(\boldsymbol{k})$ mixes with the odd one described by $\chi_i^\Gamma(\boldsymbol{k})\boldsymbol{g}(\boldsymbol{k})$. Hence, the general form of the pairing potential relevant for the realization of the superconducting state belonging to the Γ representation involves both basis

functions. Explicitly written, this leads to the form

$$\begin{aligned} V_{s_1 s_2, s_2' s_1'}(\boldsymbol{k}, \boldsymbol{k}') &= V \sum_{i=1}^{d_\Gamma} \chi_i^\Gamma(\boldsymbol{k}) \chi_i^\Gamma(\boldsymbol{k}') \Big\{ e_s \, \hat{\tau}_{s_1 s_2} \hat{\tau}^\dagger_{s_2' s_1'} \\ &\quad + e_t \left[(\boldsymbol{g}_{\boldsymbol{k}} \cdot \hat{\boldsymbol{\tau}})_{s_1 s_2} (\boldsymbol{g}_{\boldsymbol{k}'} \cdot \hat{\boldsymbol{\tau}})^\dagger_{s_2' s_1'} \right] \\ &\quad + e_m \left[(\boldsymbol{g}_{\boldsymbol{k}} \cdot \hat{\boldsymbol{\tau}})_{s_1 s_2} \hat{\tau}^\dagger_{s_2' s_1'} + \hat{\tau}_{s_1 s_2} (\boldsymbol{g}_{\boldsymbol{k}'} \cdot \hat{\boldsymbol{\tau}})^\dagger_{s_2' s_1'} \right] \Big\} . \end{aligned} \tag{3.6}$$

The first term of Eq. (3.6) is diagonal in the spin-singlet pairing channel, the second one in the protected triplet pairing channel [12]. The last term describes the scattering of Cooper pairs between the two channels, which is allowed in absence of inversion symmetry. It should be noted that this possibility has been deduced here using only symmetry arguments. In Appendix B, we provide some explanations about the microscopic origin of this last term.

3.4 Discussion and comments

The tables of Appendix A show that there are many superconducting compounds without an inversion center. However, not all of these materials are interesting. Most likely, the superconductivity in these materials is due to the electron-phonon interaction, and then it is conventional. The effect on the static uniform spin susceptibility [14] should be observed by Knight shift measurement independently of the pairing, then also for some of these superconductors. But if, in addition, the splitting of the bands $\alpha/k_B T_c$ is small, then the superconductivity does not show any anomaly. However, the literature on these compounds is rather limited. Most of these materials were discovered more than twenty years ago, when only the value of the critical temperature was investigated. In the light of new theoretical development and new experimental techniques, it is crucial to reconsider the study of these compounds. In this context, $CePt_3Si$ played an important role, because its rather short coherence length, roughly 100 Å, let Bauer *et al.* [6] observe, through the mesure of H_{c2}, the unexpected paramagnetic robustness which characterizes superconductors with large ASOC.

Another important remark abaut $CePt_3Si$ involves its $\boldsymbol{g_k}$-vector: In this case, the group analysis allowed the $\boldsymbol{g_k}$-vector to have different components, from Table A.4, $\boldsymbol{g_k} = \alpha_1(k_x\hat{y} - k_y\hat{x}) + \alpha_2(k_x^2 - k_y^2)(k_y\hat{x} + k_x\hat{y}) + \alpha_3\, k_x k_y k_z(k_x^2 - k_y^2)\hat{z}$. In our calculation in Chapter 2, we always considered $\alpha_1 >> \alpha_2, \alpha_3$, so that $\boldsymbol{g_k} \propto (k_y, -k_x, 0)$. This first component has the form of the well-known Rashba spin-orbit coupling term [30] with electric field along the z-axis. The fact that in $CePt_3Si$ the Si atom is shifted from the center of the unit cell along the z-axis [6] justifies this choice. This seems to be confirmed by band structure calculation [31].

Chapter 4

Results for large antisymmetric spin-orbit coupling

4.1 The two-band description

The ASOC term lifts the spin degeneracy by generating two bands with different spin structure. For large $\alpha >> k_B T_c$, it is convenient to diagonalize the normal state Green's function $\hat{G}_0(\boldsymbol{k}, i\omega_n)$, Eq. (2.22), into the components corresponding to the two bands, using the unitary transformation

$$\hat{U}(\boldsymbol{k}) = \cos(\theta_{\boldsymbol{k}}/2) - i\sin(\theta_{\boldsymbol{k}}/2)(\cos\phi_{\boldsymbol{k}}\hat{\sigma}_y - \sin\phi_{\boldsymbol{k}}\hat{\sigma}_x), \tag{4.1}$$

where $\boldsymbol{g}_{\boldsymbol{k}} = |\boldsymbol{g}_{\boldsymbol{k}}|(\sin\theta_{\boldsymbol{k}}\cos\phi_{\boldsymbol{k}}, \sin\theta_{\boldsymbol{k}}\sin\phi_{\boldsymbol{k}}, \cos\theta_{\boldsymbol{k}})$ defines the angles $\theta_{\boldsymbol{k}}$ and $\phi_{\boldsymbol{k}}$. This allows us to express,

$$\hat{G}_0(\boldsymbol{k}, i\omega_n) = G_1^0(\boldsymbol{k}, i\omega_n)\hat{\sigma}_1(\boldsymbol{k}) + G_2^0(\boldsymbol{k}, i\omega_n)\hat{\sigma}_2(\boldsymbol{k}) \tag{4.2}$$

through the two Green's functions,

$$G_{1,2}^0(\boldsymbol{k}, i\omega_n) = \frac{1}{i\omega_n - \xi_{1,2}(\boldsymbol{k})}, \tag{4.3}$$

where the quasi-particle bands $\xi_{1,2}(\boldsymbol{k}) \equiv \xi_{\boldsymbol{k}} \pm \alpha|\boldsymbol{g}_{\boldsymbol{k}}|$ are split by the presence of the ASOC. The spin structure in the bands is described by the 2 x 2 matrices

$$\begin{aligned} \sigma^1_{\lambda,\mu}(\boldsymbol{k}) &\equiv U_{\lambda,1}(\boldsymbol{k})U^\dagger_{1,\mu}(\boldsymbol{k}) = 1/2(\sigma_0 + (\hat{\boldsymbol{g}}_{\boldsymbol{k}} \cdot \boldsymbol{\sigma}))_{\lambda,\mu} \\ \sigma^2_{\lambda,\mu}(\boldsymbol{k}) &\equiv U_{\lambda,2}(\boldsymbol{k})U^\dagger_{2,\mu}(\boldsymbol{k}) = 1/2(\sigma_0 - (\hat{\boldsymbol{g}}_{\boldsymbol{k}} \cdot \boldsymbol{\sigma}))_{\lambda,\mu}. \end{aligned} \tag{4.4}$$

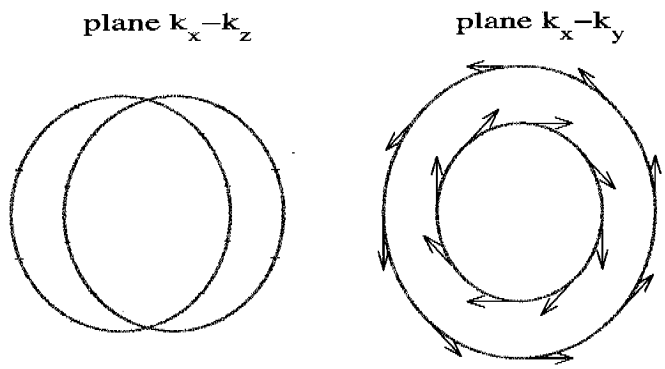

Figure 4.1: Fermi surface for $\boldsymbol{g_k} \propto (k_y, -k_x, 0)$ as in $CePt_3Si$. The arrows show the structure of the quasi-particle spin. Only along the z-axis is the spin degeneracy preserved.

which act as projection operators in spin space. Since the spins of quasiparticles in the two bands have opposite directions for a given momentum $\boldsymbol{k}$, the matrices satisfy the conditions,

$$\begin{aligned} \hat{\sigma}_1(\boldsymbol{k})\hat{\sigma}_2(\boldsymbol{k}) &= 0 \\ \hat{\sigma}^2_{1,2}(\boldsymbol{k}) &= \hat{\sigma}_{1,2}(\boldsymbol{k}) \end{aligned} \tag{4.5}$$

and are reciprocal under the inversion operation,

$$\hat{\sigma}_{1,2}(-\boldsymbol{k}) = \hat{\sigma}_{2,1}(\boldsymbol{k}). \tag{4.6}$$

Symmetry considerations of Section 3.1 lead to the following form for $\boldsymbol{g_k}$ in $CePt_3Si$ in lowest order expansion in the wave vector $\boldsymbol{k}$: $\boldsymbol{g_k} \propto (k_y, -k_x, 0)$. The resulting spin structure is visualized in Fig.4.1, where we assume, for simplicity, that the original Fermi surface is spherical. The pairing interaction is generally given by

$$\mathcal{H}_{pair} = \frac{1}{2} \sum_{\boldsymbol{k},\boldsymbol{k}'} \sum_{s,s'} V_{s_1 s_2, s'_2 s'_1}(\boldsymbol{k}, \boldsymbol{k}') c^\dagger_{\boldsymbol{k}s_1} c^\dagger_{-\boldsymbol{k}s_2} c_{-\boldsymbol{k}'s'_2} c_{\boldsymbol{k}'s'_1} , \tag{4.7}$$

where $V_{s_1 s_2, s'_2 s'_1}(\boldsymbol{k}, \boldsymbol{k}')$ is the pairing potential defined in Eq. (3.6). We should note here that in our formulation we neglect any ω-dependence of the pairing

interaction. Moreover, we assume that the superconducting state with the highest critical temperature is of the "s-wave" type. However, the generalization to other superconducting states is trivial. For the "s-wave" channel we have

$$\begin{aligned} V_{s_1 s_2, s_2' s_1'}(\boldsymbol{k}, \boldsymbol{k}') = V \Big\{ & e_s \, \hat{\tau}_{s_1 s_2} \hat{\tau}^{\dagger}_{s_2' s_1'} \\ + \; & e_t \left[(\boldsymbol{g}_{\boldsymbol{k}} \cdot \hat{\boldsymbol{\tau}})_{s_1 s_2} (\boldsymbol{g}_{\boldsymbol{k}'} \cdot \hat{\boldsymbol{\tau}})^{\dagger}_{s_2' s_1'} \right] \\ + \; & e_m \left[(\boldsymbol{g}_{\boldsymbol{k}} \cdot \hat{\boldsymbol{\tau}})_{s_1 s_2} \hat{\tau}^{\dagger}_{s_2' s_1'} + \hat{\tau}_{s_1 s_2} (\boldsymbol{g}_{\boldsymbol{k}'} \cdot \hat{\boldsymbol{\tau}})^{\dagger}_{s_2' s_1'} \right] \Big\}, \end{aligned} \tag{4.8}$$

where $\hat{\tau}_{s_1 s_2} = (i\hat{\sigma}^y)_{s_1 s_2}$, and $\hat{\boldsymbol{\tau}}_{s_1 s_2} = (i\boldsymbol{\sigma}\hat{\sigma}^y)_{s_1 s_2}$. To avoid ambiguity, we set $V > 0$, and $e_s^2 + e_t^2 + e_m^2 = 1$. The first term of Eq. (4.8) is diagonal in the conventional s-wave pairing channel, the second one for the S-triplet pairing channel [12]. The last term describes the scattering of Cooper pairs between the two channels, which is a result of the absence of inversion symmetry. The micriscopic origin of this last term is explained in Appendix B. In particular, we show the existence of a Dzyaloshinskii-Moriya [43, 44] type of interaction for both a weakly interacting Fermi liquid and for a Hubbard model near half filling. This kind of interaction gives a contribution to e_m. This can give rise to a large interaction when the derivative in the density of states is large, for example, close to a Van Hove singularity. But, a satisfying microscopical discussion of the origin of the superconductivity in $CePt_3Si$ can be done only by solving an equation of the Eliashberg type [45]. However, the potential we propose is sufficient to study, in the context of BCS theory, the different possibilities of pairing.

The Gor'kov equations are formally analogous to those obtained for systems with an inversion symmetry [28] and have already been introduced by Eqs. (2.12-2.14). The two-band structure of the normal state is more conveniently handled if we use the Green's functions $G_{1,2}$ and $F_{1,2}$, as is easily obtained by the unitary transformation (4.1),

$$\begin{aligned} \begin{pmatrix} G_1 & 0 \\ 0 & G_2 \end{pmatrix} &= \hat{U}^{\dagger}(\boldsymbol{k}) \, \hat{G} \, \hat{U}(\boldsymbol{k}) \\ - \begin{pmatrix} F_1 \, e^{-i\phi_{\boldsymbol{k}}} & 0 \\ 0 & F_2 \, e^{i\phi_{\boldsymbol{k}}} \end{pmatrix} &= \hat{U}^{\dagger}(\boldsymbol{k}) \, \hat{F} \, \hat{U}^{*}(-\boldsymbol{k}). \end{aligned} \tag{4.9}$$

The phase factor $-e^{\mp i\phi}\boldsymbol{k}$ is introduced to cancel the phase dependence of the anomalous Green's functions on the two bands [41].

The pairing interaction defined in (4.8) fixes the form of the order parameter to $\hat{\Delta}(\boldsymbol{k}) = i\{\psi + d\,(\boldsymbol{g_k}\cdot\hat{\boldsymbol{\sigma}})\}\hat{\sigma}_y$. ψ and d are complex order parameters which can be interpreted as the magnitude of the s-wave spin-singlet and S-triplet components, respectively. The particular form of $\hat{\Delta}(\boldsymbol{k})$ prevents the existence of inter-band terms in the Gorkov equations

$$\begin{aligned}\{G^0_{1,2}(\boldsymbol{k},i\omega_n)\}^{-1}G_{1,2}(\boldsymbol{k},i\omega_n) + \Delta_{1,2}(\boldsymbol{k})F^{\dagger}_{1,2}(\boldsymbol{k},i\omega_n) &= 1\\ \{G^0_{1,2}(-\boldsymbol{k},-i\omega_n)\}^{-1}F^{\dagger}_{1,2}(\boldsymbol{k},i\omega_n) - \Delta^*_{1,2}(\boldsymbol{k})G_{1,2}(\boldsymbol{k},i\omega_n) &= 0,\end{aligned} \tag{4.10}$$

where, in this case,

$$\Delta_{1,2}(\boldsymbol{k}) = (\psi \pm d|\boldsymbol{g_k}|). \tag{4.11}$$

Thus, the Gor'kov equations are diagonal in the band index. The solution of the two-band Gorkov equations is given by

$$G_{1,2}(\boldsymbol{k},i\omega_n) = -\frac{i\omega_n + \xi_{1,2}}{(\omega_n^2 + |\Delta_{1,2}|^2 + \xi^2_{1,2})}, \tag{4.12}$$

and

$$F_{1,2}(\boldsymbol{k},i\omega_n) = \frac{\Delta_{1,2}}{(\omega_n^2 + |\Delta_{1,2}|^2 + \xi^2_{1,2})}. \tag{4.13}$$

Going back to the spin basis, we find

$$\begin{aligned}\hat{G}(\boldsymbol{k},i\omega_n) &= G_1(\boldsymbol{k},i\omega_n)\hat{\sigma}_1(\boldsymbol{k}) + G_2(\boldsymbol{k},i\omega_n)\hat{\sigma}_2(\boldsymbol{k}),\\ \hat{F}(\boldsymbol{k},i\omega_n) &= \{F_1(\boldsymbol{k},i\omega_n)\hat{\sigma}_1(\boldsymbol{k}) + F_2(\boldsymbol{k},i\omega_n)\hat{\sigma}_2(\boldsymbol{k})\}i\hat{\sigma}_y.\end{aligned} \tag{4.14}$$

The gap functions of the two bands are obtained by solving the self-consistent equation

$$\Delta_\alpha(\boldsymbol{k}) = -k_B T \int \frac{d\boldsymbol{k}'}{(2\pi)^3}\sum_{n,\beta} V^{\alpha,\beta}_{\boldsymbol{k},\boldsymbol{k}'}F_\beta(\boldsymbol{k}',i\omega_n). \tag{4.15}$$

The corresponding pairing interaction is determined by

$$\begin{aligned}V^{\alpha,\beta}_{\boldsymbol{k},\boldsymbol{k}'} &= \sum_{\gamma,\delta}\sum_{s_i,s_i'} D^*_{\alpha,\gamma}(\boldsymbol{k})U^*_{s_1\gamma}(-\boldsymbol{k})\hat{U}^{\dagger}_{\gamma s_2}(\boldsymbol{k})V_{s_1s_2,s_2's_1'}(\boldsymbol{k},\boldsymbol{k}')\\ &\times\ \hat{U}_{s_2'\delta}(\boldsymbol{k}')\hat{U}^{\top}_{\delta s_1'}(-\boldsymbol{k}')D_{\delta,\beta}(\boldsymbol{k}')\end{aligned} \tag{4.16}$$

with $\hat{D}(\boldsymbol{k}')$ =diag$(-\exp(-i\phi_{\boldsymbol{k}'}), -\exp(i\phi_{\boldsymbol{k}'}))$. Using (4.8) it follows

$$\begin{aligned}\hat{V}_{\boldsymbol{k},\boldsymbol{k}'} &= \frac{V}{2}\left\{\left[e_s + e_t|\boldsymbol{g}_{\boldsymbol{k}}||\boldsymbol{g}_{\boldsymbol{k}'}|\right]\hat{\sigma}_0 + \left[e_s - e_t|\boldsymbol{g}_{\boldsymbol{k}}||\boldsymbol{g}_{\boldsymbol{k}'}|\right]\hat{\sigma}_x\right. \\ &- \left. e_m\left[|\boldsymbol{g}_{\boldsymbol{k}}| + |\boldsymbol{g}_{\boldsymbol{k}'}|\right]\hat{\sigma}_z - ie_m\left[|\boldsymbol{g}_{\boldsymbol{k}}| - |\boldsymbol{g}_{\boldsymbol{k}'}|\right]\hat{\sigma}_y\right\}.\end{aligned} \tag{4.17}$$

The evaluation of $\boldsymbol{\Delta} = (\psi, d)$ is done by solving Eq. (4.15). We approximate the sum over $\boldsymbol{k}$ by $\sum_{\boldsymbol{k}} \to N_0 \int \frac{d\Omega}{4\pi} \int d\xi$. After having performed the integral over ξ, the gap equation reads

$$\frac{1}{N_0 V}\boldsymbol{\Delta} = \pi k_B T \sum_{\omega_n > -\epsilon_c}^{\epsilon_c} \hat{Q}(i\omega_n)\boldsymbol{\Delta} \tag{4.18}$$

with

$$\begin{aligned}\hat{Q} &= \left[Q_1(i\omega_n)\begin{pmatrix} -e_s & 0 \\ e_m & 0 \end{pmatrix} + Q_2(i\omega_n)\begin{pmatrix} e_m & -e_s \\ -e_t & e_m \end{pmatrix}\right. \\ &\left. + Q_3(i\omega_n)\begin{pmatrix} 0 & e_m \\ 0 & -e_t \end{pmatrix}\right]\end{aligned} \tag{4.19}$$

where we introduced the functions

$$\begin{aligned}Q_1(i\omega_n) &\equiv \frac{1}{2}\left\langle \frac{(1+\delta_N)}{\sqrt{\omega_n^2 + |\psi + d|\boldsymbol{g}_{\boldsymbol{k}}||^2}} + \frac{(1-\delta_N)}{\sqrt{\omega_n^2 + |\psi - d|\boldsymbol{g}_{\boldsymbol{k}}||^2}}\right\rangle_{\boldsymbol{k}}, \\ Q_2(i\omega_n) &\equiv \frac{1}{2}\left\langle \frac{(1+\delta_N)|\boldsymbol{g}_{\boldsymbol{k}}|}{\sqrt{\omega_n^2 + |\psi + d|\boldsymbol{g}_{\boldsymbol{k}}||^2}} - \frac{(1-\delta_N)|\boldsymbol{g}_{\boldsymbol{k}}|}{\sqrt{\omega_n^2 + |\psi - d|\boldsymbol{g}_{\boldsymbol{k}}||^2}}\right\rangle_{\boldsymbol{k}}, \\ Q_3(i\omega_n) &\equiv \frac{1}{2}\left\langle \frac{(1+\delta_N)|\boldsymbol{g}_{\boldsymbol{k}}|^2}{\sqrt{\omega_n^2 + |\psi + d|\boldsymbol{g}_{\boldsymbol{k}}||^2}} + \frac{(1-\delta_N)|\boldsymbol{g}_{\boldsymbol{k}}|^2}{\sqrt{\omega_n^2 + |\psi - d|\boldsymbol{g}_{\boldsymbol{k}}||^2}}\right\rangle_{\boldsymbol{k}}.\end{aligned} \tag{4.20}$$

where $\langle\rangle_{\boldsymbol{k}}$ denotes the integral over the Fermi surface $\int \frac{d\Omega_{\boldsymbol{k}}}{4\pi}$. The parameter δ_N fixes the distribution of the DOS at the Fermi level of the two bands, $N_1 = N_0(1+\delta_N)$ and $N_2 = N_0(1-\delta_N)$.

4.2 Characterisation of the superconducting instability

The critical temperature and the basic structure of the gap function $\mathbf{\Delta} = (\psi, d)$, which characterizes the superconducting instability, follow from the solution of the linearized form of the self-consistent Eq. (4.18). We find

$$\frac{1}{N_0 V}\mathbf{\Delta} = f_1(\epsilon_c, k_B T)\hat{Q}^l\mathbf{\Delta} \tag{4.21}$$

with

$$f_1(\epsilon_c, k_B T) = \ln(4\gamma\epsilon_c/2\pi k_B T) \tag{4.22}$$

and

$$\hat{Q}^l = \left[\begin{pmatrix} -e_s & e_m \\ e_m & -e_t \end{pmatrix} + \delta_N\langle|\boldsymbol{g}_{\boldsymbol{k}}|\rangle \begin{pmatrix} e_m & -e_s \\ -e_t & e_m \end{pmatrix}\right], \tag{4.23}$$

where we have used the Euler's constant γ already introduced in Chapter 2. For simplicity, we have assumed the same cut-off energy ϵ_c for both bands.

Eq. (4.21) has a non-trivial solution, if at least one of the eigenvalues λ_i of the matrix $\hat{Q}^l$ is positive. In this case, the critical temperature follows the standard BCS relation $k_B T_c = 2\epsilon_c\gamma/\pi \ \exp(-1/(N_0 V\lambda'))$, where $\lambda' = \max_i(\lambda_i) > 0$. Furthermore, the nucleating form of the gap function follows from $\hat{Q}^l\mathbf{\Delta}' = \lambda'\mathbf{\Delta}'$.

In this context, we introduce the term *dominant* channel to denote the channel responsible for the superconducting transition, and we call *subdominant* the other channel characterized by $\lambda'' = \min_i(\lambda_i)$ and $\hat{Q}^l\mathbf{\Delta}'' = \lambda''\mathbf{\Delta}''$.

Solving the eigenstate problem $\hat{Q}^l\mathbf{\Delta}_i = \lambda_i\mathbf{\Delta}_i$, we find the sets

$$2\lambda' = -(e_s + e_t) + 2e_m\delta + \Lambda \tag{4.24}$$

$$\mathbf{\Delta}' \propto \begin{pmatrix} -(e_s - e_t) + \Lambda \\ 2(e_m - e_t\delta) \end{pmatrix}, \tag{4.25}$$

and

$$2\lambda'' = -(e_s + e_t) + 2e_m\delta - \Lambda, \tag{4.26}$$

$$\mathbf{\Delta}'' \propto \begin{pmatrix} -(e_s - e_t) - \Lambda \\ 2(e_m - e_t\delta) \end{pmatrix}. \tag{4.27}$$

where

$$\Lambda = \sqrt{(e_s - e_t)^2 + 4(e_m - e_s\delta)(e_m - e_t\delta)},$$

and $\delta = \delta_N\langle|\boldsymbol{g}_{\boldsymbol{k}}|\rangle$ to simplify the notation. Our interest lies in the characterization of the instability for all possible combinations of the three components of the pairing potential (4.8). From Eq. (4.24), we determine the conditions for the superconducting instability and the form of the nucleating pairing state given by Eq. (4.25).

In order to conveniently display a phase diagram of the three parameters, we use the condition $e_s^2 + e_t^2 + e_m^2 = 1$ and represent these parameters by the angles of spherical coordinates (e_s: s-wave spin-singlet, e_t: S spin-triplet, and e_m: mixing):

$$\begin{aligned} e_s &= \cos(\phi_v)\sin(\theta_v), \\ e_t &= \sin(\phi_v)\sin(\theta_v), \\ e_m &= \cos(\theta_v). \end{aligned} \tag{4.28}$$

The character of the interaction as a function of the two spherical angles (θ_v, ϕ_v) is shown in Fig. 4.2.

Obviously an attractive interaction either for spin-singlet or -triplet pairing or both would yield a superconducting instability. If both e_s and e_t are repulsive (> 0), the mixing term plays the decisive role. From Eq. (4.24) we immediately see that an instability is absent for small $|e_m|$ (grey domain with "no SC" in Fig. 4.3) :

$$|e_m| < \sqrt{e_s e_t} \text{ where } e_s,\ e_t > 0. \tag{4.29}$$

On the other hand, a large enough value of $|e_m|$ can trigger superconductivity, even with $e_s, e_t > 0$. The inter-parity scattering can lower the pairing energy and generate a positive eigenvalue of the matrix $\hat{Q}^l$. This mechanism is formally analogous to superconductivity driven by interband Cooper pair scattering in a multi-band superconductor.

A second positive eigenvalue $\lambda'' > 0$ is possible if both spin channels are attractive ($e_s, e_t < 0$) (grey domain with "e_s and e_t attr." in Fig. 4.2). From Eq. (4.26) we see that the following condition has to be satisfied:

$$|e_m| < \sqrt{e_s e_t} \text{ and } e_s,\ e_t < 0. \tag{4.30}$$

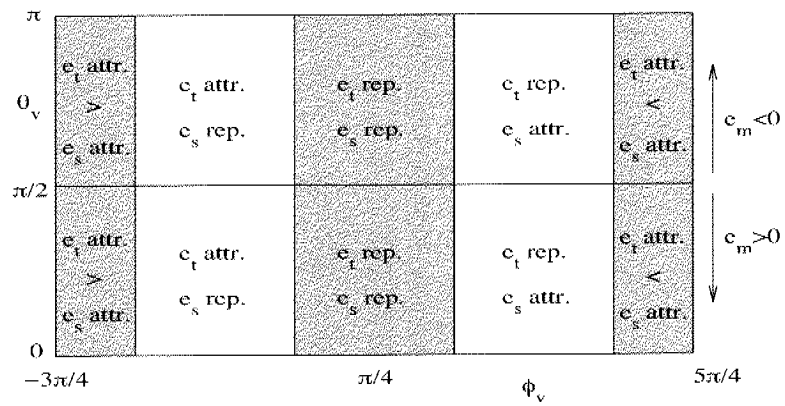

Figure 4.2: The character of the three interaction components ($e_s \equiv$ s-wave spin-singlet, $e_t \equiv$ protected spin-triplet, and $e_m \equiv$ parity violating) as a function of the two spherical angles (θ_v, ϕ_v). The abbreviations " e_s attr." and " e_s rep." mean that the s-wave component of the interaction is attractive ($e_s < 0$) or repulsive ($e_s > 0$), respectively.

The parity-mixing term tends to suppress the second instability.

It only remains to determine the form of the 2-dimensional order parameter $\Delta = (\psi, d)$ based on Eq. (4.25) which nucleates at the superconducting transition. There are four typical forms of the order parameter (ψ, d) which will help us to structure the following discussion ($\mathbf{\Delta} = (\psi, d)$):

$$\mathbf{\Delta}_s \propto \begin{pmatrix} 1 \\ 0 \end{pmatrix} \text{Spin-singlet}, \quad \mathbf{\Delta}_t \propto \begin{pmatrix} 0 \\ 1 \end{pmatrix} \text{Spin-triplet},$$
$$\mathbf{\Delta}_{m1} \propto \begin{pmatrix} 1 \\ 1 \end{pmatrix}, \qquad \mathbf{\Delta}_{m2} \propto \begin{pmatrix} 1 \\ -1 \end{pmatrix}. \tag{4.31}$$

These correspond to the pure spin-singlet pairing $\mathbf{\Delta}_s$, the pure spin-triplet pairing $\mathbf{\Delta}_t$ and two mixed pairings $\mathbf{\Delta}_{m1}$, and $\mathbf{\Delta}_{m2}$.

Before we start discussing the conditions favoring different order parameter forms, we will consider the corresponding gap topologies on the two

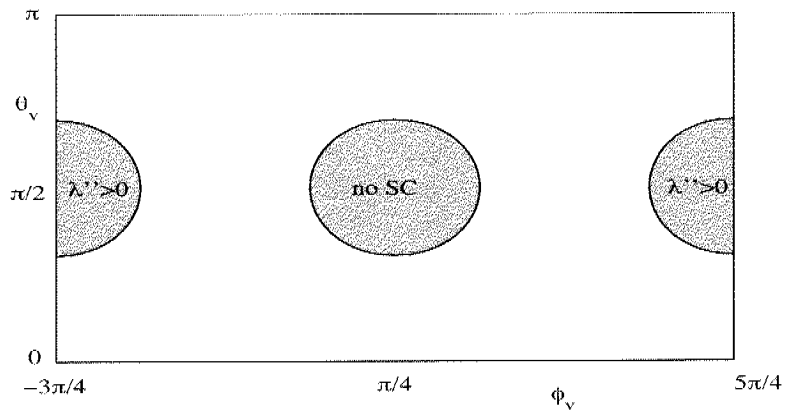

Figure 4.3: The character of the eigenvalues λ', Eq. (4.24), and λ'' , Eq. (4.26), as a function of the two spherical angles (θ_v, ϕ_v). If $\lambda' < 0$ there is no superconducting instability (grey domain with "no SC"). The white domain is charaterized by $\lambda' > 0$ and $\lambda'' < 0$. If $\lambda'' > 0$, the system is characterized by two critical temperatures (grey domain with " $\lambda'' > 0$")

bands for the four cases in Eq. (4.31). To be concrete, we now discuss the case relevant for $CePt_3Si$, i.e. $\boldsymbol{g}_{\boldsymbol{k}} \propto (k_y, -k_x, 0)$. The gap on the two Fermi surfaces is given by

$$\Delta_{1,2}(\theta) = (\psi \pm d\sqrt{3/2}|\sin(\theta)|), \tag{4.32}$$

where θ is the polar angle in $\boldsymbol{k}$-space relative to the z-axis. Fig. 4.4 displays the two-band gap function $\Delta_{1,2}$ for the three different order parameters $\boldsymbol{\Delta}_s$, $\boldsymbol{\Delta}_t$, $\boldsymbol{\Delta}_{m1}$ of Eq. (4.31). The case $\boldsymbol{\Delta}_{m2}$ can be obtained from $\boldsymbol{\Delta}_{m1}$ by exchanging Δ_1 and Δ_2.

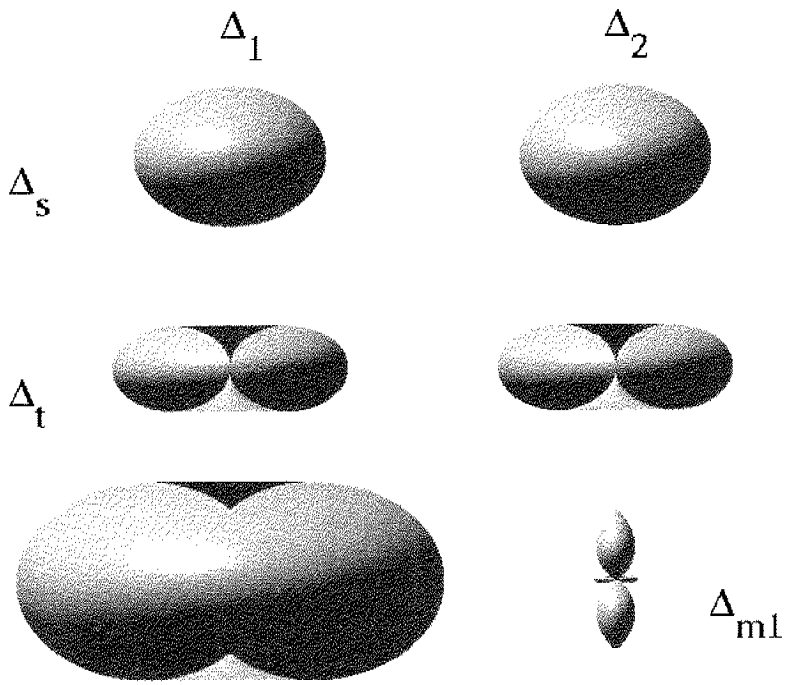

Figure 4.4: The gap amplitudes $\Delta_{1,2}$ of the two non-degenerated bands for three particular directions of the order parameter in the 2-dimensional plane, spanned by ψ, d. The directions corresponding to the two dimensional order parameter $\mathbf{\Delta}_s$, $\mathbf{\Delta}_t$, $\mathbf{\Delta}_{m1}$ are given by (4.31)

In the cases of the pure spin-singlet phase $\mathbf{\Delta}_s$ or the pure spin-triplet phase $\mathbf{\Delta}_t$, the two gap functions Δ_1 and Δ_2 have the same amplitude with the difference that in the spin-triplet case point-nodes appear along the z-axis. For $\mathbf{\Delta}_{m1}$, the gap on the first Fermi surface is much bigger than that on the second, $\Delta_1 > \Delta_2$. Furthermore, the gap function in the second band Δ_2 has two line-nodes perpendicular to the z-axis. The presence of line-nodes in one of the two non-degenerate bands is not a particularity of the mixed states

$\mathbf{\Delta}_{m1}$, but a general property of all states with $|d|C_1 > |\psi|$ and $|\psi| \neq 0$, where $C_1 = \sqrt{3/2}$ only in the case of a spherical original Fermi surface. However, in general, the topology of the nodes in the two gap functions belonging to the trivial representation A_1 of the point group C_{4v} is characterized by

$$\frac{|\psi|}{|d|} \begin{cases} = 0 & \text{2 point-nodes} \\ < C_1 & \text{2 line-nodes for one band} \perp z\text{-axis} \\ > C_1 & \text{no nodes} \end{cases} \tag{4.33}$$

Now we turn to the conditions under which the different forms of the order parameter nucleate. We expect that the order parameter appears as a pure spin-singlet Δ_s or a pure spin-triplet Δ_t if the spin-singlet potential e_s or the spin-triplet potential e_t are attractive and dominant, respectively. This is the case if the density of states on the Fermi levels is equal to $\delta = 0$ and the parity-mixing interaction e_m is absent.

From Eq. (4.25), the necessary conditions can be derived

$$\mathbf{\Delta} = \mathbf{\Delta}_s \quad \text{for} \quad e_m = e_t\delta,\ e_s < e_t, \tag{4.34}$$

$$\mathbf{\Delta} = \mathbf{\Delta}_t \quad \text{for} \quad e_m = e_s\delta,\ e_t < e_s, \tag{4.35}$$

$$\mathbf{\Delta} = \mathbf{\Delta}_{m1} \quad \text{for} \quad e_s = e_t,\ e_m > e_t\delta, \tag{4.36}$$

$$\mathbf{\Delta} = \mathbf{\Delta}_{m2} \quad \text{for} \quad e_s = e_t,\ e_m < e_t\delta. \tag{4.37}$$

Moreover, the condition in Eq. (4.29) has to be satisfied to guarantee a superconducting phase transition. The first two conditions (4.34) and (4.35) are necessary to compensate the mixing of the spin-triplet with the spin-singlet pairing channels induced when the DOS are different for the two Fermi surfaces $\delta \neq 0$. Furthermore, taking into account the condition (4.29), we see that, surprisingly, $\mathbf{\Delta}_s$ and $\mathbf{\Delta}_t$ can also nucleate in the presence of repulsive spin-singlet e_s and spin-triplet e_t potentials. If $e_s = e_t$, the conditions (4.36) and (4.37) indicate that the order parameter is either $\mathbf{\Delta}_{m1}$ or $\mathbf{\Delta}_{m2}$. For $\delta = 0$ the sign of the parity-mixing potential e_m determines which of the two order parameter appears. Fig. 4.5 shows the phase diagram of the different order parameter forms resulting from Eq. (4.31). The different black lines are plotted choosing $\delta = 0.3$. The grey ones show how the lines corresponding to the pure spin-singlet Δ_s and pure spin-triplet Δ_t are moved with varying δ. For general combinations of the three components e_s, e_t, e_m the angles

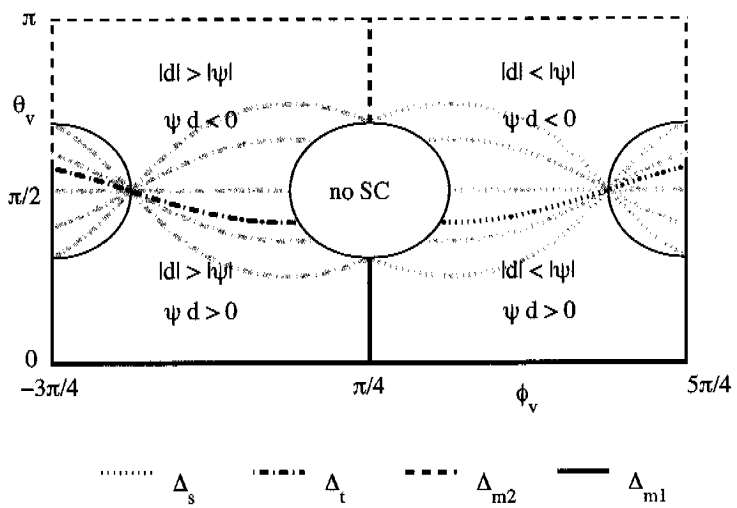

Figure 4.5: Phase diagram showing the direction of the nucleated order parameter $\mathbf{\Delta} = (\psi, d)$ as a function of the three components $e_s = \cos(\phi_v)\sin(\theta_v)$, $e_t = \sin(\phi_v)\sin(\theta_v)$, $e_m = \cos(\theta_v)$ of the pairing potential and for different values of δ. The different lines correspond to the four directions $\mathbf{\Delta}_s$, $\mathbf{\Delta}_t$, $\mathbf{\Delta}_{m1}$ and $\mathbf{\Delta}_{m2}$, see legend. The different black lines are obtained for $\delta = 0.3$, while the grey lines for values of $-1 < \delta < 1$.

θ_v, ϕ_v lie in one of the four basic domains delimited by the black lines shown in Fig. 4.5. The order parameter nucleates with intermediary values of ψ, and d.

4.3 Evolution of the gaps below T_c

To obtain the magnitude of the two-dimensional order parameter $\mathbf{\Delta} = (\psi, d)$ as a function of the temperature, we have to solve the self-consistent Eq. (4.18). This last becomes simpler at $T = 0$,

$$\mathbf{\Delta} = \hat{Q}_0(\mathbf{\Delta})\mathbf{\Delta} \tag{4.38}$$

with

$$\hat{Q}_0(\mathbf{\Delta}) = \left\{ VN_0 \left[Q_1^0(\mathbf{\Delta}) \begin{pmatrix} -e_s & 0 \\ e_m & 0 \end{pmatrix} + Q_2^0(\mathbf{\Delta}) \begin{pmatrix} e_m & -e_s \\ -e_t & e_m \end{pmatrix} + Q_3^0(\mathbf{\Delta}) \begin{pmatrix} 0 & e_m \\ 0 & -e_t \end{pmatrix} \right] + \frac{1}{\lambda'} \hat{Q}^l \right\}, \tag{4.39}$$

where $\hat{Q}^l$ and λ' have been defined in Eq. (4.23) and (4.24). The functions

$$Q_1^0(\mathbf{\Delta}) = \frac{(1+\delta_N)}{2} \left\langle \ln\left(\frac{\gamma|\psi+d|\boldsymbol{g}_{\boldsymbol{k}}||}{\pi k_B T_c}\right) \right\rangle_{\boldsymbol{k}} + \frac{(1-\delta_N)}{2} \left\langle \ln\left(\frac{\gamma|\psi-d|\boldsymbol{g}_{\boldsymbol{k}}||}{\pi k_B T_c}\right) \right\rangle_{\boldsymbol{k}},$$

$$Q_2^0(\mathbf{\Delta}) = \frac{(1+\delta_N)}{2} \left\langle |\boldsymbol{g}_{\boldsymbol{k}}| \ln\left(\frac{\gamma|\psi+d|\boldsymbol{g}_{\boldsymbol{k}}||}{\pi k_B T_c}\right) \right\rangle_{\boldsymbol{k}} - \frac{(1-\delta_N)}{2} \left\langle |\boldsymbol{g}_{\boldsymbol{k}}| \ln\left(\frac{\gamma|\psi-d|\boldsymbol{g}_{\boldsymbol{k}}||}{\pi k_B T_c}\right) \right\rangle_{\boldsymbol{k}},$$

$$Q_3^0(\mathbf{\Delta}) = \frac{(1+\delta_N)}{2} \left\langle |\boldsymbol{g}_{\boldsymbol{k}}|^2 \ln\left(\frac{\gamma|\psi+d|\boldsymbol{g}_{\boldsymbol{k}}||}{\pi k_B T_c}\right) \right\rangle_{\boldsymbol{k}} + \frac{(1-\delta_N)}{2} \left\langle |\boldsymbol{g}_{\boldsymbol{k}}|^2 \ln\left(\frac{\gamma|\psi-d|\boldsymbol{g}_{\boldsymbol{k}}||}{\pi k_B T_c}\right) \right\rangle_{\boldsymbol{k}},$$

are obtained from Eq. (4.20). The eigenproblem $\lambda_i^0 \mathbf{\Delta}_i^0 = \hat{Q}_0(\mathbf{\Delta}_i^0)\mathbf{\Delta}_i^0$ determines the ratio $\nu_0 = \psi_0/d_0$ between the s-wave spin-singlet ψ_0 and the S-triplet d_0 component at $T = 0$. However, the additional condition $\lambda_i^0(\mathbf{\Delta}_i^0) = 1$ is necessary to determine the magnitude of the two components of the order parameter.

The parameters involved in Eq. (4.18) and (4.38) are the three components of the pairing interaction (e_s, e_t, e_m), the density of states on the two non-degenerate bands δ and the strength of the interaction $1/N_0V$. To simplify the study of such equations, it is more convenient to derive the three components of the pairing interaction (e_s, e_t, e_m) from parameters which characterize the superconducting instability. These are the ratio between the spin-singlet and the spin-triplet components at the critical temperature

$$\nu_l \equiv \lim_{T \to T_c} \frac{\psi}{d} = -\frac{(e_s - e_t) + \Lambda}{2(e_m - e_t\delta)}, \tag{4.40}$$

and a second parameter ρ which characterizes the subdominant channel,

$$\rho \equiv \frac{1}{N_0 V} \frac{\lambda'' - \lambda'}{\lambda'\lambda''}. \tag{4.41}$$

λ'' has been defined in Eq. (4.26). If the subdominant channel is attractive, then $\rho = \ln(T_c''/T_c)$, otherwise $\rho = 1/N_0V_{eff}$, where

$$\frac{1}{N_0V_{eff}} = \frac{1}{N_0V\lambda'} - \frac{1}{N_0V\lambda''}$$

defines the effective interaction in the case of a repulsive subdominant channel.

Introducing

$$\frac{1}{\kappa} \equiv \sum_{0 \le n < (\frac{\epsilon_c}{2\pi k_B T_c} - \frac{1}{2})} \frac{2}{2n+1} = \frac{1}{N_0 V \lambda'} \tag{4.42}$$

and through substitution of λ' and λ'' in Eqs. (4.40, 4.41, 4.42), we find $(e_s, e_t, e_m) = (\lambda_s, \lambda_t, \lambda_m)/\sqrt{\lambda_s^2 + \lambda_t^2 + \lambda_m^2}$ with

$$\begin{aligned}
\lambda_s &= -\frac{\kappa(1+\nu_l^2+2\nu_l\delta+\kappa\nu_l^2(\delta^2-1)\rho)}{(1+\nu_l^2+2\nu_l\delta)(\delta^2-1)(\kappa\rho-1)} \\
\lambda_t &= -\frac{\kappa(1+\nu_l^2+2\nu_l\delta+\kappa(\delta^2-1)\rho)}{(1+\nu_l^2+2\nu_l\delta)(\delta^2-1)(\kappa\rho-1)} \\
\lambda_m &= \frac{\kappa(\kappa\nu_l(\delta^2-1)\rho-\delta(1+\nu_l^2+2\nu_l\delta))}{(1+\nu_l^2+2\nu_l\delta)(\delta^2-1)(\kappa\rho-1)}.
\end{aligned}$$

The case $\lambda'' = 0$.

We start the discussion considering the case where the subdominant channel is inactive, $\lambda'' = 0$. In this case, the interaction parameters e_s, e_t, and, e_m lie on a line given by

$$|e_m| = \sqrt{e_s e_t} \text{ with } e_s,\ e_t < 0, \tag{4.43}$$

which corresponds to the circle centered in $\phi_v = 5\pi/4 \equiv -3\pi/4$ in the phase diagram of Figs. 4.3 and 4.5. In this limit, the parameter $|\rho| \to \infty$.

The only eigenvector of the matrix $\hat{Q}_{T=0}(\mathbf{\Delta}_0)$ with a non-vanishing eigenvalue corresponds to $\mathbf{\Delta}_0 = \mathbf{\Delta}'$, which is given by Eq. (4.25). Thus, the ratio between the spin-singlet and the spin-triplet components at $T = 0$ is equal to that obtained for $T = T_c$, i.e. $\nu_0 = \nu_l$. This result is a first indication that the form of the order parameter is unchanged upon temperature when the subdominant channel is inactive. This is confirmed by the numerical solution of Eq. (4.18).

Fig. 4.6 shows the spin-singlet ψ and the spin-triplet component d as a function of temperature obtained for $\nu = 0.5$ and $\delta = -0.5$. The inset shows

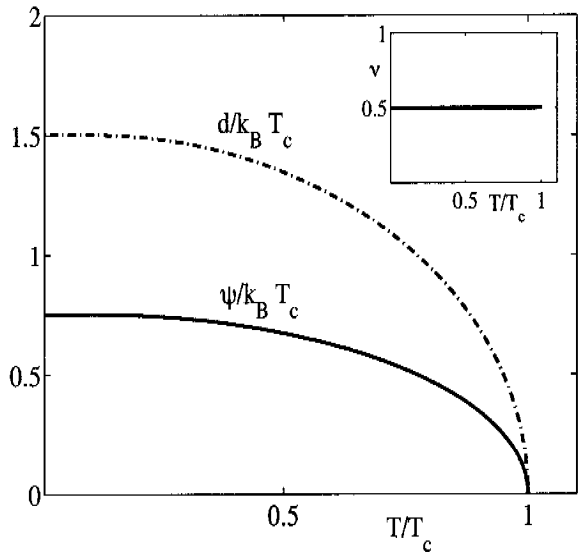

Figure 4.6: The order parameter $\mathbf{\Delta} = (\psi, d)$ as a function of the temperature when the subdominant channel is inactive, i.e. $\lambda'' = 0$. The inset plot shows the ratio $\nu = \psi/d$. ($\nu_l = 0.5$, $\delta = -0.5$).

the ratio $\nu = \psi/d$. This does not depend on temperature. Furthermore, in this case there are explicit expressions for the two components

$$\frac{d_0\gamma}{k_B T_c \pi} = \exp\left\{ -\frac{\left\langle (1+\delta_N)(\nu+|\boldsymbol{g}_{\boldsymbol{k}}|)^2 \ln(|\nu+|\boldsymbol{g}_{\boldsymbol{k}}||) + (1-\delta_N)(\nu-|\boldsymbol{g}_{\boldsymbol{k}}|)^2 \ln(|\nu-|\boldsymbol{g}_{\boldsymbol{k}}||) \right\rangle}{\left\langle (1+\delta_N)(\nu+|\boldsymbol{g}_{\boldsymbol{k}}|)^2 + (1-\delta_N)(\nu-|\boldsymbol{g}_{\boldsymbol{k}}|)^2 \right\rangle} \right\}$$

$$\frac{\psi_0\gamma}{k_B T_c \pi} = \exp\left\{ -\frac{\left\langle (1+\delta_N)(\nu+|\boldsymbol{g}_{\boldsymbol{k}}|)^2 \ln\left(|1+\frac{|\boldsymbol{g}_{\boldsymbol{k}}|}{\nu}|\right) + (1-\delta_N)(\nu-|\boldsymbol{g}_{\boldsymbol{k}}|)^2 \ln\left(|1-\frac{|\boldsymbol{g}_{\boldsymbol{k}}|}{\nu}|\right) \right\rangle}{\left\langle (1+\delta_N)(\nu+|\boldsymbol{g}_{\boldsymbol{k}}|)^2 + (1-\delta_N)(\nu-|\boldsymbol{g}_{\boldsymbol{k}}|)^2 \right\rangle} \right\} \tag{4.44}$$

of the order parameter. For a *pure* spin-singlet order parameter, $\nu \to \infty$, and for the *pure* protected spin-triplet state, $\nu = 0$, we recover the standard result: $\psi_0/k_B T_c = \pi/\gamma \approx 1.76$, and $d_0/k_B T_c = \pi/\gamma \exp\langle -|\boldsymbol{g}_{\boldsymbol{k}}|^2 \ln(|\boldsymbol{g}_{\boldsymbol{k}}|)\rangle \approx 1.65$ for $\boldsymbol{g}_{\boldsymbol{k}} \propto (k_y, -k_x, 0)$, respectively.

The case $\lambda'' \neq 0$.

However, if the subdominant channel is active, the ratio between the spin-singlet and the spin-triplet components,

$$\nu_0 \equiv \frac{\psi_0}{d_0} = -\frac{(Q_3^0 - Q_2^0\delta)(1+\nu_l^2+2\nu_l\delta) - (1-\delta^2)(Q_3^0\kappa + \nu_l(Q_2^0\kappa+\nu_l+\delta))\rho}{(Q_2^0 - Q_1^0\delta)(1+\nu_l^2+2\nu_l\delta) - (Q_2^0\kappa - \nu_l + Q_1^0\kappa\nu_l - \delta)(1-\delta^2)\rho} \tag{4.45}$$

at $T = 0$ is in general different from that obtained for $T = T_c$. Moreover, ν_0 depends on the cut-off energy ϵ_c via κ. The magnitude of the order parameter, which follows combining Eq. (4.45) with the equation

$$\frac{\rho\,[\nu_l^2 Q_1^0 + Q_3^0 + 2\nu_l Q_2^0]}{\nu_l^2 + 1 + 2\nu_l\delta} = \frac{(Q_1^0 Q_3^0 - Q_2^{0^2})}{(1-\delta^2)}, \tag{4.46}$$

which is obtained from the condition $\lambda_i^0(\mathbf{\Delta}_i^0) = 1$, also depends on ϵ_c. However, no changes in the qualitative behaviors of the gaps as a function of temperature have been observed solving Eq. (4.18) for different values of the cut-off energy ϵ_c.

Comparing the condensation energy at T=0,

$$\begin{aligned} F_c &= -\frac{N_1}{4}\langle|\Delta_1(\boldsymbol{k})|^2\rangle_{\boldsymbol{k}} - \frac{N_2}{4}\langle|\Delta_2(\boldsymbol{k})|^2\rangle_{\boldsymbol{k}} \\ &= -\frac{N_0}{2}(|\psi_0|^2 + |d_0|^2 + 2\delta\psi_0 d_0) \end{aligned} \tag{4.47}$$

obtained for different cases, we found that

$$|E_c^A| > |F_c^0| > |E_c^R|. \tag{4.48}$$

Here, we introduce E_c^R and E_c^A to denote the condensation energy obtained in the presence of a repulsive, $\lambda'' < 0$, and attractive, $\lambda'' > 0$, subdominant channel, respectively. F_c^0 denotes the limit case characterized by $\lambda'' = 0$. The Copper pair gains condensation energy if the subdominant channel is attractive. On the contrary, the condensation energy of the pairs decreases in the presence of a repulsive subdominant channel.

Fig. 4.7 shows the order parameter as a function of the temperature obtained for two representative cases. The first case is characterised by a repulsive, $\lambda'' < 0$, subdominant channel with $\lambda''/\lambda' \approx -5000$, while the

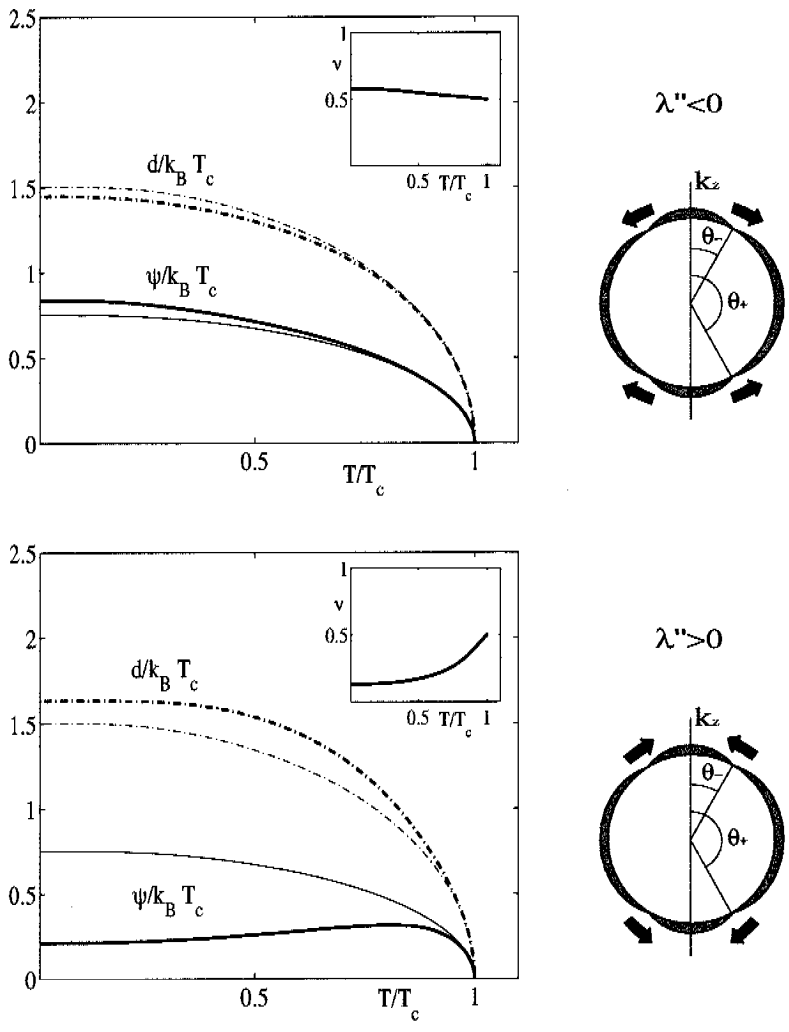

Figure 4.7: The order parameter $\mathbf{\Delta} = (\psi, d)$ as a function of temperature. The first plot shows the case with a repulsive, $\lambda'' < 0$, subdominant channel, and $\lambda''/\lambda' \approx -5000$. The second plot shows the result obtained when the subdominant channel is attractive, $\lambda'' > 0$, and characterized by $T_c''/T_c = 0.7$. The thin lines are obtained for $\lambda'' = 0$. ($\nu_l = \psi/d = 0.5$, $\delta = -0.5$, $\epsilon_c = 60 k_B T_c$).

second is characterized by an attractive, $\lambda'' > 0$, subdominant channel with $T_c''/T_c = 0.7$. In both cases, $\nu = \psi/d = 0.5$ and $\boldsymbol{g_k} \propto (k_y, -k_x, 0)$. This means that the nucleation of the superconducting state is characterized in both cases by two line nodes, perpendicular to the z-axis, on the gap amplitude, $\Delta_2(\theta) = (\psi - d\sqrt{3/2}|\sin(\theta)|)$, of the second non-degenerated band. The polar angle $\theta_\pm$ determines the position of those nodes. In our example, the two line nodes are characterised by $\theta_\pm = \pi/2 \pm (\pi/2 - \arcsin(\sqrt{2/3}\nu))$ (we suppose a native spherical Fermi surface). From the insets of Fig. 4.7 we see that the ratio ν between the spin-singlet and the spin-triplet component now changes with the temperature. Thus the position of the nodes also now depends upon temperature. To the right of the graphs in Fig. 4.7 we draw the gap structure on the second Fermi surface schematically. The arrows show the directions along which the accidental line nodes move, decreasing the temperature. This last depends on the character of the subdominant channel.

In the case of an attractive subdominant channel there is the possibility of a second phase transition. This is the case if there is a second solution $\Delta_0'' = (\psi_0'', d_0'')$ for Eqs. (4.45), (4.46) with

$$|\psi_0''|^2 + |d_0''|^2 + 2\delta\psi_0''d_0'' > |\psi_0|^2 + |d_0|^2 + 2\delta\psi_0 d_0. \tag{4.49}$$

Our numerical investigation seems to show that in general there is no second phase transition. The solution nucleating at the highest critical temperature seems to maintain the highest condensation energy, changing its structure continuously with temperature. The only exception affects systems with constant density of state, $\delta = 0$, and with no mixing pairing interaction component, $e_m = 0$. In this particular case, we could have a second transition between a spin-triplet state and a spin-singlet state.

4.4 Static uniform spin susceptibility

In Section 2.5, we discussed the spin suceptibility of the superconducting state supposing the same density of state for the two non-degenerated bands. We have treated only the specific cases of *pure* spin-singlet and *pure* spin-triplet order parameters. This result was reported in [14]. The spin suscep-

tibility tensor introduced in Eq. (4.50) can easily be expressed using the two band formalism,

$$\chi^s_{ij} = -\mu_B^2 k_B T \sum_{\boldsymbol{k}} \sum_{\omega_n} \mathrm{Tr}\left\{\hat{\sigma}_i \left[\left((G_1^2+F_1^2)\,\hat{\sigma}_1(\boldsymbol{k}) + (G_2^2+F_2^2)\hat{\sigma}_2(\boldsymbol{k})\right)\hat{g}_{\boldsymbol{k},j} + (G_1G_2+F_1F_2)\left(\hat{\sigma}_j - \hat{g}_{\boldsymbol{k},j}(\hat{\boldsymbol{g}}_{\boldsymbol{k}}\cdot\hat{\boldsymbol{\sigma}})\right)\right]\right\}. \tag{4.50}$$

The spin susceptibility of the normal state is given by Eq. (2.44), which reads

$$\chi^n_{i,i} = \mu_B^2 \sum_{\boldsymbol{k}} \left\{ \frac{n_F(\xi_1)-n_F(\xi_2)}{\alpha|\boldsymbol{g}_{\boldsymbol{k}}|}(1-\hat{g}^2_{\boldsymbol{k},i}) + \left(\frac{\partial n_F(\xi_1)}{\partial \xi_1} + \frac{\partial n_F(\xi_2)}{\partial \xi_2}\right)\hat{g}^2_{\boldsymbol{k},i}\right\}. \tag{4.51}$$

The first term of Eq. (4.51) comes from the interband transitions between the two non-degenerated bands, and is of the Van Vleck type [46], while the last term is the Pauli contribution. Without the assumption of constant density of state, the uniform static spin susceptibility is in general anisotropic and different from the Pauli susceptibility $\chi^n \neq \chi_P \equiv 2\mu_B^2 N_0$. To the second order in α, this gives

$$\begin{aligned}\chi^n_{i,i} &= \mu_B^2 \sum_{\boldsymbol{k}} 2\frac{\partial n_F(\xi)}{\partial \xi} + \frac{\partial^3 n_F(\xi)}{\partial \xi^3}\frac{\alpha^2}{3}(|\boldsymbol{g}_{\boldsymbol{k}}|^2 + 2g^2_{\boldsymbol{k},i}) \\ &= \chi_P\left(\delta_{i,j} + \frac{\alpha^2 N_0''}{3N_0}\left\langle |\boldsymbol{g}_{\boldsymbol{k}}|^2 + 2g^2_{\boldsymbol{k},i}\right\rangle_{\boldsymbol{k}}\right).\end{aligned} \tag{4.52}$$

This means that the spin susceptibility of $CePt_3Si$ in the normal state is different for fields along the z-axis and for fields in the xy-plane.

If the splitting of the two Rashba bands is large, $\alpha/k_BT_c >> 1$, then the transition into the superconducting state does not affect the Van Vleck susceptibility. This was already pointed out by Samokhin [47]. In fact, the sum over $\boldsymbol{k}$ of the mix products G_1G_2 and F_1F_2

$$\begin{aligned}\sum_{\boldsymbol{k}} G_1G_2\Big(\sum_{\boldsymbol{k}} F_1F_2\Big) = \frac{\pi N_0}{2\left(4\alpha^2|\boldsymbol{g}_{\boldsymbol{k}}|^2 + \left(\sqrt{\omega_n^2+\Delta_1^2}+\sqrt{\omega_n^2+\Delta_2^2}\right)^2\right)} \\ \left[(\psi^2 \pm d^2|\boldsymbol{g}_{\boldsymbol{k}}|^2)\left(\frac{1}{\sqrt{\omega_n^2+\Delta_1^2}}+\frac{1}{\sqrt{\omega_n^2+\Delta_2^2}}\right)\right. \\ \left. +2(d|\boldsymbol{g}_{\boldsymbol{k}}|\psi + i\alpha|\boldsymbol{g}_{\boldsymbol{k}}|\omega_n)\left(\frac{1}{\sqrt{\omega_n^2+\Delta_2^2}}-\frac{1}{\sqrt{\omega_n^2+\Delta_2^2}}\right)\right]\end{aligned}$$

becomes negligible at sufficiently large α values. Consequently, the temperature dependency of the spin susceptibility in the superconducting state is given by the change in the Pauli contribution,

$$\chi_{ii}^{s} = \chi_P \left\{(1+c_1) + c_2 \left\langle g_{\boldsymbol{k},i}^2 \right\rangle_{\boldsymbol{k}} \right. \\ \left. - \; k_B T \pi \sum_{\omega_n} \left\langle \left[\frac{(1+\delta_N)}{2} \frac{|\Delta_1(\boldsymbol{k})|^2 \hat{g}_{\boldsymbol{k},i}^2}{(\omega_n^2 + |\Delta_1(\boldsymbol{k})|^2)^{3/2}} \; \frac{(1-\delta_N)}{2} \frac{|\Delta_2(\boldsymbol{k})|^2 \hat{g}_{\boldsymbol{k},i}^2}{(\omega_n^2 + |\Delta_2(\boldsymbol{k})|^2)^{3/2}} \right] \right\rangle_{\boldsymbol{k}} \right\}, \tag{4.53}$$

where at large $\alpha/k_B T_c$ the relation $2c_1 = c_2 = 2\alpha^2 N_0''/3N_0$ derived in Eq. (4.52) for small $\alpha/k_B T_c$ is inadequate. In that limit, it is more realistic to consider the density of state close to the Fermi levels as constant, but different for each non-degenerated band. It follows

$$\chi_{ii}^{s} = \chi_P \left\{1 + \left\langle c_1(\boldsymbol{k}) \left(1 - \hat{g}_{\boldsymbol{k},i}^2\right) \right\rangle_{\boldsymbol{k}} + \right. \\ \left. - \; k_B T \pi \sum_{\omega_n} \left\langle \left[\frac{(1+\delta_N)}{2} \frac{|\Delta_1(\boldsymbol{k})|^2 \hat{g}_{\boldsymbol{k},i}^2}{(\omega_n^2 + |\Delta_1(\boldsymbol{k})|^2)^{3/2}} \; \frac{(1-\delta_N)}{2} \frac{|\Delta_2(\boldsymbol{k})|^2 \hat{g}_{\boldsymbol{k},i}^2}{(\omega_n^2 + |\Delta_2(\boldsymbol{k})|^2)^{3/2}} \right] \right\rangle_{\boldsymbol{k}} \right\}, \tag{4.54}$$

where the value of $c_1(\boldsymbol{k})$,

$$c_1(\boldsymbol{k}) \;=\; \int d\xi \frac{N(\xi,\boldsymbol{k})}{2N_0} \frac{n_F(\xi_1) - n_F(\xi_2)}{\alpha |\boldsymbol{g}_{\boldsymbol{k}}|} - 1 \tag{4.55}$$

will strongly depend on the details of the density of state $N(\xi,\boldsymbol{k})$ in the two non-degenerated bands. An alternative expression to Eq. (4.53) is given, first summing over the Matsubara frequencies,

$$\chi_{ii}^{s} \;=\; \chi_P \left\{ \left\langle (1+c_1(\boldsymbol{k})) \left(1 - \hat{g}_{\boldsymbol{k},i}^2\right) \right\rangle_{\boldsymbol{k}} \right. \\ \left. + \; \frac{(1+\delta_N)}{2} \left\langle Y_1(\boldsymbol{k},T) \hat{g}_{\boldsymbol{k},i}^2 \right\rangle_{\boldsymbol{k}} + \frac{(1-\delta_N)}{2} \left\langle Y_2(\boldsymbol{k},T) \hat{g}_{\boldsymbol{k},i}^2 \right\rangle_{\boldsymbol{k}} \right\}, \tag{4.56}$$

where $Y_{1,2}$ is the Yosida function defined by,

$$Y_{1,2}(\boldsymbol{k},T) = \frac{1}{4k_B T} \int \frac{d\xi_{1,2}}{\cosh^2(E_{\boldsymbol{k}}^{1,2}/2k_B T)} \tag{4.57}$$

with $E_{\boldsymbol{k}}^{1,2} = \sqrt{\xi_{1,2}^2 + |\Delta_{1,2}(\boldsymbol{k})|^2}$. In the specific case of $CePt_3Si$, the uniform static susceptibility of the superconducting state for fields along the z-axis ($\chi_\parallel = \chi_{zz}$) remains unchanged as already predicted in Section 2.5, this because we supposed $\boldsymbol{g}_{\boldsymbol{k}} \propto (k_y, -k_x, 0)$. On the contrary, Samokhin found a variation of the susceptibility with temperature for this field orientation also. He supposed $g_{\boldsymbol{k},z} \propto k_y k_x k_z (k_x^2 - k_y^2) \neq 0$. But there are indications, see Section 3.4, that this component can be neglected. Instead, for fields in the xy-plane ($\chi_\perp = \chi_{xx} = \chi_{yy}$), the static uniform spin susceptibility should decrease considerably, its value at T=0 now dependent on the details of the band structure. However, its low-temperature limit $T \to 0$ only depends on the standard behaviors of the Yosida function [5],

$$Y_{1,2}(T) = \langle Y_{1,2}(\boldsymbol{k}, T) \rangle_{\boldsymbol{k}} \propto \begin{cases} e^{-\langle \Delta_{1,2}^0(\boldsymbol{k}) \rangle / T}, & \Delta_{1,2}(\boldsymbol{k}) \neq 0, \\ T^2, & \Delta_{1,2}(\boldsymbol{k}) \text{ has nodes at isolated points}, \\ T, & \Delta_{1,2}(\boldsymbol{k}) \text{ has lines nodes}. \end{cases}$$

Recent experimental data of the nuclear magnetic relaxation rate T_1^{-1} [21, 22], the London penetration depth [23] and thermal conductivity [24] give evidence for the possible presence of line nodes.

4.5 Discussion and conclusions

In this chapter we have characterized the superconducting state belonging to the trivial representation A_1 in a material without an inversion center and strong antisymmetric spin-orbit coupling. However, all results can be easily generalized to any other representation of the point group. The corresponding pairing state involves spin-singlet s-wave pairing as well as a spin-triplet component specific to the spin-orbit coupling. In addition to the pure spin-singlet s-wave and spin-triplet pairing, the pairing interaction includes a parity mixing contribution corresponding to an inter-parity scattering of Cooper pairs.

The combination of the three types of pairing interaction (e_s, e_l, e_m) and the distribution of the density of states on the two non-degenerated bands δ determine the form of the order parameter represented by a singlet and

a triplet component $\Delta = (\psi, d)$. The two-component structure of the order parameter allows for two distinct pairing channels, a *dominant* and a *subdominant* one. The pairing instability of the clean system is completely characterized by the property of the *dominant* channel. However, decreasing the temperature the structure of the order parameter is strongly affected by the presence of the *subdominant* channel. The condensation energy at $T = 0$ of the superconducting state increases in the case of an attractive *subdominant* channel.

For the case of $CePt_3Si$, we found that if $|d| > |\psi|$ and $|\psi| \neq 0$, one Fermi surface would have line nodes perpendicular to the z-axis in the quasiparticle gap. We would also like to mention that the presence of line nodes may leave its specific low-temperature features in various thermodynamic quantities, such as the specific heat, the London penetration depth and so on. Recent experimental data of the nuclear magnetic relaxation rate T_1^{-1} [21, 22], the London penetration depth [23] and thermal conductivity [24] give evidence for the possible presence of line nodes. We show that in the presence of line nodes, the uniform static spin-susceptibility for fields in the xy-plane should be $\propto T$ at low temperatures, see also [47].

Moreover, the position of line nodes will, in general, depend upon both temperature and character of the *subdominant* channel. The temperature dependence of the position could be measured by thermal conductivity [48]. The displacement direction as a function of the temperature will indicate if the *subdominant* channel is attractive or repulsive.

The presence of two instabilities in the linearized gap equation, the *dominant* and *subdominant* one, provide the possibility that two superconducting phase transitions might appear. From our study, this possibility seems to be reduced to an exception.

Chapter 5

Calculation of disorder effects

5.1 Born approximation

Effects of disorder are described by potential scattering of the quasiparticles, which in real-space representation is given by

$$\mathcal{H}_{imp} = \sum_i \mathcal{H}_i, \quad \mathcal{H}_i = \int u(\boldsymbol{r} - \boldsymbol{r}_i)\psi_s^\dagger(\boldsymbol{r})\psi_s(\boldsymbol{r})d\boldsymbol{r}, \tag{5.1}$$

where $u(\boldsymbol{r})$ is the potential of a non-magnetic impurity, which we consider rather short-ranged, such that s-wave scattering is dominant. We are interested in the disorder-averaged normal and anomalous Green's functions $\hat{G}$ and $\hat{F}$,

$$\begin{aligned} G_{\lambda\mu}(r - r') &= -\langle T_\tau\{\psi_\lambda(r)\psi_\mu^\dagger(r')\}\rangle \\ F_{\lambda\mu}(r - r') &= \langle T_\tau\{\psi_\lambda(r)\psi_\mu(r')\}\rangle \\ F_{\lambda\mu}^\dagger(r - r') &= \langle T_\tau\{\psi_\lambda^\dagger(r)\psi_\mu^\dagger(r')\}\rangle, \end{aligned} \tag{5.2}$$

with $r = (\boldsymbol{r}, \tau)$ and where the bracket denotes the thermal average.

For the impurity average, we use the Born approximation [28], neglecting the possibility of more than two scattering events at the same impurity, which is valid provided that the potential is small in comparison with the characteristic electron energy scale ϵ_F (ϵ_F= Fermi energy, or analogue the band width).

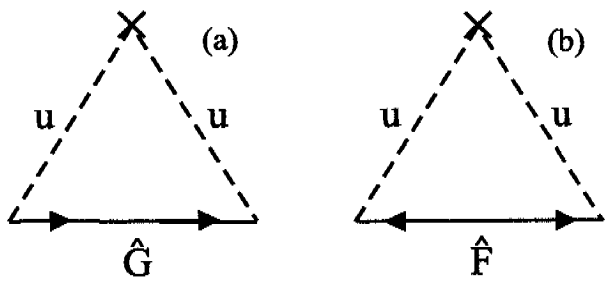

Figure 5.1: The-self energy contributions due to impurity scattering in the Born approximation, of normal type Σ_G (a) and of anomalous type Σ_F (b).

Formally, the impurity scattering enters the self-energy of the Greens function of the normal, $\hat{\Sigma}_G$, Fig. 5.1(a), and the anomalous type, $\hat{\Sigma}_F$, see Fig. 5.1(b). Their mathematical expressions read

$$\begin{aligned} \hat{\Sigma}_G(i\omega_n) &= \frac{\Gamma}{\pi N_0}\int \frac{d\boldsymbol{k}'}{(2\pi)^3}\hat{G}(\boldsymbol{k}', i\omega_n) \\ \hat{\Sigma}_F(i\omega_n) &= \frac{\Gamma}{\pi N_0}\int \frac{d\boldsymbol{k}'}{(2\pi)^3}\hat{F}(\boldsymbol{k}', i\omega_n), \end{aligned} \tag{5.3}$$

where $\Gamma \equiv \pi n_{imp} N_0 u^2$ is the averaged scattering rate, $N_0 \equiv (N_1 + N_2)/2$ and $N_{1,2}$ are the densities of state (DOS) of the two bands at the Fermi level. In addition, we have introduced the impurity concentration n_{imp} and the s-wave scattering potential u^2.

The Gor'kov equations with these self-energy contributions are formally analogous to those obtained for systems with an inversion symmetry [28]

$$\begin{aligned} \left(\hat{G}_0^{-1}(\boldsymbol{k}, i\omega_n) - \hat{\Sigma}_G(i\omega_n)\right)\hat{G}(\boldsymbol{k}, i\omega_n) & \\ + \left(\hat{\Delta}(\boldsymbol{k}) + \hat{\Sigma}_F(i\omega_n)\right)\hat{F}^\dagger(\boldsymbol{k}, i\omega_n) &= \hat{\sigma}_0 \\ \left(\hat{G}_0^{-1^\top}(-\boldsymbol{k}, -i\omega_n) + \hat{\Sigma}_G^\top(-i\omega_n)\right)\hat{F}^\dagger(\boldsymbol{k}, i\omega_n) & \\ - \left(\hat{\Delta}^\dagger(\boldsymbol{k}) + \hat{\Sigma}_F^\dagger(i\omega_n)\right)\hat{G}(\boldsymbol{k}, i\omega_n) &= 0. \end{aligned} \tag{5.4}$$

The two-band Green's functions $G_{1,2}$ and $F_{1,2}$, are derived by unitary trans-

formation (4.1), as already done for the clean system (4.9).

$$\begin{aligned}\left(\{G^0_{1,2}(\boldsymbol{k},i\omega_n)\}^{-1}-\Sigma_G(i\omega_n)\right)G_{1,2}(\boldsymbol{k},i\omega_n)&\\ +\left(\Delta_{1,2}(\boldsymbol{k})+\Sigma_F(i\omega_n)\right)F^\dagger_{1,2}(\boldsymbol{k},i\omega_n) &= 1\\ \left(\{G^0_{1,2}(-\boldsymbol{k},-i\omega_n)\}^{-1}+\Sigma_G(-i\omega_n)\right)F^\dagger_{1,2}(\boldsymbol{k},i\omega_n)&\\ -\left(\Delta^*_{1,2}(\boldsymbol{k})+\Sigma_F(i\omega_n)\right)G_{1,2}(\boldsymbol{k},i\omega_n) &= 0,\end{aligned}\tag{5.5}$$

where, in this case,

$$\begin{aligned}\Sigma_G(i\omega_n) &= \frac{\Gamma}{2\pi N_0}\int\frac{d\boldsymbol{k}'}{(2\pi)^3}\left\{G_1(\boldsymbol{k}',i\omega_n)+G_2(\boldsymbol{k}',i\omega_n)\right\}\\ \Sigma_F(i\omega_n) &= \frac{\Gamma}{2\pi N_0}\int\frac{d\boldsymbol{k}'}{(2\pi)^3}\left\{F_1(\boldsymbol{k}',i\omega_n)+F_2(\boldsymbol{k}',i\omega_n)\right\},\end{aligned}\tag{5.6}$$

and,

$$\Delta_{1,2}(\boldsymbol{k})=(\psi\pm d|\boldsymbol{g}_{\boldsymbol{k}}|).\tag{5.7}$$

Thus the Gor'kov equations are still diagonal in the band index. The scattering on an impurity does not change the spin of a quasiparticle and with the impurity-average a certain translational symmetry is restored such that the two bands do not mix in this approximation. Interband effects occur only through virtual processes.

Introducing the modified gap functions $\tilde{\Delta}_{1,2}(\boldsymbol{k},i\omega_n)=\Delta_{1,2}(\boldsymbol{k})+\Sigma_F(i\omega_n)$ and frequencies $i\tilde{\omega}_n=i\omega_n-\Sigma_G(i\omega_n)$, the solution of the two-band Gor'kov equations is given by

$$G_{1,2}(\boldsymbol{k},i\omega_n)=-\frac{i\tilde{\omega}_n+\xi_{1,2}}{(\tilde{\omega}_n^2+|\tilde{\Delta}_{1,2}|^2+\xi^2_{1,2})},\tag{5.8}$$

$$F_{1,2}(\boldsymbol{k},i\omega_n)=\frac{\tilde{\Delta}_{1,2}}{(\tilde{\omega}_n^2+|\tilde{\Delta}_{1,2}|^2+\xi^2_{1,2})},\tag{5.9}$$

in which $\tilde{\Delta}_{1,2}(\boldsymbol{k},i\omega_n)$ and $\tilde{\omega}_n$ have to be determined self-consistently. The corresponding equations are given by the substitution of Eqs. (5.8) and (5.9) into Eqs. (4.15) and (5.6),

$$\tilde{\omega}_n = \omega_n+\tilde{\omega}_n\Gamma Q_1(i\tilde{\omega}_n),\tag{5.10}$$

$$\tilde{\psi} = \psi+\tilde{\psi}\,\Gamma Q_1(i\tilde{\omega}_n)+d\,\Gamma Q_2(i\tilde{\omega}_n),\tag{5.11}$$

$$\frac{1}{N_0V}\boldsymbol{\Delta} = \pi k_BT\sum_{\omega_n>-\epsilon_c}^{\epsilon_c}\hat{Q}(i\tilde{\omega}_n)\boldsymbol{\Delta},\tag{5.12}$$

where in the last equation $\mathbf{\Delta} = (\psi, d)$, and

$$\begin{aligned}\hat{Q}(i\tilde{\omega}_n) &= \frac{Q_1(i\tilde{\omega}_n)}{1-\Gamma Q_1(i\tilde{\omega}_n)}\begin{pmatrix} -e_s & 0 \\ e_m & 0 \end{pmatrix} \\ &+ \frac{Q_2(i\tilde{\omega}_n)}{1-\Gamma Q_1(i\tilde{\omega}_n)}\begin{pmatrix} e_m & -e_s \\ -e_t & e_m \end{pmatrix} \\ &+ \left\{ Q_3(i\tilde{\omega}_n) + \frac{\Gamma Q_2^2(i\tilde{\omega}_n)}{1-\Gamma Q_1(i\tilde{\omega}_n)} \right\}\begin{pmatrix} 0 & e_m \\ 0 & -e_t \end{pmatrix} \end{aligned} \tag{5.13}$$

is defined using the functions Q_1, Q_2, Q_3, which are obtained by substituting ψ and ω_n by $\tilde{\psi}$ and $\tilde{\omega}_n$ in Eq (4.20), respectively.

Going back to the spin basis, we find formally the same equation as Eq. (4.14)

$$\begin{aligned}\hat{G}(\boldsymbol{k}, i\omega_n) &= G_1(\boldsymbol{k}, i\omega_n)\hat{\sigma}_1(\boldsymbol{k}) + G_2(\boldsymbol{k}, i\omega_n)\hat{\sigma}_2(\boldsymbol{k}), \\ \hat{F}(\boldsymbol{k}, i\omega_n) &= \{F_1(\boldsymbol{k}, i\omega_n)\hat{\sigma}_1(\boldsymbol{k}) + F_2(\boldsymbol{k}, i\omega_n)\hat{\sigma}_2(\boldsymbol{k})\} i\hat{\sigma}_y. \end{aligned} \tag{5.14}$$

5.2 Effect on T_c

The effect of disorder on the superconducting instability is deduced by the solution of the linearized form of the self-consistent system of Eqs. (5.10-5.12). Using standard summation techniques [5], we find

$$\frac{1}{N_0 V}\mathbf{\Delta} = \left\{ f_1(c_c, k_B T)\hat{Q}^l + f_2(\Gamma, k_B T)\hat{Q}^l_\Gamma \right\}\mathbf{\Delta}, \tag{5.15}$$

where f_1 and $\hat{Q}^l$ have been defined in Eq. (4.22) and Eq. (4.23), respectively. Instead, f_2 is defined by

$$f_2(\Gamma, k_B T) = \Psi\left(\frac{1}{2} + \frac{\Gamma}{2\pi k_B T}\right) - \Psi\left(\frac{1}{2}\right) \tag{5.16}$$

and

$$\hat{Q}^l_\Gamma = (1 - \delta_N^2(|\boldsymbol{g}_{\boldsymbol{k}}|)^2)\begin{pmatrix} 0 & -e_m \\ 0 & e_t \end{pmatrix}. \tag{5.17}$$

Here we have used the digamma function $\Psi(z)$ defined by $\Psi(z) \equiv d/dz \ln(z!)$.

First, we would like to note that the zeros in the first column of the matrix $\hat{Q}^l_\Gamma$ are a consequence of Anderson's theorem [26], i.e. the conventional s-wave pairing state is not affected by non-magnetic impurities. For more general states in our two-dimensional order parameter space, T_c decreases with growing disorder. We distinguish two basically different cases here: For the pure system either both eigenvalues λ', λ'' are positive, or one of the two, λ'' is negative. In the first case, there is a second lower (bare) critical temperature $k_B T_c'' = 1.14 \epsilon_c \exp(-1/(N_0 V \lambda''))$.

The case: $\lambda'' = 0$

Before starting the discussion of these two general cases, we consider the boundary situation with $\lambda'' = 0$. The only eigenvector of the matrix $\hat{Q}^l_\Gamma$ with a non-vanishing eigenvalue corresponds to the form of $\mathbf{\Delta}'$ given by in Eq. (4.25). Hence, in this case, disorder would not alter the structure of the nucleating order parameter

$$\mathbf{\Delta} = \begin{pmatrix} \psi \\ d \end{pmatrix} \propto \mathbf{\Delta}' \propto \begin{pmatrix} \sqrt{|e_s|} \\ \mathrm{sign}(e_m)\sqrt{|e_t|} \end{pmatrix}. \tag{5.18}$$

The instability equation (5.15) becomes

$$\frac{1}{N_0 V} = \lambda' f_1(\epsilon_c, k_B T) + e_t(1-\delta^2) f_2(\Gamma, k_B T), \tag{5.19}$$

where $e_t(1-\delta^2)$ is the eigenvalue of the matrix $\hat{Q}^l_\Gamma$. We replace $f_1 = \ln(T_c/T) + 1/N_0 V \lambda'$ and $\lambda' = -(e_s + e_t) + 2e_m\delta$ in Eq. (5.19) and find

$$\ln(T_c/T) = \frac{e_t(1-\delta^2)}{(e_s + e_t) - 2e_m\delta} f_2(\Gamma, k_B T). \tag{5.20}$$

Using Eq. (5.18) we obtain

$$\ln\left(\frac{1}{t}\right) = \frac{1}{1+\eta} f_2(\gamma, t), \tag{5.21}$$

where

$$\eta = \frac{(\psi + \delta d)^2}{d^2(1-\delta^2)}, \tag{5.22}$$

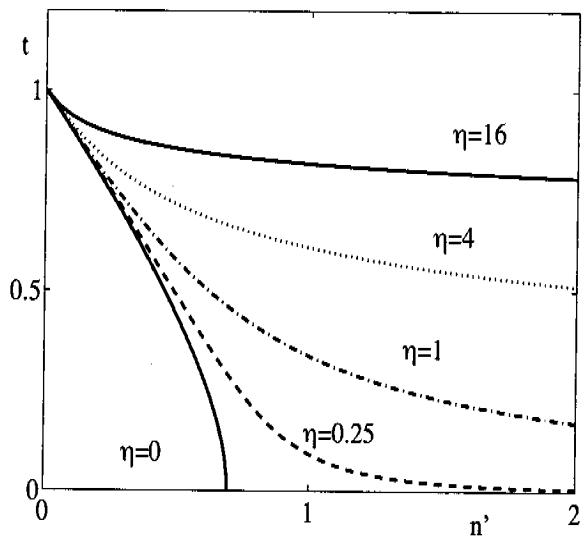

Figure 5.2: The critical temperature as a function of the impurity concentration reduced so as to have a slope of -1 at $t = 1$ for different values of η. For the value of η, see Eq. (5.51). This result is valid only for $\lambda'' = 0$.

with $t = T/T_c$ and $\gamma = \Gamma/k_B T_c$. The effect of impurity scattering affects T_c as in unconventional superconductors in general [49]. However, a distinctive point is the presence of the pre-factor $1/(1+\eta)$. A similar result was obtained for the s+g-superconductivity in borocarbides [50].

In order to visualize the behavior of the onset temperature of superconductivity depending on impurity concentrations, we introduce the normalization with respect to the initial slope of T_c-reduction.

$$n' = \frac{n_{imp}}{(-dn_{imp}/dt)_{t=1}} = \frac{\tilde{\gamma}}{(-d\tilde{\gamma}/dt)_{t=1}}. \tag{5.23}$$

Fig. 5.2 shows the evolution of t as a function of n' for different values of η when the *subdominant* channel has $\lambda'' = 0$.

For $\eta > 0$, the superconducting instability extends to large impurity

concentrations n' with the asymptotical behavior of the critical temperature

$$0.88\, t^{-\eta} - t = \frac{4(1+\eta)}{\pi} n'. \tag{5.24}$$

Hence, we observe a variation of the robustness against non-magnetic impurities. For $\eta = 0$, the standard behavior of an unconventional superconductor is found, while for $\eta \to \infty$ the non-sensitivity against disorder analogous to a conventional superconducting phase is realized. The latter case coincides with the suppression of the spin-triplet component in the pure phase. The exponent η can be interpreted as the product of two ratios

$$\eta = \eta_1 \eta_2 \text{ with } \eta_{1,2} = \frac{\langle N_1 \Delta_1(\boldsymbol{k}) + N_2 \Delta_2(\boldsymbol{k}) \rangle}{N_{1,2} \langle \Delta_1(\boldsymbol{k}) - \Delta_2(\boldsymbol{k}) \rangle}, \tag{5.25}$$

where $\eta_{1,2}$ corresponds to the ratio between the s-wave spin-singlet component (numerator) and the spin-triplet component lying in the first and second band (denominator), respectively. Once $\langle N_1 \Delta_1(\boldsymbol{k}) + N_2 \Delta_2(\boldsymbol{k}) \rangle \neq 0$, the robustness of the superconducting state against disorder is introduced by the presence of a s-wave spin-singlet contribution.

For other unconventional pairing states which do not belong to the trivial representation A_1, the impurity contribution to the self-energy of anomalous type is zero and we recover exactly the result obtained by Larkin [49].

The case: $\lambda'' \neq 0$

In this case, the eigenvectors of the two matrices $\hat{Q}^l$ and $\hat{Q}^l_\Gamma$ are different, such that we need to diagonalize the matrix appearing in Eq. (5.15). The highest eigenvalue and its eigenvector read

$$2\lambda = 2\lambda' f_1 + c_1 - c_2 + \sqrt{c_2^2 + c_3}, \tag{5.26}$$

$$\boldsymbol{\Delta} \propto \begin{pmatrix} \psi' + \frac{\sqrt{c_2^2+c_3}-c_4}{f_1 c_5} \\ d' \end{pmatrix}, \tag{5.27}$$

where (ψ', d') are normalized ($\psi'^2 + d'^2 = 1$). Furthermore, the parameters c_i are defined as

$$\begin{aligned}
c_1 &= (1-\delta^2)\left[e_t - \frac{e_t(e_t - e_s - 2e_m\delta) + 2e_m^2}{\Lambda}\right] f_2, \\
c_2 &= \Lambda f_1 - \frac{(1-\delta^2)}{2}\left\{\Lambda + \frac{e_t^2 + e_s[4\delta(e_m - e_t\delta) - e_s]}{\Lambda}\right\} f_2, \\
c_3 &= -\frac{4(e_m^2 - e_s e_t)(e_m - e_t\delta)^2(\delta^2-1)^2}{\Lambda^2} f_2^2, \\
c_4 &= \Lambda f_1 + e_t(1-\delta^2) f_2, \\
c_5 &= \sqrt{4(e_m - e_t\delta)^2 + (e_t - e_s + \Lambda)^2}.
\end{aligned} \tag{5.28}$$

The equation determining the critical temperature can be expressed as

$$\frac{2}{N_0 V} = 2\lambda' f_1(\epsilon_c, k_B T) + c_1 - c_2 + \sqrt{c_2^2 + c_3}. \tag{5.29}$$

When we again use the relation $f_1 = \ln(T_c/T) + 1/N_0 V\lambda'$, we can cancel the $2/N_0V$ term appearing on the left-hand side of Eq. (5.29) and reach a new convenient representation,

$$\left[2\lambda' \ln\left(\frac{1}{t}\right) + c_1\right]^2 - 2\left[2\lambda' \ln\left(\frac{1}{t}\right) + c_1\right] c_2 - c_3 = 0. \tag{5.30}$$

We assume now that the second channel is attractive, $\lambda'' > 0$, so that the clean system is characterized by a second lower (bare) critical temperature $t'' = T_c''/T_c$. We use the relation $f_1 = \ln(T_c/T) + \ln(t'')\lambda''/(\lambda'' - \lambda')$ to simplify Eq. (5.30). This leads to an equation of the second order in $\ln(t)$ of the following form which allows us to determine both transition temperatures ($t = T/T_c$ or $t = T''/T_c$)

$$\ln\left(\frac{1}{t}\right)(\ln(t'') - f_2(\gamma, t) - \ln(t)) = \frac{1}{1+\eta} f_2(\gamma, t)\ln(t''), \tag{5.31}$$

where η is now given by the form of the order parameter in the clean system

$$\eta = \frac{(\psi' + \delta d')^2}{d'^2(1-\delta^2)}, \tag{5.32}$$

and (ψ', d') are connected to the pairing potential via Eq. (4.25).

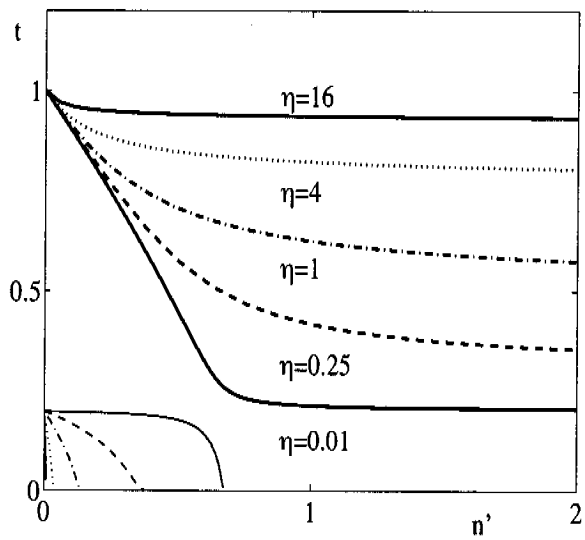

Figure 5.3: The critical temperature as a function of the impurity concentration and for different values of η. Those corresponding to the *dominant* channel, thick lines, have been reduced so as to have a slope of -1 at $t = 1$. The thin lines show the evolution of the *subdominant* channel. This result is obtained supposing that the *subdominant* channel is attractive and $t'' = 0.2$.

Fig. 5.3 shows the solutions of Eq. (5.31) for different values of η and for $t_0'' = 0.2$ in the pure case. The thick line shows the onset temperature of superconductivity as a function of n'. The thin line correspond to the bare transition temperature of *subdominant* instability, as obtained from the square root appearing in Eq. (5.29).

The presence of an attractive *subdominant* channel supports the survival of superconductivity under non-magnetic impurity scattering. The lowest limit for the critical temperature is given by

$$\lim_{n' \to \infty} t = t_0''^{\frac{1}{1+\eta}}.$$

Using Eq. (5.29) to simplify Eq. (5.27), we find that the form of the order

parameter nucleating at the critical temperature t is given by

$$\begin{pmatrix} \psi \\ d \end{pmatrix} \propto \begin{pmatrix} 1+f_3(t) & \delta f_3(t) \\ 0 & 1 \end{pmatrix} \begin{pmatrix} \psi' \\ d' \end{pmatrix}, \tag{5.33}$$

where we have introduced the function $f_3(t)$ defined as

$$f_3(t) = -\frac{(1+\eta)\ln(t)}{(1+\eta)\ln(t) - \ln(t'')}. \tag{5.34}$$

The spin-singlet component of the order parameter increases with disorder. In the limit of a dirty system, the character of the order parameter is purely spin-singlet. Note that the *subdominant* instability is, in any case, suppressed by the disorder. The larger η, the stronger the suppression.

The behavior of the spin-singlet component ψ of the normalized order parameter as a function of the critical temperature t and for different values of η is shown in the Fig. 5.4. The order-parameter of the clean system is supposed to be in the spin-triplet channel.

The case with a repulsive *subdominant* channel, $\lambda'' < 0$, can be easily treated within Eqs. (5.31) and (5.34), substituting $\ln(t'')$ with $1/N_0V_{eff}$, where

$$\frac{1}{N_0V_{eff}} = \frac{1}{N_0V\lambda'} - \frac{1}{N_0V\lambda''}. \tag{5.35}$$

From Eq. (5.31) we find that superconductivity disappears for sufficiently high impurity concentrations. The critical impurity concentration n_c' is given by

$$0.88\, e^{\frac{1}{N_0V_{eff}}\frac{\eta}{1+\eta}} = \frac{4(1+\eta)}{\pi} n_c'. \tag{5.36}$$

Furthermore, the spin-singlet component of the nucleating order parameter decreases with disorder evolving towards

$$\begin{pmatrix} \psi_c \\ d_c \end{pmatrix} \propto \begin{pmatrix} -\delta d' \\ d' \end{pmatrix} \tag{5.37}$$

at the critical impurity concentration n_c'.

It has to be noted that, for almost every combination of the pairing interaction, $\lambda'' \neq 0$. However, the realization of one of the two scenarios described in this chapter can be observed only if $|\lambda''|$ is very close to or bigger than λ', respectively. This means that, in general, we will observe behavior very similar to that described by $\lambda'' = 0$.

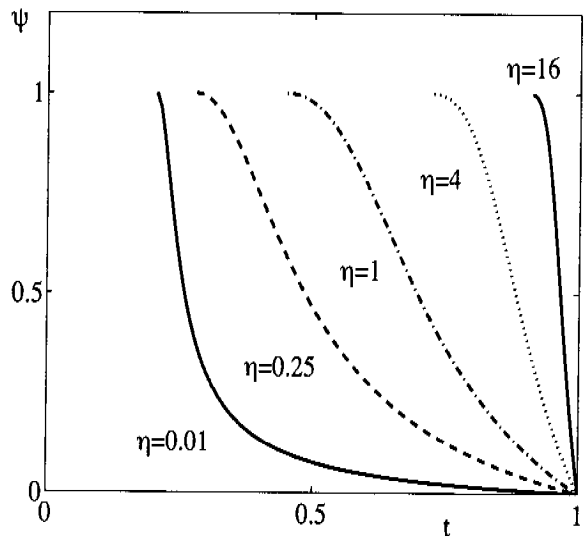

Figure 5.4: The spin-singlet component ψ of the normalized order parameter as a function of the critical temperature t and for different values of η. This result is obtained supposing that the *subdominant* channel is attractive with $t'' = 0.2$ and that the order parameter of the clean system is spin-triplet .

5.3 Static uniform spin susceptibility

The expression for the static uniform spin suceptibility formulated in real space reads

$$\chi_{ij} = -\mu_B \lim_{\substack{\tau' \to \tau \\ r' \to r}} \int_0^\beta d\tau'' \int d\boldsymbol{r}'' \, \mathrm{Tr} \left\{ \sigma^i_{\beta,\alpha} \left\langle T_\tau \left(\overline{\psi_\alpha(r')\psi^\dagger_\gamma(r'')\sigma^j_{\gamma,\delta}\psi_\delta(r'')\psi^\dagger_\beta(r')} \right) \right\rangle \right\},$$

where the *bar* denotes the average over the impurity position [51]. We introduce the notation,

$$\begin{aligned} \Pi^1_{j,\alpha\beta}(r-r'', r''-r') &= \left\langle T_\tau \left(\overline{\psi_\alpha(r)\psi^\dagger_\gamma(r'')\sigma^j_{\gamma,\delta}\psi_\delta(r'')\psi^\dagger_\beta(r')} \right) \right\rangle \\ &= \{ \overline{\hat{G}(r-r'')\hat{\sigma}_j\hat{G}(r''-r')} - \overline{\hat{F}(r-r'')\hat{\sigma}_j^{\mathsf{T}}\hat{F}^\dagger(r''-r')} \}_{\alpha\beta} \end{aligned}$$

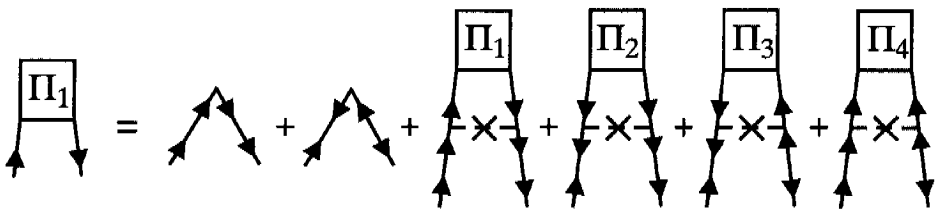

Figure 5.5: Required diagrams for Π^1.

for its kernel. Since the average of a product of two Green's functions does not equal the product of the two separate averages, the expressions (5.8, 5.9) for the normal and anomalous Green's functions are not sufficient to compute the susceptibility.

Abrikosov and Gor'kov present the relevant set of diagrams necessary to compute this average in the context of the Born approximation [52, 53]. The required graphs are of the *ladder* type and they can be generated self-consistently by the set of diagrams shown in Fig. 5.5. The last four diagrams are obtained by the following decomposition

$$\begin{aligned}
&\left\langle T_\tau \left(\psi_\lambda(y)\psi^\dagger_\alpha(r)\psi_\alpha(r)\psi^\dagger_\gamma(r'')\sigma^j_{\gamma,\delta}\psi_\delta(r'')\psi^\dagger_\beta(r')\psi_\beta(r')\psi^\dagger_\eta(y')\right)\right\rangle \\
= \;& \left\langle T_\tau \left(\psi_\lambda(y)\psi^\dagger_\alpha(r)\right)\right\rangle \left\langle T_\tau \left(\psi_\alpha(r)\psi^\dagger_\gamma(r'')\sigma^j_{\gamma,\delta}\psi_\delta(r'')\psi^\dagger_\beta(r')\right)\right\rangle \left\langle T_\tau \left(\psi_\beta(r')\psi^\dagger_\eta(y')\right)\right\rangle \\
- \;& \left\langle T_\tau \left(\psi_\lambda(y)\psi_\alpha(r)\right)\right\rangle \left\langle T_\tau \left(\psi^\dagger_\alpha(r)\psi^\dagger_\gamma(r'')\sigma^j_{\gamma,\delta}\psi_\delta(r'')\psi^\dagger_\beta(r')\right)\right\rangle \left\langle T_\tau \left(\psi_\beta(r')\psi^\dagger_\eta(y')\right)\right\rangle \\
+ \;& \left\langle T_\tau \left(\psi_\lambda(y)\psi_\alpha(r)\right)\right\rangle \left\langle T_\tau \left(\psi^\dagger_\alpha(r)\psi^\dagger_\gamma(r'')\sigma^j_{\gamma,\delta}\psi_\delta(r'')\psi_\beta(r')\right)\right\rangle \left\langle T_\tau \left(\psi^\dagger_\beta(r')\psi^\dagger_\eta(y')\right)\right\rangle \\
- \;& \left\langle T_\tau \left(\psi_\lambda(y)\psi^\dagger_\alpha(r)\right)\right\rangle \left\langle T_\tau \left(\psi_\alpha(r)\psi^\dagger_\gamma(r'')\sigma^j_{\gamma,\delta}\psi_\delta(r'')\psi_\beta(r')\right)\right\rangle \left\langle T_\tau \left(\psi^\dagger_\beta(r')\psi^\dagger_\eta(y')\right)\right\rangle .
\end{aligned} \tag{5.38}$$

Thus, to determine $\hat{\Pi}^1_j$ we require three other quantities. We introduce them as the Fourier transform

$$\hat{\Pi}^i_j(k,k') = \int\int_0^{1/T} d\tau d\tau' \int\int d\boldsymbol{r} d\boldsymbol{r}' \, \hat{\Pi}^i_j(r,r') \exp^{-i(\boldsymbol{k}\cdot\boldsymbol{r}-\omega_n\tau)-i(\boldsymbol{k}'\cdot\boldsymbol{r}'-\omega'_n\tau')}$$

of the following quantities

$$\begin{aligned}
\hat{\Pi}^2_j(r-r'',r''-r') &= i\hat{\sigma}_y \left\langle T_\tau \left(\overline{\psi^\dagger(r)\psi^\dagger(r'')\hat{\sigma}_j\psi(r'')\psi^\dagger(r')} \right) \right\rangle \\
\hat{\Pi}^3_j(r-r'',r''-r') &= i\hat{\sigma}_y \left\langle T_\tau \left(\overline{\psi^\dagger(r)\psi^\dagger(r'')\hat{\sigma}_j\psi(r'')\psi(r')} \right) \right\rangle i\hat{\sigma}_y \\
\hat{\Pi}^4_j(r-r'',r''-r') &= \left\langle T_\tau \left(\overline{\psi(r)\psi^\dagger(r'')\hat{\sigma}_j\psi(r'')\psi(r')} \right) \right\rangle i\hat{\sigma}_y .
\end{aligned}$$

Introducing the averaged functions

$$\hat{\Lambda}^i_j = n_{imp} \int \frac{d\boldsymbol{k}'}{(2\pi)^3} |u(\boldsymbol{k}-\boldsymbol{k}')|^2 \, \hat{\Pi}^i_j(k',k') = \frac{\Gamma}{\pi N_0} \int \frac{d\boldsymbol{k}'}{(2\pi)^3} \hat{\Pi}^i_j(k',k'), \tag{5.39}$$

we can easily derive the equation corresponding to Fig. 5.5,

$$\begin{aligned}
\hat{\Pi}^1_j(k,k) &= \hat{G}(k)\hat{\sigma}_j\hat{G}(k) - \hat{F}(k)\hat{\sigma}_j^{\mathsf{T}}\hat{F}^\dagger(k) \\
&+ \hat{G}(k)\hat{\Lambda}^1_j\hat{G}(k) + \hat{F}(k)(-i\hat{\sigma}_y)\hat{\Lambda}^2_j\hat{G}(k) \\
&+ \hat{F}(k)(-i\hat{\sigma}_y)\hat{\Lambda}^3_j(-i\hat{\sigma}_y)\hat{F}^\dagger(k) + \hat{G}(k)\hat{\Lambda}^4_j(-i\hat{\sigma}_y)\hat{F}^\dagger(k).
\end{aligned} \tag{5.40}$$

The analogous set of ladder diagrams for $\Pi^2_j(k,k)$ can be obtained from the decomposition,

$$\begin{aligned}
&\left\langle T_\tau \left(\psi^\dagger_{\lambda'}(y)\psi^\dagger_\alpha(r)\psi_\alpha(r)\psi^\dagger_\gamma(r'')\sigma^j_{\gamma,\delta}\psi_\delta(r'')\psi^\dagger_\beta(r')\psi_\beta(r')\psi^\dagger_\eta(y') \right) \right\rangle \\
= &\left\langle T_\tau \left(\psi^\dagger_{\lambda'}(y)\psi^\dagger_\alpha(r) \right) \right\rangle \left\langle T_\tau \left(\psi_\alpha(r)\psi^\dagger_\gamma(r'')\sigma^j_{\gamma,\delta}\psi_\delta(r'')\psi^\dagger_\beta(r') \right) \right\rangle \left\langle T_\tau \left(\psi_\beta(r')\psi^\dagger_\eta(y') \right) \right\rangle \\
+ &\left\langle T_\tau \left(\psi_\alpha(r)\psi^\dagger_{\lambda'}(y) \right) \right\rangle \left\langle T_\tau \left(\psi^\dagger_\alpha(r)\psi^\dagger_\gamma(r'')\sigma^j_{\gamma,\delta}\psi_\delta(r'')\psi^\dagger_\beta(r') \right) \right\rangle \left\langle T_\tau \left(\psi_\beta(r')\psi^\dagger_\eta(y') \right) \right\rangle \\
- &\left\langle T_\tau \left(\psi_\alpha(r)\psi^\dagger_{\lambda'}(y) \right) \right\rangle \left\langle T_\tau \left(\psi^\dagger_\alpha(r)\psi^\dagger_\gamma(r'')\sigma^j_{\gamma,\delta}\psi_\delta(r'')\psi_\beta(r') \right) \right\rangle \left\langle T_\tau \left(\psi^\dagger_\beta(r')\psi^\dagger_\eta(y') \right) \right\rangle \\
- &\left\langle T_\tau \left(\psi^\dagger_{\lambda'}(y)\psi^\dagger_\alpha(r) \right) \right\rangle \left\langle T_\tau \left(\psi_\alpha(r)\psi^\dagger_\gamma(r'')\sigma^j_{\gamma,\delta}\psi_\delta(r'')\psi_\beta(r') \right) \right\rangle \left\langle T_\tau \left(\psi^\dagger_\beta(r')\psi^\dagger_\eta(y') \right) \right\rangle .
\end{aligned} \tag{5.41}$$

The corresponding equation reads

$$\begin{aligned}\hat{\Pi}_j^2(k,k) &= -i\hat{\sigma}_y\hat{F}^\dagger(k)\hat{\sigma}_j\hat{G}(k) - i\hat{\sigma}_y\hat{G}^\top(-k)\hat{\sigma}_j^\top\hat{F}^\dagger(k) \\ &- i\hat{\sigma}_y\hat{F}^\dagger(k)\hat{\Lambda}_j^1\hat{G}(k) + i\hat{\sigma}_y\hat{G}^\top(-k)(-i\hat{\sigma}_y)\hat{\Lambda}_j^2\hat{G}(k) \\ &+ i\hat{\sigma}_y\hat{G}^\top(-k)(-i\hat{\sigma}_y)\hat{\Lambda}_j^3(-i\hat{\sigma}_y)\hat{F}^\dagger(k) - i\hat{\sigma}_y\hat{F}^\dagger(k)\hat{\Lambda}_j^4(-i\hat{\sigma}_y)\hat{F}^\dagger(k).\end{aligned} \tag{5.42}$$

To be able to construct the system of equations necessary to calculate $\hat{\Pi}_j^1$, we should also determine the equations for $\hat{\Pi}_j^3$ and $\hat{\Pi}_j^4$. However, as for the superconducting alloys [52] it turns out that,

$$\hat{\Lambda}_j^1(i\omega_n) = -\hat{\Lambda}_j^3(i\omega_n) \quad \text{and} \quad \hat{\Lambda}_j^2(i\omega_n) = -\hat{\Lambda}_j^4(i\omega_n).$$

thus only two equations are necessary to calculate $\hat{\Pi}_j^1$. We rewrite Eqs. (5.40) and (5.42) using the two band formalism

$$\begin{aligned}\hat{\Pi}_j^1(k,k) &= \left[\left(G_1^2(k) + F_1^2(k)\right)\hat{g}_{\boldsymbol{k},j}\hat{\sigma}_1(\boldsymbol{k}) + \left(G_2^2(k) + F_2^2(k)\right)\hat{g}_{\boldsymbol{k},j}\hat{\sigma}_2(\boldsymbol{k})\right](1+\Lambda_1) \\ &+ \left[G_1(k)F_1(k)\hat{g}_{\boldsymbol{k},j}\hat{\sigma}_1(\boldsymbol{k}) + G_2(k)F_2(k)\hat{g}_{\boldsymbol{k},j}\hat{\sigma}_2(\boldsymbol{k})\right]2\Lambda_2.\end{aligned} \tag{5.43}$$

$$\begin{aligned}\hat{\Pi}_j^2(k,k) &= \Big[\left(G_1(-k) - G_1(k)\right)F_1(k)\hat{g}_{\boldsymbol{k},j}\hat{\sigma}_1(\boldsymbol{k}) \\ &\quad + \left(G_2(-k) - G_2(k)\right)F_2(k)\hat{g}_{\boldsymbol{k},j}\hat{\sigma}_2(\boldsymbol{k})\Big](1+\Lambda_1) \\ &\quad + \Big[\left(G_1(-k)G_1(k) - F_1^2(k)\right)\hat{g}_{\boldsymbol{k},j}\hat{\sigma}_1(\boldsymbol{k}) \\ &\quad + \left(G_2(-k)G_2(k) - F_2^2(k)\right)\hat{g}_{\boldsymbol{k},j}\hat{\sigma}_2(\boldsymbol{k})\Big]\Lambda_2.\end{aligned} \tag{5.44}$$

Since we are interested in the diagonal component of the susceptibility, we expressed the matrices $\hat{\Lambda}_j$ as $\hat{\Lambda}_j = \Lambda_j\hat{\sigma}_j$. Furthermore, we neglected all interband contributions. As we saw in Section 4.4, this choice is justified if $\alpha/k_BT_c >> 1$. Using this notation, we can substitute Eqs. (5.43) and (5.44) in (5.39) to perform the average on the impurities' position. The resulting set of equations reads,

$$\begin{aligned}\Lambda_j^1 &= \Gamma\left[R_j^3\left(1+\Lambda_j^1\right) - i\tilde{\omega}_nR_j^2\,\Lambda_j^2\right] \\ \Lambda_j^2 &= \Gamma\left[i\tilde{\omega}_nR_j^3\left(1+\Lambda_j^1\right) + \tilde{\omega}_n^2R_j^1\,\Lambda_j^2\right],\end{aligned} \tag{5.45}$$

where,

$$
\begin{aligned}
R_j^1 &\equiv \frac{1}{2}\left\langle\left(\frac{(1+\delta_N)}{(\tilde{\omega}_n^2+|\tilde{\psi}+d|\boldsymbol{g_k}||^2)^{3/2}}+\frac{(1-\delta_N)}{(\tilde{\omega}_n^2+|\tilde{\psi}-d|\boldsymbol{g_k}||^2)^{3/2}}\right)\hat{g}_{j,\boldsymbol{k}}^2\right\rangle_{\boldsymbol{k}},\\
R_j^2 &\equiv \frac{1}{2}\left\langle\left(\frac{(1+\delta_N)(\tilde{\psi}+d|\boldsymbol{g_k}|)}{(\tilde{\omega}_n^2+|\tilde{\psi}+d|\boldsymbol{g_k}||^2)^{3/2}}+\frac{(1-\delta_N)(\tilde{\psi}-d|\boldsymbol{g_k}|)}{(\tilde{\omega}_n^2+|\tilde{\psi}-d|\boldsymbol{g_k}||^2)^{3/2}}\right)\hat{g}_{j,\boldsymbol{k}}^2\right\rangle_{\boldsymbol{k}},\\
R_j^3 &\equiv \frac{1}{2}\left\langle\left(\frac{(1+\delta_N)|\tilde{\psi}+d|\boldsymbol{g_k}||^2}{(\tilde{\omega}_n^2+|\tilde{\psi}+d|\boldsymbol{g_k}||^2)^{3/2}}+\frac{(1-\delta_N)|\tilde{\psi}-d|\boldsymbol{g_k}||^2}{(\tilde{\omega}_n^2+|\tilde{\psi}-d|\boldsymbol{g_k}||^2)^{3/2}}\right)\hat{g}_{j,\boldsymbol{k}}^2\right\rangle_{\boldsymbol{k}}.
\end{aligned}
\tag{5.46}
$$

We obtain

$$
\Lambda_j^1=\frac{\Gamma R_j^3+\Gamma^2\tilde{\omega}_n^2\left[(R_j^2)^2-R_j^1R_j^3\right]}{1-\Gamma(R_j^3+\tilde{\omega}_n^2R_j^1)-\Gamma^2\tilde{\omega}_n^2\left[(R_j^2)^2-R_j^1R_j^3\right]}. \tag{5.47}
$$

The diagonal part of the susceptibility as a function of disorder follows straightforward by

$$
\begin{aligned}
\chi_{jj} &= -\mu_B^2k_BT\int\frac{d\boldsymbol{k}'}{(2\pi)^3}\sum_{\omega_n}\mathrm{Tr}\left\{\hat{\sigma}_j\hat{\Pi}_j^1(k,k)\right\}\\
&= \chi_P\left\{1+\left\langle c_1(\boldsymbol{k})\left(1-\hat{g}_{\boldsymbol{k},j}^2\right)\right\rangle_{\boldsymbol{k}}\right\}\\
&- \mu_B^2k_BT\sum_{\omega_n}\mathrm{Tr}\left\{\hat{\sigma}_j\int\frac{d\boldsymbol{k}'}{(2\pi)^3}\hat{\Pi}_j^1(k,k)\right\}\\
&= \chi_P\left\{1+\left\langle c_1(\boldsymbol{k})\left(1-\hat{g}_{\boldsymbol{k},j}^2\right)\right\rangle_{\boldsymbol{k}}-\pi k_BT\sum_{\omega_n}\frac{\Lambda_j^1}{\Gamma}\right\}.
\end{aligned}
\tag{5.48}
$$

Substituting (5.47) in (5.48) we find

$$
\begin{aligned}
\chi_{jj} = \chi_P\Bigg\{&1+\left\langle c_1(\boldsymbol{k})\left(1-\hat{g}_{\boldsymbol{k},j}^2\right)\right\rangle_{\boldsymbol{k}}\\
&-\pi k_BT\sum_{\omega_n}\frac{R_j^3+\Gamma\tilde{\omega}_n^2\left[(R_j^2)^2-R_j^1R_j^3\right]}{1-\Gamma(R_j^3+\tilde{\omega}_n^2R_j^1)-\Gamma^2\tilde{\omega}_n^2\left[(R_j^2)^2-R_j^1R_j^3\right]}\Bigg\}.
\end{aligned}
\tag{5.49}
$$

We are now able to study the effect of the disorder on the static uniform spin susceptibility. In general, we first have to solve the set of Eqs. (5.10)

to (5.13) for deriving $\tilde{\omega}_n$ and $\tilde{\psi}$, which are necessary to compute Eq. (5.49). However, in the case of a *pure* s-wave spin-singlet order parameter this is not necessary. In fact, in that case, Anderson's theorem still holds, so that

$$\tilde{\psi} = \psi w, \quad \tilde{\omega}_n = \omega_n w, \quad \text{with} \quad w = 1 + \Gamma \frac{1}{\sqrt{\omega_n^2 + \psi^2}},$$

and the susceptibility can be expressed directly via ψ and ω_n,

$$\chi_{j,j} = \chi_P \Bigg\{ 1 + \Big\langle c_1(\boldsymbol{k}) \left(1 - \hat{g}^2_{\boldsymbol{k},j}\right) \Big\rangle_{\boldsymbol{k}} - \pi k_B T \sum_{\omega_n} \frac{\Gamma |\psi|^2 \langle \hat{g}^2_{j,\boldsymbol{k}} \rangle_{\boldsymbol{k}}}{(\omega_n^2 + |\psi|^2) \left[\sqrt{\omega_n^2 + |\psi|^2} + \Gamma (1 - \langle \hat{g}^2_{j,\boldsymbol{k}} \rangle_{\boldsymbol{k}}) \right]} \Bigg\}. \tag{5.50}$$

In the case of $CePt_3Si$ in which $\boldsymbol{g}_{\boldsymbol{k}} \propto (k_y, -k_x, 0)$, we expect that the susceptibility shows a temperature dependence only for fields along the xy-plane ($\chi_\perp = \chi_{xx} = \chi_{yy}$). The top plot of Fig. 5.6 shows the solution of Eq. (5.50) for $\chi_\perp$ as a function of temperature and for different impurity scattering rates Γ. For simplicity we set c_1 to be zero. The spin susceptibiliy changes considerably with disorder and its value increases. For large impurity scattering rates, the value of the spin susceptibility in the superconducting state approaches that characterizing the normal state. Conventional superconductivity usually does not show this effect [51]. However, in the presence of strong spin-orbit scattering, a similar behavior has been predicted and observed [38, 54].

The bottom plot of Fig. 5.6 shows the paramagnetic spin susceptibility in the case of a *pure* spin triplet order parameter with constant density of state $\delta = 0$. The spin susceptibility increases while the critical temperature decreases. At sufficiently large impurity scattering ($\Gamma = 0.88 k_B T_c$), the superconducting transition is suppressed.

For the general form of order-parameter, the behavior of the the spin susceptibility with disorder depends essentially on two factors. The first is the value of $\eta = (\nu_l + \delta)^2/(1 - \delta^2)$, which has been defined in Eq. (5.32). The second is the character of the subdominant channel.

If the value of η is relatively small and the subdominant channel is repulsive, then the spin susceptibility behaves qualitatively like the pure spin

triplet order parameter with constant density of state. The top plot of Fig. 5.7 shows the case characterized by $\nu_l = 0.5$ and where the subdominant channel is repulsive, $\lambda'' < 0$, and characterized by $\lambda''/\lambda' \approx 14$. Instead, if η is sufficiently large or the subdominant channel is attractive, the spin susceptibility increases considerably with disorder, while the critical temperature changes only marginally. In that case, the behavior of the spin susceptibility is similar to that obtained for the pure spin-singlet order parameter. η is clearly large if the spin-singlet component is much larger than that of the spin-triplet ($\nu_l >> 1$). However, for $CePt_3Si$, there is experimental evidence [21–24] about the presence of line nodes; then ν_l is perhaps small. In that case, η can be large only if the density of state is distributed mainly in one band. The alternative lies in the presence of an attractive subdominant channel.

The bottom plot of Fig. 5.7 shows the case characterized by $\nu_l = 0.8$ and where the subdominant channel is attractive, $\lambda'' > 0$, and characterized by $T_c''/T_c = 0.5$. In that case, the critical temperature decreases with disorder upto $T/T_c = T_c''/T_c^{1/(1+\eta)} \approx 0.8$. Because, in our case, $\eta = (\nu_l + \delta)^2/(1 - \delta^2) = 2.25\bar{3}$, with $\delta = 0.5$. The spin susceptibility increases with disorder approaching the value of the normal state susceptibility. This behavior is similar to that showed by the pure spin singlet order parameter in the (top) plot of Fig 5.6. This can be explained by the fact that the triplet component of the order parameter is gradually suppressed with disorder in the presence of an attractive subdominant channel [17], see also Section 5.2. This means than the line nodes present in the clean system disappear with disorder. This last phenomenon is indirectly showed by the temperature dependence at low T of the spin susceptibility. The bottom plot of Fig. 5.7 shows a linear temperature dependence for the spin susceptibility of a clean system, while the dirty system shows an exponential temperature dependence.

5.4 Discussion and conclusion

In this chapter, we looked at the effect of disorder on the superconducting state belonging to the trivial representation A_1. We used, for this study, the well known Born approximation, which is valid provided that the impu-

rity potential is small in comparision with the characteristic electron energy scale. We have shown that, depending on the properties characterizing the *dominant* and the *subdominant* pairing channels, the A_1-phase is affected by non-magnetic impurities in different ways.

In particular, the critical temperature T_c is unaffected by non-magnetic impurities only in the case of a *pure* s-wave spin singlet order parameter. In the general case, T_c decreases with disorder. Its behavior depends on

$$\eta = \frac{(\psi + \delta d)^2}{d^2(1-\delta^2)},$$

and on the character of the subdominant channel. In particular, the superconductivity survives to the disorder in the case of an attractive subdominant channel. In that case, the critical temperature of the dirty system is reduced to

$$T_c = T_c''^{\frac{1}{1+\eta}}.$$

where T_c'' is the critical temperature of the bare subdominant channel. Instead, if the subdominant channel is repulsive, the superconductivity disappears at a critical impurity concentration. In all cases, the dependence of T_c on the impurity concentration is very characteristic and could be used to establish the realization of the A_1-phase and the property of the subdominant pairing channels.

The effect of disorder on the static uniform susceptibility also depends on η and on the character of the subdominant channel. We studied the temperature dependence of the susceptibility for fields along the xy-plane ($\chi_\perp = \chi_{xx} = \chi_{yy}$) in the case of $CePt_3Si$. If η is sufficiently large or the subdominant channel is attractive, the spin susceptibility increases considerably with disorder, while the critical temperature changes only marginally. For large impurity scattering rates the value of the spin susceptibility in the superconducting state approaches that characterizing the normal state.

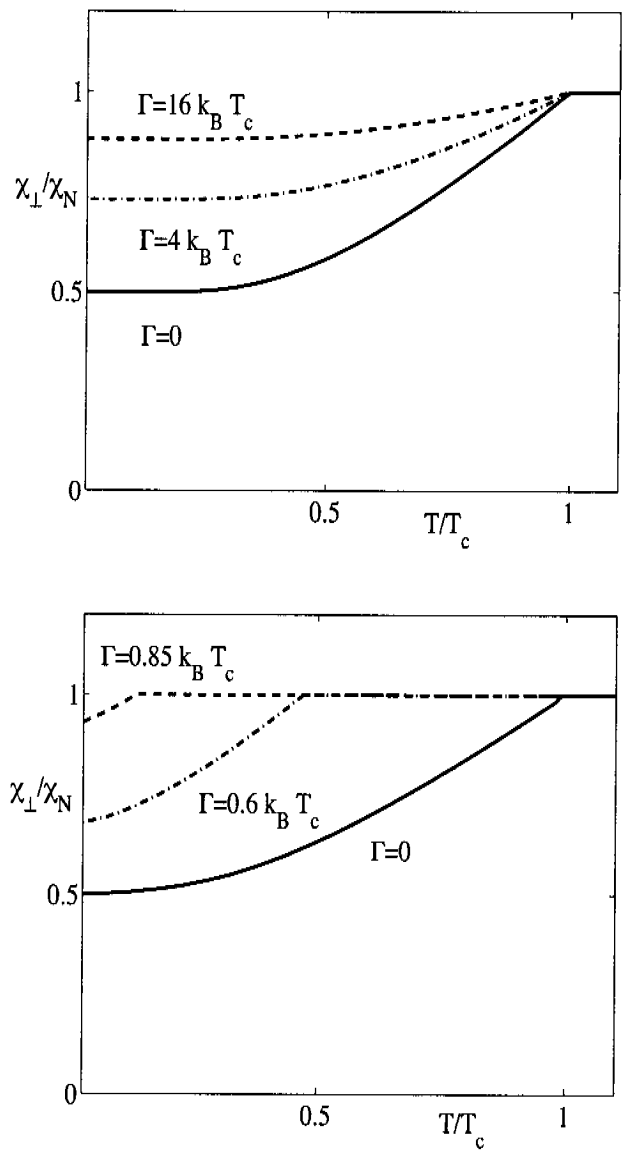

Figure 5.6: The static uniform spin susceptibility for fields in the xy-plane, $\chi_\perp$ as a function of the temperature and for different value of the impurity scattering rate Γ. We chose $\boldsymbol{g_k} \propto (-k_y, k_x, 0)$ ($CePt_3Si$). The top plot shows the spin susceptibility for a *pure* s-wave spin-singlet order parameter, while the bottom plot shows the result for a *pure* protected spin-triplet state. In both cases, we assume constant density of state $\delta = 0$.

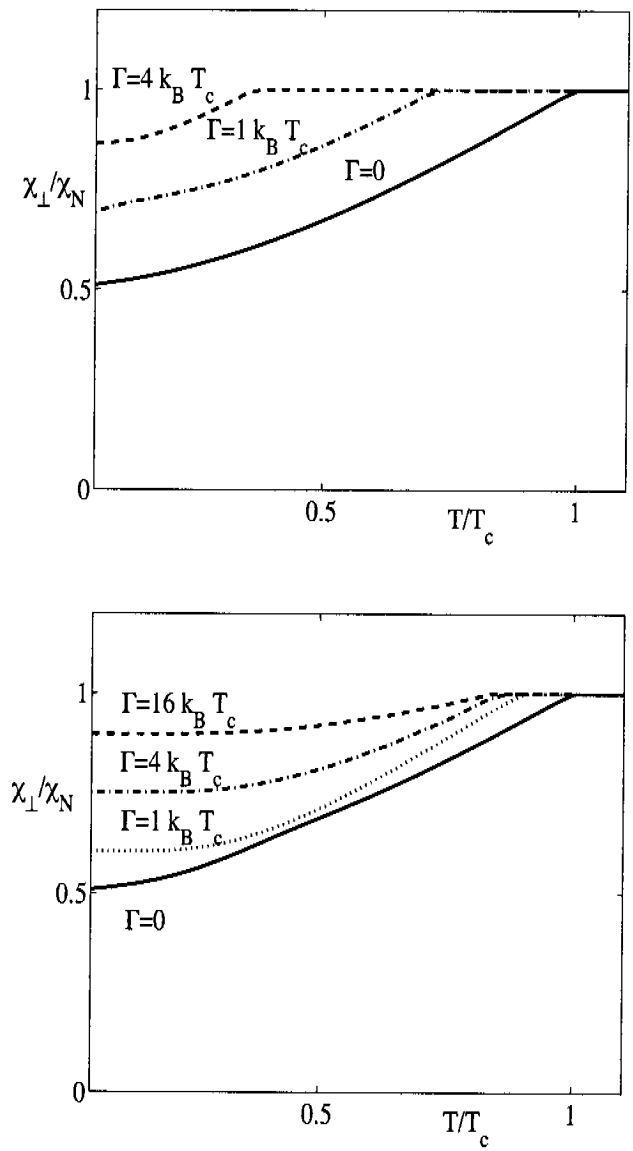

Figure 5.7: The static uniform spin susceptibility for fields in the xy-plane, $\chi_\perp$ as a function of the temperature and for different values of the impurity scattering rate Γ. We chose $\boldsymbol{g_k} \propto (-k_y, k_x, 0)$ ($CePt_3Si$). The top plot shows the spin susceptibility for $\nu_l = \psi/d = 0.5$, in the case of a repulsive, $\lambda'' < 0$, *subdominant* channel. The bottom plot shows the result for $\nu_l = 0.8$ and an attractive, $\lambda'' > 0$, *subdominant* channel, characterized by $T_c'' = 0.5$. ($\delta = 0.5$, $\epsilon_c = 30 k_B T_c$).

Chapter 6

Conclusions and outlook

In this thesis, we have studied basic aspects of superconductivity in materials without an inversion center. All results of this thesis derive from the presence of an antisymmetric ($\boldsymbol{g_k} = -\boldsymbol{g_{-k}}$) spin orbit coupling term

$$\alpha \boldsymbol{g_k} \cdot \boldsymbol{S} \tag{6.1}$$

in the single particle Hamiltonian, which is used to describe the normal state of the material. The strength of our results lies in the fact that the $\boldsymbol{g_k}$-vector function is determined only by symmetry arguments. $\boldsymbol{g_k}$ is different from zero only in crystals without an inversion center, and its structure has been determined for all twentyone point groups without the inversion element, see Appendix A. On the contrary, the coupling strength α has a microscopic origin. α is expected to become significant compared to the electron energy scale ϵ_F in material with heavy nucleons.

However, we have shown that the energy scales determining the superconducting regime are α and $k_B T_c$. If $\alpha >> k_B T_c$, then only spin triplet states with $\boldsymbol{d}(\boldsymbol{k}) || \boldsymbol{g_k}$ survive to the lack of inversion symmetry. This class of protected spin-triplet states mixes with spin-singlet states which are in general unaffected by the lack of the inversion symmetry. The general form for the superconducting order parameter has been deduced

$$\hat{\Delta}_\Gamma(\boldsymbol{k}) = \sum_{i=1}^{d_\Gamma} \chi_i^\Gamma(\boldsymbol{k}) \hat{\Delta}_s(\boldsymbol{k})$$

where

$$\hat{\Delta}_s(\boldsymbol{k}) = \left[\psi + d(\boldsymbol{g}_{\boldsymbol{k}} \cdot \hat{\boldsymbol{\sigma}})\right] i\sigma_y,$$

is the most symmetric superconducting state, called "s-wave", and $\chi_i^{\Gamma}(\boldsymbol{k})$ are basis functions belonging to the even irreducible representation of the different Laue classes, see Appendix A. In addition to the pure spin-singlet e_s and spin-triplet e_t pairing, the pairing interaction includes a parity mixing contribution e_m corresponding to an inter-parity scattering of Cooper pairs. The microscopic origin of this last term can be found in the Dzyaloshinskii-Moriya magnetic interaction, which is present in systems without inversion symmetry, see Appendix B. The role played by this last term is not yet clear. However, our calculations show that the form of the order parameter, represented by a singlet and a triplet component $\boldsymbol{\Delta} = (\psi, d)$, is determined by the combinations of the three types of pairing interaction (e_s, e_t, e_m) and the distribution of the density of states on the two non-degenerated bands δ. The two-component structure of the order parameter allows for two distinct pairing channels. The dominant channel determines the superconducting transition for the clean system, while the dependence of superconductivity on temperature and non-magnetic impurity is determined by the character of the subdominant channel.

We have applied this theory to the study of the "s-wave" state in the context of $CePt_3Si$. In particular, we found that if $|d| > |\psi|$ and $\psi \neq 0$ one Fermi surface would have accidental nodes perpendicular to the z-axis. This is the case if the spin-triplet pairing interaction is more attractive than the spin-singlet interaction, i.e. $e_t < 0$ with $e_t < e_s$. Moreover, we need $e_m \neq e_s\delta$. There is important experimental evidence confirming the realization of this superconducting state in $CePt_3Si$. In particular, the analysis of the results concerning the nuclear magnetic relaxation rate $1/T_1T$, obtained by Pt-NMR [10, 21, 22], see Fig. 1.3 , shows two behaviors which contradict the conventional picture of superconductivity. The NMR relaxation rate shows the Hebel-Slichter coherence peak, indicating an s-wave-like pairing, and at low temperature shows a power law, indicating unconventional pairing. Recent numerical calculations of $1/T_1T$ [25] show that this situation is compatible with the realization of the "s-wave" state which we propose. Fig. 6.1 shows the numerical result. The W_{FF} (dashed line) is related to the co-

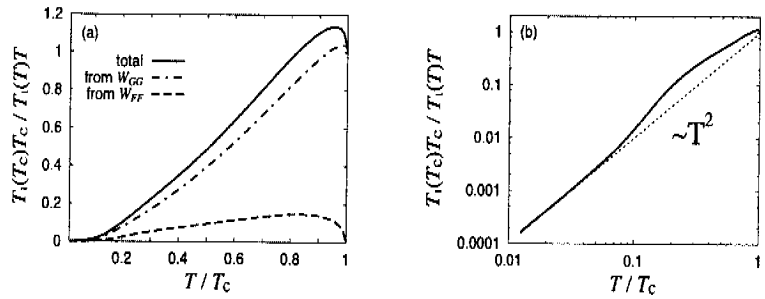

Figure 6.1: Numerical result for the temperature dependence of the nuclear spin lattice relaxation rate $1/T_1T$, from N. Hayashi *et al.* [25]

herence effect and gives the dominant contribution to the peak below T_c. In contrast, W_{GG} (dashed-dotted line) describes the contribution of the density of states. The temperature dependence of $1/T_1T_c$ exibits a T^2 power law at low temperatures, characteristic of the presence of line nodes in the gap. Such a gap with line nodes is also suggested by measurements of the London penetration depth [23] and thermal conductivity [24]. Numerical estimation of the superfluid density demonstrates that our pairing model is compatible with the observed London penetration depth [55]. Furthermore, the superconducting state which we propose should be confirmed by other experimental studies. For example, we expect surface bound states with subgap energies similar to unconventional superconductors [56]. Those should leave their signature in the tunneling conductance. Moreover, the angle-resolved thermal conductivity and Josephson effect could give information on the character of the subdominant pairing channel. This methods are sensitive to the position of the line nodes. A possible movement of the line node with temperature should be detected. If after decreasing the temperature the length of the line nodes increases, then the subdominant channel is repulsive. The character of the subdominant channel could also be investigated studying the dependence of T_c on the non-magnetic impurity concentration. However, the problem of non-magnetic impurities in $CePt_3Si$ seems to be more complex than in our simple treatment. The chemical substitution of Ce by non-magnetic La have

been studied [57]. However, Ce is magnetic and the La substitution results in being more like a magnetic impurity substitution. Quite a small concentration of La, $\approx$ 2%, almost completely suppresses superconductivity. The La substitution also strongly suppresses the Néel transition. The substitution of Si by Ge has also been investigated [10]. In this case, the volume of the sample and the Néel transition increase with the Ge concentration. The superconductivity is suppressed for concentrations of Ge of the order of 10%.

Another important part of this thesis is devoted to the study of the paramagnetic limiting of the superconducting phase. The spin-singlet state becomes more robust against paramagnetic depairing in systems without an inversion center. In particular, we found that for large values of α/k_BT_c, the paramagnetic limiting field and the static uniform spin susceptibility have similar behaviors for both spin-singlet or protected spin-triplet states. These quantities suggest a large anisotropy of H_{c2} in $CePt_3Si$. However, measurements in a single crystal, see Fig. 1.2, show that the anisotropy of H_{c2} between fields along the z-axis and fields lying in the xy-plane is relatively small. Kaur *et al.* were able to show that this reduction of the anisotropy is possibly induced by the presence of a finite-$\boldsymbol{q}$ helical phase and they propose a Josephson junction experiment that can unambiguously identify the helical order [35]. In particular, the Josephson current should display an interference pattern for a field perpendicular to the junction. Several research groups are also trying to deduce the static uniform spin susceptibility by Knight shift measurement. In particular, the group of M. Yogi is looking at the Knight shift by a ^{29}Si-NMR study [58]. For this measurement, the single crystal is reduced in powder to allow the magnetic field to penetrate in the simple. The powder is aligned under high magnetic field. The spin susceptibility for fields along the z-axis seems to remain constant in the supeconducting phase. The behavior for fields in the xy-plane is not yet clear. However, in the case of $CePt_3Si$, the utilization of powder can induce a strong deviation of the results from what we expect for the single crystal. This is because we expect that the effect of spin-reversing scattering due to the boundaries of the small specimens is important in this material with heavy nucleons. It is well known that this effect can drastically reduce the Knight shift [38,54]. In the last chapter of this thesis, we have shown that the presence of non-magnetic

impurity in superconductors without an inversion center can further reduce the Knight shift.

There are other non-centrosymmetric superconductors with noticeable properties. For example, the heavy fermion compound UIr, which has a monoclinic crystal structure. This material becomes a superconductor under a pressure of $\approx 2.6 - 2.65$GPa and at very low temperature $T_c \approx 0.14K$ [59]. The superconducting dome lies close to the quantum critical point separating the ferromagnetic and the paramagnetic phases. Its exact position is not yet clear. However, the question of coexistence and competition of superconductivity and ferromagnetism in superconductors without an inversion center is an interesting problem by itself [60]. More recently, the discovery of the system $Li_2Pd_{3(1-x)}$ $Pt_{3x}B$, with generating point group O, seems to give the possibility to study, in a continous way, the transition between a conventional superconductor $x = 0$ and a more unconventional one observed for $x = 1$ [61–64].

In this thesis, we also provided an extensive list of further non-centrosymmetric superconductors. We leave to the experimentalist the task of checking if some exotic unconventional superconductors belong to these compounds.

Appendix A

Tables and Figures for various crystal symmetries

The symbols used to draw the symmetry transformations for the three-dimensional representation of the point groups

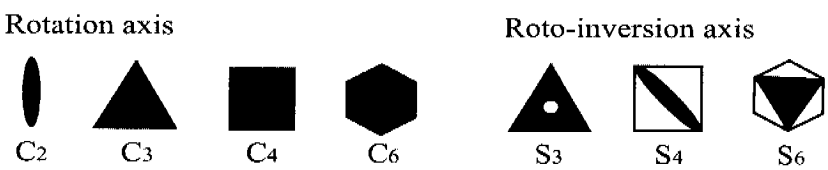

A.1 Cubic crystal systems

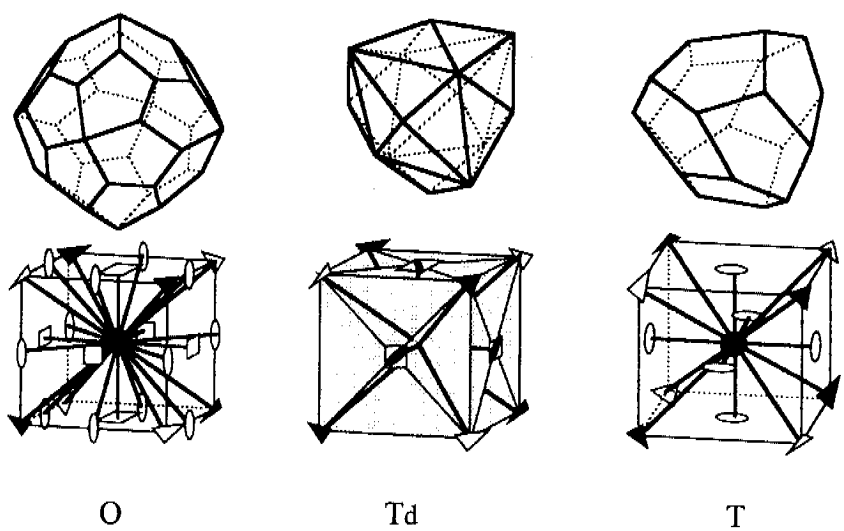

Figure A.1: Three-dimensional representation of the three point groups without inversion symmetry for cubic crystal systems.

G'	$\Gamma(G)$	$\boldsymbol{g_k}$
O	A_{1u}	$k_x\hat{x} + k_y\hat{y} + k_z\hat{z}$
T_d	A_{2u}	$k_x(k_z^2 - k_y^2)\hat{x} + k_y(k_x^2 - k_z^2)\hat{y} + k_z(k_y^2 - k_x^2)\hat{z}$
T	A_{1u}	$\alpha_1(k_x\hat{x} + k_y\hat{y} + k_z\hat{z})$
	A_{2u}	$+\alpha_2[k_x(k_z^2 - k_y^2)\hat{x} + k_y(k_x^2 - k_z^2)\hat{y} + k_z(k_y^2 - k_x^2)\hat{z}]$

Table A.1: The $\boldsymbol{g_k}$-vector for the three point groups G' without the inversion symmetry for cubic crystal systems. The basic point group G is O_h.

G'	Compound	Space Group	T_c	Ref.
O	Mo_3Al_2C	$P4_132$	10K	[65, 66]
	$La_3Rh_4Sn_{13}$	$I4_132$	3.2K	[67, 68]
	$La_2Pd_{3(1-x)}Pt_{3x}$	$P4_332$	2.5-8K	[61, 62, 69]
T_d	Ti_5Re_{24} type, e.g $Nb_{0.24}Tc_{0.76}$	$I\bar{4}3m$	12.9K	[70–72]
	Pu_2C_3 type, e.g. Y_2C_3	$I\bar{4}3d$	17K	[73–77]
				[78–82]
	Th_3P_4 type, e.g. La_3S_4	$I\bar{4}3d$	8.06K	[83]
	Th_4D_{15}	$I\bar{4}3d$	7.63K	[84, 85]
T	LaRhSi	$P2_13$	4.35K	[86]
	LaIrSi	$P2_13$	2.3K	[86, 87]

Table A.2: List of compounds with cubic space group generating by point groups without the inversion operator.

G'	$\Gamma(G')$	$\chi_i^{\Gamma}(\boldsymbol{k})$
O, T_d	A_1	$\beta_1 + \beta_2(k_x^2 + k_y^2 + k_z^2)$
	A_2	$(k_x^2 - k_y^2)(k_y^2 - k_z^2)(k_z^2 - k_x^2)$
	E	$2k_z^2 - k_x^2 - k_y^2 \equiv u$
		$\sqrt{3}(k_x^2 - k_y^2) \equiv v$
	F_1	$k_y k_z(k_y^2 - k_z^2)$
		$k_z k_x(k_z^2 - k_x^2)$
		$k_x k_y(k_x^2 - k_y^2)$
	F_2	$k_y k_z$
		$k_z k_x$
		$k_x k_y$
T	A_1	$\beta_1 + \beta_2(k_x^2 + k_y^2 + k_z^2)$
		$+\beta_3(k_x^2 - k_y^2)(k_y^2 - k_z^2)(k_z^2 - k_x^2)$
	A_2	$1/\sqrt{2}(u - v)$
	B_1	$1/\sqrt{2}(u + v)$
		$\sqrt{3}(k_x^2 - k_y^2)$
	F_1	$\beta_1 k_y k_z(k_y^2 - k_z^2) + \beta_2 k_y k_z$
		$\beta_1 k_z k_x(k_z^2 - k_x^2) + \beta_2 k_z k_x$
		$\beta_1 k_x k_y(k_x^2 - k_y^2) + \beta_2 k_x k_y$

Table A.3: Basis functions for the superconducting state in the case of cubic crystal systems.

A.2 Tetragonal crystal systems

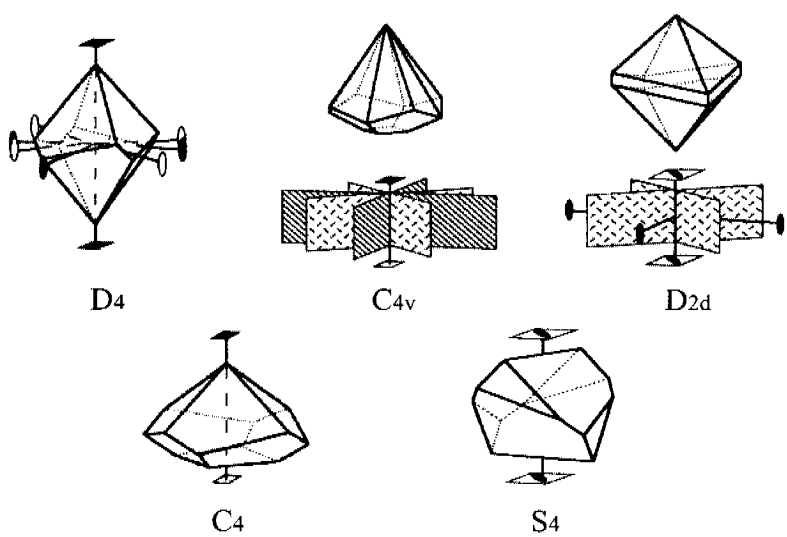

Figure A.2: Three-dimensional representation of the five point groups without inversion symmetry for tetragonal crystal systems.

G'	Γ	$\boldsymbol{g_k}$
D_4	A_{1u}	$\alpha_1 k_z\hat{z} + \alpha_2(k_x\hat{x} + k_y\hat{y})$
C_{4v}	A_{2u}	$\alpha_1(k_x\hat{y} - k_y\hat{x}) + \alpha_2(k_x^2 - k_y^2)(k_y\hat{x} + k_x\hat{y})$
		$+\alpha_3\, k_xk_yk_z(k_x^2 - k_y^2)\hat{z}$
D_{2d}	B_{1u}	$\alpha_1(k_x\hat{x} - k_y\hat{y}) + \alpha_2 k_z(k_x^2 - k_y^2)\hat{z}$
C_4	A_{1u}	$\alpha_1 k_z\hat{z} + \alpha_2(k_x\hat{x} + k_y\hat{y})$
	A_{2u}	$+\alpha_3(k_x\hat{y} - k_y\hat{x}) + \alpha_4(k_x^2 - k_y^2)(k_y\hat{x} + k_x\hat{y})$
S_4	B_{1u}	$\alpha_1(k_x\hat{x} - k_y\hat{y}) + \alpha_2 k_z(k_x^2 - k_y^2)\hat{z}$
	B_{2u}	$+\alpha_3(k_x\hat{y} + k_y\hat{x}) + \alpha_4 k_xk_yk_z\hat{z}$

Table A.4: The $\boldsymbol{g_k}$-vector for the five tetragonal point groups without inversion symmetry. The basic point group G is D_{4h}.

G'	Compound	Space Group	T_c	Ref.
D_4	-	-	-	-
C_{4v}	LaPtSi type, e.g. ThIrSi	$I4_1md$	6.5K	[88–92]
	$CePt_3Si$	P4mm	0.75K	[6]
D_{2d}	-	-	-	-
C_4	$La_5B_2C_6$ type	P4	6.9K	[93–96]
S_4	Ni_3P type, e.g. Mo_3P	$I\bar{4}$	5.31K	[97, 98]

Table A.5: List of compounds with tetragonal space group generating by point groups without the inversion operator.

G'	$\Gamma(G')$	$\chi_i^{\Gamma}(\boldsymbol{k})$
D_4, C_{4v}, D_{2d}	A_1	$\beta_1 + \beta_2(k_x^2 + k_y^2) + \beta_3 k_z^2$
	A_2	$k_x k_y (k_x^2 - k_y^2)$
	B_1	$k_x^2 - k_y^2$
	B_2	$k_x k_y$
	E	$k_x k_z$
		$k_y k_z$
C_4, S_4	A_1	$\beta_1 + \beta_2(k_x^2 + k_y^2) + \beta_3 k_z^2$
		$+\beta_4 k_x k_y (k_x^2 - k_y^2)$
	A_2	$\beta_1(k_x^2 - k_y^2) + \beta_2 k_x k_y$
	B_1	$-(k_x + ik_y)k_z$
	B_2	$(k_x - ik_y)k_z$

Table A.6: Basis functions for the superconducting state in the case of tetragonal crystal systems.

A.3 Hexagonal crystal systems

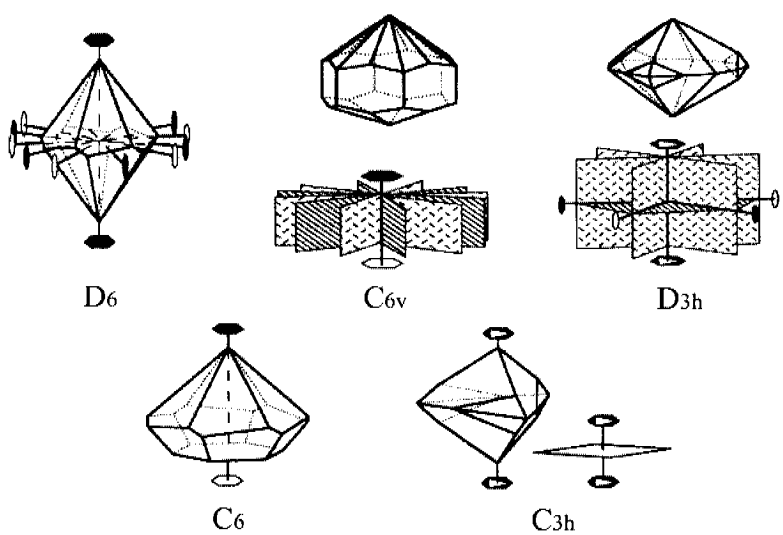

Figure A.3: Three-dimensional representation of the five point groups without inversion symmetry for hexagonal crystal systems.

G'	Γ	$\boldsymbol{g_k}$
D_6	A_{1u}	$\alpha_1 k_z \hat{z} + \alpha_2 (k_x \hat{x} + k_y \hat{y})$
C_{6v}	A_{2u}	$\alpha_1 (k_x \hat{y} - k_y \hat{x}) + \alpha_2 k_z (k_x^3 - 3k_x k_y^2)(k_y^3 - 3k_y k_x^2) \hat{z}$
D_{3h}	B_{2u}	$\alpha_1 (k_y^3 - 3k_y k_x^2) \hat{z} + \alpha_2 k_z [(k_x^2 - k_y^2) \hat{y} - 2k_x k_y \hat{x}]$
C_6	A_{1u}	$\alpha_1 k_z \hat{z} + \alpha_2 (k_x \hat{x} + k_y \hat{y})$
	A_{2u}	$+\alpha_3 (k_x \hat{y} - k_y \hat{x}) + \alpha_4 (k_x^3 - 3k_x k_y^2)(k_y^3 - 3k_y k_x^2) \hat{z}$
C_{3h}	B_{2u}	$\alpha_1 (k_y^3 - 3k_y k_x^2) \hat{z} + \alpha_2 k_z [(k_x^2 - k_y^2) \hat{y} - 2k_x k_y \hat{x}]$
	B_{1u}	$\alpha_3 (k_x^3 - 3k_x k_y^2) \hat{z} + \alpha_4 k_z [(k_x^2 - k_y^2) \hat{x} - 2k_x k_y \hat{y}]$

Table A.7: The $\boldsymbol{g_k}$-vector for the five hexagonal point groups without inversion symmetry. The basic point group G is D_{6h}.

G'	Compound	Space Group	T_c	Ref.
D_6	-	-	-	-
C_{6v}	MoN	$P6_3mc$	15.1K	[99]
	GaN	$P6_3mc$	5.85K	[100, 101]
	$Li_{0.3}Ti_{1.1}S_2$	$P6_3mc$	13K	[102, 103]
D_{3h}	MoC	$P\bar{6}m2$	9.26K	[104, 105]
	NbSe	$P\bar{6}m2$	6.3K	[106–108]
	ZrNiAl type, e.g. ZrRuP	$P\bar{6}2m$	12.93K	[109, 110]
C_6	-	-	-	-
C_{3h}	-	-	-	-

Table A.8: List of compounds with hexagonal space group generating by point groups without the inversion operator.

G'	$\Gamma(G')$	$\chi_i^\Gamma(\boldsymbol{k})$
D_6, C_{6v}, D_{3h}	A_1	$\beta_1 + \beta_2(k_x^2 + k_y^2) + \beta_3 k_z^2$
		$+\beta_4(k_x^6 - 15k_x^4k_y^2 + 15k_x^2k_y^4 - k_y^6)$
	A_2	$(k_x^3 - 3k_xk_y^2)(k_y^3 - 3k_yk_x^2)$
	B_1	$k_z(k_x^3 - 3k_xk_y^2)$
	B_2	$k_z(k_y^3 - 3k_yk_x^2)$
	E_1	k_zk_x
		k_zk_y
	E_2	$k_x^2 - k_y^2$
		$2k_xk_y$
C_6, C_{3h}	A_1	$\beta_1 + \beta_2(k_x^2 + k_y^2) + \beta_3 k_z^2$
		$+\beta_4(k_x^6 - 15k_x^4k_y^2 + 15k_x^2k_y^4 - k_y^6)$
		$+\beta_5(k_x^3 - 3k_xk_y^2)(k_y^3 - 3k_yk_x^2)$
	A_2	$(k_x - ik_y)^2$
	B_1	$(k_x + ik_y)^2$
	B_2	$\beta_1 k_z(k_x^3 - 3k_xk_y^2) + \beta_2 k_z(k_y^3 - 3k_yk_x^2)$
	C_1	k_zk_y
	C_2	k_zk_x

Table A.9: Basis functions for the superconducting state in case of hexagonal crystal systems.

A.4 Trigonal crystal systems

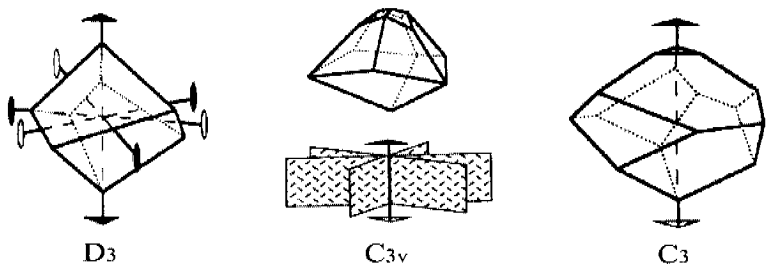

Figure A.4: Three-dimensional representation of the three point groups without inversion symmetry for trigonal crystal systems.

G'	Γ	$\boldsymbol{g_k}$
D_3	A_{1u}	$\alpha_1 k_z \hat{z} + \alpha_2(k_x \hat{x} + k_y \hat{y})$
C_{3v}	A_{2u}	$(k_x \hat{y} - k_y \hat{x})$
C_3	A_{1u}	$\alpha_1 k_z \hat{z} + \alpha_2(k_x \hat{x} + k_y \hat{y})$
	A_{2u}	$+\alpha_3(k_x \hat{y} - k_y \hat{x})$

Table A.10: The $\boldsymbol{g_k}$-vector for the three trigonal point groups without inversion symmetry. The basic point group G is D_{3d}.

G'	Compound	Space Group	T_c	Ref.
D_3	-	-	-	-
C_{3v}	3R-MoS_2 type, e.g. $Ba_{0.2}(NH_3)_yMoS_2$	R3m	5.7K	[111–115]
C_3	-	-	-	-

Table A.11: List of compounds with trigonal space group generating by point groups without the inversion operator.

G'	$\Gamma(G')$	$\chi_i^\Gamma(\boldsymbol{k})$
D_3, C_{3v}	A_1	$\beta_1 + \beta_2(k_x^2 + k_y^2) + \beta_3 k_z^2$
	A_2	$\beta_1(k_x^3 - 3k_x k_y^2)(k_y^3 - 3k_y k_x^2) + \beta_2 k_z(k_y^3 - 3k_y k_x^2)$
	E	$\beta_1(k_x^2 - k_y^2) + \beta_2 k_z k_x$
		$\beta_3 2k_x k_y + \beta_4 k_z k_y$
C_3	A_1	$\beta_1 + \beta_2(k_x^2 + k_y^2) + \beta_3 k_z^2$
		$+\beta_4(k_x^3 - 3k_x k_y^2)(k_y^3 - 3k_y k_x^2) + \beta_5 k_z(k_y^3 - 3k_y k_x^2)$
	A_2	$\beta_1(k_x^2 - k_y^2) + \beta_2 k_z k_x$
	B_1	$\beta_3 2k_x k_y + \beta_4 k_z k_y$

Table A.12: Basis functions for the superconducting state in case of trigonal crystal systems.

A.5 Orthorhombic crystal systems

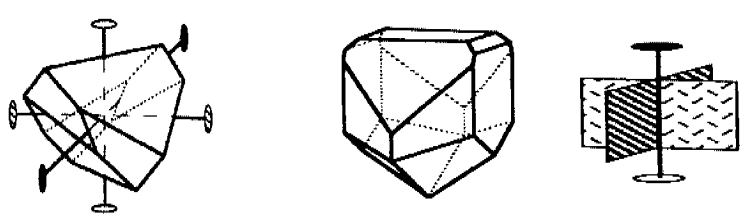

Figure A.5: Three-dimensional representation of the two point groups without inversion symmetry for orthorhombic crystal systems.

G'	Γ	$\boldsymbol{g_k}$
D_2	A_{1u}	$\alpha_1 k_x \hat{x} + \alpha_2 k_y \hat{y} + \alpha_3 k_z \hat{z}$
C_{2v}	B_{1u}	$\alpha_1 k_y \hat{x} + \alpha_2 k_x \hat{y}$

Table A.13: The $\boldsymbol{g_k}$-vector for the two orthorhombic point groups without inversion symmetry. The basic point group G is D_{2h}.

G'	Compound	Space Group	T_c	Ref.
D_2	-	-	-	-
C_{2v}	TiFeSi type, e.g. NbReSi	Ima2	5.1K	[92, 116]

Table A.14: List of compounds with orthorhombic space group generating by point groups without the inversion operator.

G'	$\Gamma(G')$	$\chi_i^{\Gamma}(\boldsymbol{k})$
D_2, C_{2v}	A_1	$\beta_1 + \beta_2 k_x^2 + \beta_3 k_y^2 + \beta_4 k_z^2$
	A_2	$k_z k_x$
	B_1	$k_x k_y$
	B_2	$k_y k_z$

Table A.15: Basis functions for the superconducting state in case of orthorombic crystal systems.

A.6 Monoclinic crystal systems

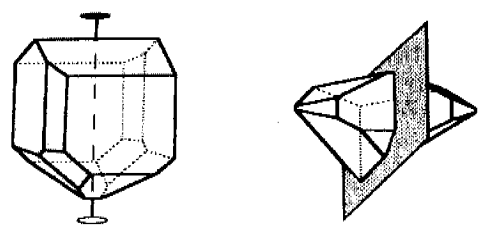

Figure A.6: Three dimensional representation of the two point groups without inversion symmetry for monoclinic crystal systems.

G'	Γ	$\boldsymbol{g_k}$
C_2	A_{1u}	$\alpha_1 k_x \hat{x} + \alpha_2 k_y \hat{y} + \alpha_3 k_z \hat{z}$
		$\alpha_4 k_x \hat{y} + \alpha_5 k_y \hat{x}$
C_s	A_{2u}	$\alpha_1 k_x \hat{z} + \alpha_2 k_y \hat{z} + \alpha_3 k_z \hat{x} + \alpha_2 k_z \hat{y}$

Table A.16: The $\boldsymbol{g_k}$-vector for the two monoclinic point groups without inversion symmetry. The basic point group G is C_{2h}.

G'	Compound	Space Group	T_c	Ref.
C_2	UIr	$P2_1$	0.1K	[59]
C_s	-	-	-	-

Table A.17: List of compounds with monoclinic space group generating by point groups without the inversion operator.

G'	$\Gamma(G')$	$\chi_i^{\Gamma}(\boldsymbol{k})$
C_2, C_s	A_1	$\beta_1 + \beta_2 k_x^2 + \beta_3 k_y^2 + \beta_4 k_z^2 + \beta_5 k_x k_y$
	A_2	$\beta_1 k_z k_x + \beta_2 k_z k_y$

Table A.18: Basis functions for the superconducting state in case of Monoclinic crystal system.

A.7 Triclinic crystal systems

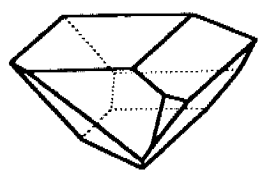

C_1

Figure A.7: Three-dimensional representation of the point group without inversion symmetry for the triclinic crystal system.

G'	Γ	$\boldsymbol{g_k}$
C_1	A_{1u}	$\alpha_1 k_x \hat{x} + \alpha_2 k_y \hat{y} + \alpha_3 k_z \hat{z}$
		$\alpha_4 k_x \hat{y} + \alpha_5 k_y \hat{x}$
		$\alpha_6 k_y \hat{z} + \alpha_7 k_z \hat{y}$
		$\alpha_8 k_z \hat{x} + \alpha_9 k_x \hat{z}$

Table A.19: The $\boldsymbol{g_k}$-vector for the triclinic point group C_1 without inversion symmetry. The basic point group G is C_i.

The list of compounds with triclinic space group generating by point groups without the inversion operator can be found in [40], these are charge-transfer Salts .

G'	$\Gamma(G')$	$\chi_i^{\Gamma}(\boldsymbol{k})$
C_1	A_1	$\beta_1 + \beta_2 k_x^2 + \beta_3 k_y^2 + \beta_4 k_z^2 + \beta_5 k_x k_y$
		$+\beta_6 k_z k_x + \beta_7 k_z k_y$

Table A.20: Basis function for the superconducting state in case of the Triclinic crystal system.

Appendix B

The origin of mixed singlet-triplet pairing interaction e_m

In this appendix, we consider a microscopic origin for the mixed singlet-triplet pairing interaction e_m given in Eq. (4.8). In particular, we show that that the Dzyaloshinskii-Moriya [43, 44] (DM) magnetic interaction gives a contribution to e_m. Such an interaction is well known to exist for magnetic systems that break inversion symmetry. We then show how this interaction can arise from the single particle Hamiltonian given in Eq. (2.16) for both a weakly interacting Fermi liquid and for a Hubbard model near half filling. Note that the DM interaction is not the only microscopic interaction that contributes to e_m. Nevertheless, this discussion suffices to show that e_m is not in general zero and in some cases may provide a substantial contribution to the superconducting condensation energy.

B.1 DM Interaction

The DM interaction can be written

$$H_{DM} = \frac{1}{N}\sum_{\boldsymbol{q}} i\boldsymbol{D}(\boldsymbol{q}) \cdot \boldsymbol{S}_{\boldsymbol{q}} \times \boldsymbol{S}_{-\boldsymbol{q}}, \tag{B.1}$$

where $\boldsymbol{D}(\boldsymbol{q})$ is a real vector that satisfies $\boldsymbol{D}(\boldsymbol{q}) = -\boldsymbol{D}(-\boldsymbol{q})$. Invariance of H_{DM} under point group operations leads to the constraint $\tilde{R}\boldsymbol{D}_{\mathrm{R}\boldsymbol{q}} = \boldsymbol{D}_{\boldsymbol{q}}$, where $\tilde{R}$ is the proper part of the rotation ($\tilde{R} = Det(R) \times R$). Note that $\boldsymbol{g}(\boldsymbol{k})$ satisfies the same symmetry relation ($\tilde{R}\boldsymbol{g}_{\mathrm{R}\boldsymbol{k}} = \boldsymbol{g}_{\boldsymbol{k}}$). Consequently, the two vectors $\boldsymbol{D}(\boldsymbol{q})$ and $\boldsymbol{g}_{\boldsymbol{q}}$ are not orthogonal. Extracting the pairing contribution from Eq. B.1 leads to the following mixed singlet-triplet pairing interaction

$$[-\boldsymbol{D}(\boldsymbol{k}-\boldsymbol{k}')\cdot\hat{\tau}]_{s_1s_2}\hat{\tau}^{\dagger}_{s_2's_1'} + \hat{\tau}_{s_1s_2}[\boldsymbol{D}(\boldsymbol{k}-\boldsymbol{k}')\cdot\hat{\tau}]^{\dagger}_{s_2's_1'}. \tag{B.2}$$

If we assume the form $\boldsymbol{D}(\boldsymbol{k}-\boldsymbol{k}') = e_m(\boldsymbol{g}_{\boldsymbol{k}'} - \boldsymbol{g}_{\boldsymbol{k}})$ and impose symmetry constraints that arise from Pauli exclusion, we arrive at the mixed parity term in Eq. (4.8). As will be shown below, this form for $\boldsymbol{D}$ can be justified.

B.2 DM Interaction in a weakly interacting Fermi liquid

The DM interaction is known to exist in materials without inversion symmetry. This implies that the DM interaction should arise as a consequence of the existence of $\boldsymbol{g}_{\boldsymbol{k}}$ in the single particle Hamiltonian. Here, we calculate the contribution of $\boldsymbol{g}_{\boldsymbol{k}}$ to the DM interaction through a calculation of the spin susceptibility. In the normal state, the static spin-susceptibility is given by

$$\chi_{ij}(\boldsymbol{q}) = -\mu_B^2 k_B T \sum_{\boldsymbol{k}} \sum_{\omega_n} \mathrm{Tr}\{\hat{\sigma}_i \hat{G}(\boldsymbol{k},\omega_n)\hat{\sigma}_j \hat{G}(\boldsymbol{k}+\boldsymbol{q},\omega_n))\} \tag{B.3}$$

Upon using the form for the normal state Green's functions and carrying out the trace over the spins, it can be shown

$$\begin{aligned}
\chi_{ij}(\boldsymbol{q}) &= -2\mu_B^2 k_B T \sum_{\boldsymbol{k}} \sum_{\omega_n} \Big\{ \Big[\delta_{ij}(1 - \hat{\boldsymbol{g}}_{\boldsymbol{k}} \cdot \hat{\boldsymbol{g}}_{\boldsymbol{k}+\boldsymbol{q}}) \\
&+ (\hat{\boldsymbol{e}}_i \cdot \hat{\boldsymbol{g}}_{\boldsymbol{k}})(\hat{\boldsymbol{e}}_j \cdot \hat{\boldsymbol{g}}_{\boldsymbol{k}+\boldsymbol{q}}) + (\hat{\boldsymbol{e}}_i \cdot \hat{\boldsymbol{g}}_{\boldsymbol{k}+\boldsymbol{q}})(\hat{\boldsymbol{e}}_j \cdot \hat{\boldsymbol{g}}_{\boldsymbol{k}}) \\
&+ i(\hat{\boldsymbol{e}}_i \times \hat{\boldsymbol{e}}_j) \cdot (\hat{\boldsymbol{g}}_{\boldsymbol{k}+\boldsymbol{q}} - \hat{\boldsymbol{g}}_{\boldsymbol{k}})\Big] G_1(\boldsymbol{k}, \omega_n) G_1(\boldsymbol{k}+\boldsymbol{q}, \omega_n) \\
&+ \Big[\delta_{ij}(1 - \hat{\boldsymbol{g}}_{\boldsymbol{k}} \cdot \hat{\boldsymbol{g}}_{\boldsymbol{k}+\boldsymbol{q}}) + (\hat{\boldsymbol{e}}_i \cdot \hat{\boldsymbol{g}}_{\boldsymbol{k}})(\hat{\boldsymbol{e}}_j \cdot \hat{\boldsymbol{g}}_{\boldsymbol{k}+\boldsymbol{q}}) \\
&+ (\hat{\boldsymbol{e}}_i \cdot \hat{\boldsymbol{g}}_{\boldsymbol{k}+\boldsymbol{q}})(\hat{\boldsymbol{e}}_j \cdot \hat{\boldsymbol{g}}_{\boldsymbol{k}}) - i(\hat{\boldsymbol{e}}_i \times \hat{\boldsymbol{e}}_j) \cdot (\hat{\boldsymbol{g}}_{\boldsymbol{k}+\boldsymbol{q}} - \hat{\boldsymbol{g}}_{\boldsymbol{k}})\Big] \\
&\cdot G_2(\boldsymbol{k}, \omega_n) G_2(\boldsymbol{k}+\boldsymbol{q}, \omega_n) \\
&+ \Big[\delta_{ij}(1 + \hat{\boldsymbol{g}}_{\boldsymbol{k}} \cdot \hat{\boldsymbol{g}}_{\boldsymbol{k}+\boldsymbol{q}}) - (\hat{\boldsymbol{e}}_i \cdot \hat{\boldsymbol{g}}_{\boldsymbol{k}})(\hat{\boldsymbol{e}}_j \cdot \hat{\boldsymbol{g}}_{\boldsymbol{k}+\boldsymbol{q}}) \\
&- (\hat{\boldsymbol{e}}_i \cdot \hat{\boldsymbol{g}}_{\boldsymbol{k}+\boldsymbol{q}})(\hat{\boldsymbol{e}}_j \cdot \hat{\boldsymbol{g}}_{\boldsymbol{k}}) - i(\hat{\boldsymbol{e}}_i \times \hat{\boldsymbol{e}}_j) \cdot (\hat{\boldsymbol{g}}_{\boldsymbol{k}+\boldsymbol{q}} + \hat{\boldsymbol{g}}_{\boldsymbol{k}})\Big] \\
&\cdot G_1(\boldsymbol{k}, \omega_n) G_2(\boldsymbol{k}+\boldsymbol{q}, \omega_n) \\
&+ \Big[\delta_{ij}(1 + \hat{\boldsymbol{g}}_{\boldsymbol{k}} \cdot \hat{\boldsymbol{g}}_{\boldsymbol{k}+\boldsymbol{q}}) - (\hat{\boldsymbol{e}}_i \cdot \hat{\boldsymbol{g}}_{\boldsymbol{k}})(\hat{\boldsymbol{e}}_j \cdot \hat{\boldsymbol{g}}_{\boldsymbol{k}+\boldsymbol{q}}) \\
&- (\hat{\boldsymbol{e}}_i \cdot \hat{\boldsymbol{g}}_{\boldsymbol{k}+\boldsymbol{q}})(\hat{\boldsymbol{e}}_j \cdot \hat{\boldsymbol{g}}_{\boldsymbol{k}}) + i(\hat{\boldsymbol{e}}_i \times \hat{\boldsymbol{e}}_j) \cdot (\hat{\boldsymbol{g}}_{\boldsymbol{k}+\boldsymbol{q}} + \hat{\boldsymbol{g}}_{\boldsymbol{k}})\Big] \\
&+ G_2(\boldsymbol{k}, \omega_n) G_1(\boldsymbol{k}+\boldsymbol{q}, \omega_n)\Big\}
\end{aligned}$$

The DM interaction is antisymmetric under interchange of i and j, this implies

$$\begin{aligned}
\boldsymbol{D}(\boldsymbol{q}) &= -2\mu_B^2 k_B T \sum_{\boldsymbol{k}, \omega_n} \{[G_1(\boldsymbol{k}, \omega_n) G_1(\boldsymbol{k}+\boldsymbol{q}, \omega_n) \\
&\quad - G_2(\boldsymbol{k}, \omega_n) G_2(\boldsymbol{k}+\boldsymbol{q}, \omega_n)]\, [\hat{\boldsymbol{g}}_{\boldsymbol{k}+\boldsymbol{q}} - \hat{\boldsymbol{g}}_{\boldsymbol{k}}] \\
&\quad + [G_2(\boldsymbol{k}, \omega_n) G_1(\boldsymbol{k}+\boldsymbol{q}, \omega_n) \\
&\quad - G_1(\boldsymbol{k}, \omega_n) G_2(\boldsymbol{k}+\boldsymbol{q}, \omega_n)]\, [\hat{\boldsymbol{g}}_{\boldsymbol{k}+\boldsymbol{q}} + \hat{\boldsymbol{g}}_{\boldsymbol{k}}]\Big\}\,.
\end{aligned} \tag{B.4}$$

Carrying out the sum over Matsubara frequencies, expanding the expression for $\boldsymbol{D}(\boldsymbol{q})$ to a linear order in $\boldsymbol{q}$ one finds

$$\begin{aligned}\boldsymbol{D}(\boldsymbol{q}) &= 2\mu_B^2 \sum_{\boldsymbol{k}} \left\{ \left[\frac{\boldsymbol{\nabla} n_2 \cdot \boldsymbol{q}}{\boldsymbol{\nabla}\xi_2 \cdot \boldsymbol{q}} - \frac{\boldsymbol{\nabla} n_1 \cdot \boldsymbol{q}}{\boldsymbol{\nabla}\xi_1 \cdot \boldsymbol{q}} \right] \boldsymbol{q} \cdot \boldsymbol{\nabla}\hat{\boldsymbol{g}} \right. \\ &\left. + \hat{\boldsymbol{g}}\boldsymbol{q} \cdot \left[\frac{n_1 - n_2}{(\xi_1 - \xi_2)^2} (\boldsymbol{\nabla}\xi_1 + \boldsymbol{\nabla}\xi_2) - \frac{\boldsymbol{\nabla} n_1 + \boldsymbol{\nabla} n_2}{\xi_1 - \xi_2} \right] \right\},\end{aligned} \tag{B.5}$$

where $\xi_i = \xi_i(\boldsymbol{k})$, $n_i = (e^{\xi_i/k_BT} + 1)^{-1}$ is the Fermi distribution function for band i, and $\boldsymbol{\nabla} = \boldsymbol{\nabla}_{\boldsymbol{k}}$. To linear order in α, this gives

$$\boldsymbol{D}(\boldsymbol{q}) = -\frac{8\mu_B^2\alpha}{3} \sum_{\boldsymbol{k}} \frac{d^2 n(\epsilon_{\boldsymbol{k}})}{d\epsilon_{\boldsymbol{k}}^2} \boldsymbol{q} \cdot \boldsymbol{\nabla}_{\boldsymbol{k}} \boldsymbol{g}_{\boldsymbol{k}}. \tag{B.6}$$

For example, if $\boldsymbol{g}_{\boldsymbol{k}} = \boldsymbol{k}/k_F$ (valid for a material with point group O), this gives

$$\boldsymbol{D}(\boldsymbol{q}) = -\frac{8\mu_B^2\alpha}{3} \left. \frac{dN_0}{d\xi} \right|_{\xi=0} \frac{\boldsymbol{q}}{k_F}, \tag{B.7}$$

where $\frac{dN}{d\xi_F}|_{\xi=0}$ is the the derivative of the density of states evaluated at the Fermi surface. This can give rise to a large interaction when the derivative in the density of states is large, for example, near a Van Hove singularity.

B.3 DM interaction within the Hubbard for finite ASOC

Here we derive the DM interaction in the strong coupling regime by finding the effective Hamiltonian that governs the low-energy excitations of the Hubbard model with ASOC in the large U/t regime. The technique used to extract the Hamiltonian for the low-energy excitations is similar to that used for the derivation of the t-J model starting from the Hubbard model.

We choose as the zeroth-order Hamiltonian the on site Coulomb repulsion

$$\mathcal{U} = U \sum_i n_{i\uparrow} n_{i\downarrow}. \tag{B.8}$$

The eigenstates of $\mathcal{U}$ are Fock states in the Wannier representation. $\mathcal{U}$ divides the Fock space into two sub-spaces:

$$\begin{aligned} S &= [|n_{1\uparrow}, n_{1\downarrow}, n_{2\uparrow}, \cdots\rangle : \forall n_{i\downarrow} + n_{i\uparrow} \leq 1] \\ D &= [|n_{1\uparrow}, n_{1\downarrow}, n_{2\uparrow}, \cdots\rangle : \exists n_{i\downarrow} + n_{i\uparrow} = 2] . \end{aligned} \tag{B.9}$$

D contains at least one doubly occupied site, and S are all configurations with either one or zero electrons per site. The hopping

$$\mathcal{T} = \mathcal{T}^s + \mathcal{T}^a, \tag{B.10}$$

where

$$\begin{aligned} \mathcal{T}^s &= -\sum_{ij,ss'} t_{ij}\sigma_0 c^\dagger_{is} c_{js'} \\ \mathcal{T}^a &= -\sum_{ij,ss'} i\boldsymbol{\alpha}_{ij}\cdot\boldsymbol{\sigma}_{ss'} c^\dagger_{is} c_{js'} \end{aligned} \tag{B.11}$$

now contains an antisymmetric term ($\boldsymbol{\alpha}_{ij} = -\boldsymbol{\alpha}_{ji}$) corresponding to the ASOC contribution. This means that the effective interaction resulting from the superexchange process also has an antisymmetric part. This last corresponds to the DM interaction

$$\begin{aligned} \mathcal{H}^{DM} &= -\sum_{ij,s_1\cdots s_4} i\frac{t_{ij}\boldsymbol{\alpha}_{ij}\cdot(\boldsymbol{\sigma}_{s_1s_2}\delta_{s_3s_4} - \boldsymbol{\sigma}_{s_3s_4}\delta_{s_1s_2})}{U} \\ &\quad c^\dagger_{is_1} c_{js_2} n_{j\uparrow} n_{j\downarrow} c^\dagger_{js_3} c_{is_4} \\ &= \sum_{ij} \frac{4it_{ij}}{U}\boldsymbol{\alpha}_{ij}\cdot(\boldsymbol{S}_i \times \boldsymbol{S}_j) . \end{aligned} \tag{B.12}$$

The interaction $\mathcal{H}^{DM}$ is a factor α/t smaller than the usual spin-spin interaction constant J. While α/t will be less than one, it is not necessarily small.

Acknowledgment

First of all I would like to thank Manfred Sigrist and Maurice Rice. Manfred presented to me with a wonderful subject for my thesis, which was full of small surprises. Even though he was perpetually overloaded with work, he always found the time to talk. Maurice proposed to me to start this dissertation with Manfred; he always showed interest in what I was doing, and he helped me to find my way in physics.

During this period, I had the opportunity to collaborate with many people, whom I would also like to thank: Carsten Honerkamp for initiating me into the research in theoretical physics. Daniel Agterberg for the high consideration he always showed towards my work. Akihisa Koga, Nobuhiku Hayashi and Katsunori Wakabayashi for giving me a taste of Japan, which is so different but similar to Switzerland.

I would like also to thank the two co-examinators Ernst Bauer and Dirk Manske. The first for having discovered superconductivity in $CePt_3Si$, without which my work probably would not exist. The second for his contagious humor and for the tips concerning the outline of this thesis.

I thank all the members of the institute. In particular Igor Milat, Alvise de Col, Martin Indergand, Samuel Wehrli and Jérôme Koopmann, for having been more than just colleagues. Igor has provided me with a roof during these last six months and he helped me both outside and inside the realm of physics, always keeping the right distance. I started and I finished my thesis at the same time as Alvise. With him I shared the full emotional cycle characterizing PhD studies. We spent long hours discussing, complaining, and dreaming. Of Martin, I appreciate his goodness and his skill in explaining physics. With Sam and Jérôme I have shared pleasant moments ever since

our diploma thesis. Moreover, thanks to the other PhD students and Post-Docs that I had the chance to know, which are more or less responsible for the nice atmosphere in the institute: Elena Bascones, Paola Gentile, Marlene Weiss, Benedikt Binz, Masashige Matsumoto, Andreas Rüegg, Sebastian Pilgram, Fabian Hassler, Sebastian Huber, Helmut Katzgraber, Mathias Körner, Urs Aeberhard, Andreas Schnyder, Philippe Corboz, Emanuel Gull, Guido Schmid, Prakash Dayal, Martin Puchwein, Christian Helm, Philipp Werner, Raphael Micha.

I am very grateful to my parents and to my brothers Ale and Mauro who supported me in all moments of this experience. I am also grateful to Francesca, who shared with me a significant and important period of my life. I would like also thank all my friends who helped me to be what I am.

Curriculum Vitae

Personal Data

Name:	Paolo Antonio Frigeri
Date of Birth:	November 14, 1973 (Sorengo, Switzerland)
Nationality:	Swiss and Italian citizen

Education

1979-1988	**Primary and secondary school in Ticino (Switzerland)**
1988-1992	**Federal certificate of ability as a multimedia technician**
	Scuola cantonale per elettronici audio e video
	6952 Canobbio, Switzerland
1992-1996	**Microelectronic engineer diploma HTL**
	Diploma thesis at the EIVD, 1401 Yverdon, Switzerland
	"Mémoire FIFO 8K x 16 bits 50Mhz"
	Advisor: Prof. Bertrand Hochet
1995-1997	**Undergraduate student, physics department**
	EPF Lausanne, Switzerland
1997-2001	**Undergraduate student, physics department**
	ETH Zürich, Switzerland
2001	**Degree in physics at the ETHZ**
	"Perturbative analysis of the t-t' Hubbard model"
	Advisor: Prof. T. M. Rice
2001-2005	**PhD student**
	ETH Zürich, Advisor: Prof. M. Sigrist

List of Publications

1 P.A. Frigeri, C. Honerkamp, T.M. Rice
Landau-Fermi liquid analysis of the 2D t-t ' Hubbard model,
Eur. Phys. J. B 28 (1), 61-70 (2002).

2 P.A. Frigeri, D.F. Agterberg, A. Koga and M. Sigrist,
Superconductivity without inversion symmetry: MnSi versus CePt3Si,
Phys. Rev. Lett. 92 (9), 097001 (2004).

3 P.A. Frigeri, D.F. Agterberg and M. Sigrist,
Spin susceptibility in superconductors without inversion symmetry
New J. Phys. 6, 115 (2004).

4 P.A. Frigeri, D.F. Agterberg, A. Koga, M. Sigrist,
Superconductivity without inversion symmetry in CePt3Si
Physica B 359-361 (2005) 371-373.

5 N. Hayashi, K. Wakabayashi, P.A. Frigeri, M. Sigrist,
Temperature Dependence of the Superfluid Density in a Noncentrosymmetric Superconductor
Phys. Rev. B 73 (2), 024504 (2006).

6 N. Hayashi, K. Wakabayashi, P.A. Frigeri, M. Sigrist,
Nuclear Magnetic Relaxation Rate in a Noncentrosymmetric Superconductor
Phys. Rev. B 73 (9), 092508 (2006).

7 P.A. Frigeri, D.F. Agterberg, I. Milat, and M. Sigrist,
Superconductivity without an inversion center of symmetry: The s-wave State, cond-mat/0505108.

8 N. Hayashi, K. Wakabayashi, P.A. Frigeri, Y. Kato, M. Sigrist, *Spatially Resolved NMR Relaxation Rate in a Noncentrosymmetric Superconductor*, cond-mat/0510547.

9 N. Hayashi, Y. Kato, P.A. Frigeri, K. Wakabayashi, M. Sigrist, *Basic Properties of a Vortex in a Noncentrosymmetric Superconductor* cond-mat/0510548.

Bibliography

[1] J. Bardeen, L. Cooper, and J. Schrieffer, Phys. Rev. **108**, 1175 (1957).

[2] A. J. Leggett, Rev. Mod. Phys. **47**, 331 (1975).

[3] H. R. Ott et al., Phys. Rev. Lett. **52**, 1915 (1984).

[4] M. Sigrist and K. Ueda, Rev. Mod. Phys. **63**, 239 (1991).

[5] V. P. Mineev and K. V. Samokhin, *Introduction to Unconventional Superconductivity*, Gordon and Breach Science Publisher, 1998.

[6] E. Bauer et al., Phys. Rev. Lett. **92**, 027003 (2004).

[7] N. Metoki et al., Physica B **359**, 383 (2005).

[8] A. Amato, E. Bauer, and C. Baines, Phys. Rev. B **71**, 092501 (2005).

[9] M. Nicklas, G. Sparn, R. Lackner, E. Bauer, and F. Steglich, Physica B **359**, 386 (2005).

[10] E. Bauer et al., Physica B **359**, 360 (2005).

[11] T. Yasuda et al., J. Phys. Jpn. **73**, 1657 (2004).

[12] P. A. Frigeri, D. F. Agterberg, A. Koga, and M. Sigrist, Phys. Rev. Lett. **92**, 097001 (2004).

[13] L. N. Bulaevskii, A. Guseinov, and A. Rusinov, JETP **44**, 1243 (1976).

[14] P. A. Frigeri, M. Sigrist, and D. F. Agterberg, New Journal of Physics **6**, 115 (2004).

[15] K. Samokhin, Phys. Rev. B **72**, 054514 (2005).

[16] V. P. Mineev, Phys. Rev. B **71**, 012509 (2005).

[17] P. A. Frigeri, D. F. Agterberg, I. Milat, and M. Sigrist, pp. cond-mat/0505108 .

[18] V. M. Edelstein, Phys. Rev. Lett. **68**, 1244 (1989).

[19] L. P. Gor'kov and E. I. Rashba, Phys. Rev. Lett. **87**, 0370041 (2001).

[20] V. Barzykin and L. P. Gor'kov, Phys. Rev. Lett. **89**, 227002 (2002).

[21] M. Yogi et al., Phys. Rev. Lett **93**, 027003 (2004).

[22] M. Yogi et al., Physica B **359**, 389 (2005).

[23] I. Bonalde, W. Brämer-Escamilla, and E. Bauer, Phys. Rev. Letter **94**, 207002 (2005).

[24] K. Izawa et al., Phys. Rev. Lett. **94**, 197002 (2005).

[25] N. Hayashi, K. Wakabayashi, P. A. Frigeri, and M. Sigrist, Phys. Rev. B **73**, 092508 (2006).

[26] P. W. Anderson, J. Phys. Chem. Solids **11**, 26 (1959).

[27] P. W. Anderson, Phys. Rev. B **30**, 4000 (1984).

[28] A. A. Abrikosov, L. Gor'kov, and I. E. Dzyaloshnskii, *Methods of Quantum Field Theory in Statistical Physics*, Dover, New York, 1975.

[29] G. Dresselhaus, Phys. Rev. **100**, 580 (1955).

[30] E. I. Rashba, Sov. Phys. Solid State , 1109 (1960).

[31] K. V. Samokhin, E. S. Zijlstra, and S. K. Bose, Phys. Rev. B **69**, 094514 (2004).

[32] P. Fulde and K. Maki, Phys. Rev. **141**, 275 (1966).

[33] N. R. Werthamer, E. Helfand, and P. C. Hohenberg, Phys. Rev. **147**, 295 (1966).

[34] K. Maki, Phys. Rev. **148**, 362 (1966).

[35] R. P. Kaur, D. F. Agterberg, and M. Sigrist, Phys. Rev. Lett. **94**, 137002 (2005).

[36] K. Ishida et al., Nature **396**, 658.

[37] I. I. Boiko and E. I. Rashba, Sov. Phys. Solid State **2**, 1692 (1960).

[38] A. A. Abrikosov and L. Gor'kov, Sov. Phys. JETP **15**, 752 (1962).

[39] N. Metoki et al., J. Phys. Condens. Matter **16**, L207 (2004).

[40] J. Charles P. Poole, *Handbook of Superconductivity*, Academic Press, 525 B Street, Suite 1900, San Diego, CA 92101-4495, USA, 2000.

[41] I. A. Sergienko and S. H. Curnoe, Phys. Rev. B **70**, 214510 (2004).

[42] V.P.Mineev, Int. J. Mod. Phys. B **18**, 2963 (2004).

[43] I. Dzyaloshinskii, J. Phys. Chem. Solids **4**, 241 (1958).

[44] T. Moriya, Phys. Rev. **120**, 91 (1960).

[45] D. Manske, *Theory of Unconventional Superconductors*, Springer, 2004.

[46] S. K. Yip, Phys. Rev. B **65**, 144508 (2002).

[47] K. V. Samokhin, Phys. Rev. Lett. **94**, 027004 (2005).

[48] K. Izawa et al., Phys. Rev. Lett. **86**, 2653 (2001).

[49] A. I. Larkin, Sov. Phys. JETP Lett. **2**, 130 (1965).

[50] Q. Yuan et al., Phys. Rev. B **68**, 174510 (2003).

[51] A. A. Abrikosov and L. P. Gor'kov, Sov. Phys. JETP **12**, 337 (1961).

[52] A. A. Abrikosov and L. P. Gor'kov, Sov. Phys. JETP **8**, 1090 (1959).

[53] A. A. Abrikosov and L. Gor'kov, Sov. Phys. JETP **9**, 220 (1959).

[54] W. A. Hines and W. D. Knight, Phys. Rev. B **4**, 893 (1971).

[55] N. Hayashi, K. Wakabayashi, P. A. Frigeri, and M. Sigrist, Phys. Rev. B **73**, 024504 (2006).

[56] U. May, Diplomathesis ETHZ (2005).

[57] D. P. Young, M. Moldovan, X. S. Wu, P. W. Adams, and J. Y. Chan, Phys. Rev. Lett. **94**, 107001 (2005).

[58] M. Yogi et al., SCES 2005, to be publish in Physica B .

[59] T. Akazawa et al., J. Phys. Soc. Jpn. **73**, 1 (2004).

[60] M. Sigrist, News and Comments in J. Phys. Soc. Jpn. (Nov. 2004) www.ipap.jp/jpsj/news/jpsj-nov2004.htm .

[61] K. Togano et al., Phys. Rev. Lett. **93**, 247004 (2004).

[62] P. Badica, T. Kondo, and K. Togano, J. Phys. Soc. Jpn. **74**, 1014 (2005).

[63] M. Nishiyama, Y. Inada, and G. Zheng, Phys. Rev. B **71**, 220505 (2005).

[64] H. Q. Yuan, D. Vandervelde, M. B. Salamon, P. Badica, and K. Togano, cond-mat/0506771 .

[65] W. Jeiltschko, H. Nowotny, and F. Benesovsky, Monatsh. Chemie **94**, 247 (1963).

[66] J. Johnston, L. Toth, K. Kennedy, and E. R. Parker, Solid State Commun. **2**, 123 (1964).

[67] G. P. Espinosa, A. S. Cooper, and H. Barz, Mater. Res. Bull. **17**, 963 (1982).

[68] P. Bordet, D. E. Cox, G. P. Espinosa, J. L. Hodeau, and M. Marezio, Solid State Commun. **78**, 359 (1991).

[69] U. Eibenstein and W. Jung, J. Solid State Chem. **133**, 21 (1997).

[70] A. L. Giorgi and E. G. Szklarz, J. Less-Common Met. **20**, 173 (1970).

[71] W. Trzebiatowski and J. Niemiec, Rocz. Chem. **29**, 277 (1955).

[72] B. T. Matthias, V. B. Compton, and E. Corenzwit, J. Phys. Chem. Solids **19**, 130 (1961).

[73] N. H. Krikorian, A. L. Bowman, M. C. Krupka, and G. P. Arnold, High-Temp. Sci. **1**, 360 (1969).

[74] N. H. Krikorian, A. L. Giorgi, E. G. Szklarz, M. C. Krupka, and B. T. Matthias, J. Less-Common Met. **19**, 253 (1969).

[75] H. Rassaerts, H. Nowotny, G. Vinek, and F. Benesovsky, Monatsh. Chem **98**, 460 (1967).

[76] M. C. Krupka, A. L. Giorgi, N. H. Krikorian, and E. G. Szklarz, J. Less-Common Met. **19**, 113 (1969).

[77] V. I. Novokshonov, Russ. J. Inorg. Chem. **25**, 375.

[78] M. C. Krupka, A. L. Giorgi, N. H. Krikorian, and E. G. Szklarz, J. Less-Common Met. **17**, 91 (1969).

[79] A. L. Giorgi, E. G. Szklarz, M. C. Krupka, and N. H. Krikorian, J. Less-Common Met. **17**, 121 (1969).

[80] V. I. Novokshonov, E. P. Khlybov, and V. Evdokimova, Russ. J. Metall. **3**, 167 (1980).

[81] M. C. Krupka, A. L. Giorgi, and E. G. Szklarz, J. Less-Common Met. **30**, 217 (1973).

[82] G. Amano, S. Akutagawa, T. Muranaka, Y. Zenitani, and J. Akimitsu, J. Phys. Soc. Japan **73**, 530 (2003).

[83] E. Bucher et al., Phys. Rev. B **11**, 500 (1975).

[84] M. H. Mueller et al., J. Appl. Cryst. **10**, 79 (1977).

[85] M. Dietrich, W. Gey, H. Rietschel, and C. B. Satterthwaite, Solid State Commun. **15**, 941 (1974).

[86] B. Chevalier, P. Lejay, A. Cole, M. Vlasse, and J. Etourneau, Solid State Commun. **41**, 801 (1982).

[87] K. Klepp and E. Parthé, Acta Cryst. B **38**, 1541 (1982).

[88] J. Evers, G. Oehlinger, A. Weiss, and C. Probst, Solid State Commun. **50**, 63 (1984).

[89] K. Klepp and E. Parthé, Acta Cryst. **B38**, 1105 (1982).

[90] P. Lejay, B. Chevalier, J. Etourneau, J. M. Tarascon, and P. Hagenmuller, Materials Research Bulletin **18**, 67 (1983).

[91] E. Hovestreydt, N. Engel, K. Klepp, B. Chabot, and E. Parthé, J. Less-Commun Met. **85**, 247 (1982).

[92] G. V. S. Rao et al., Bull. Mater. Sci. India **7**, 215 (1985).

[93] J. Bauer and O. Bars, J. Less-Common Met. **95**, 267 (1983).

[94] J. Bauer and C. Politis, J. Less-Common Met. **88**, L1 (1982).

[95] J. Bauer and O. Bars, J. Less-Common Met. **83**, 17 (1982).

[96] J. Bauer, P. Venneguès, and J. L. Vergneau, J. Less-Common Met. **110**, 295 (1985).

[97] N. Schönberg, Acta Chem. Scand. **8**, 226 (1954).

[98] R. D. Blaugher, J. K. Hulm, and P. N. Yocom, J. Phys. Chem. Solids **26**, 2037 (1965).

[99] A. Bezinge, K. Yvon, J. Muller, W. Lengaeur, and P. Ettmayer, Solid State Commun. **63**, 141 (1987).

[100] H. Schulz and K. H. Thiemann, Solid State Commun. **23**, 815 (1977).

[101] N. E. Alekseevskii and N. N. Mikhailov, Sov. Phys. JETP **16**, 1493 (1963).

[102] L.-J. Norrby and H. F. Franzen, J. Solid State Chem. **2**, 36 (1970).

[103] H. E. Barz et al., Science **175**, 884 (1972).

[104] J. Schuster, E. Rudy, and H. Nowotny, Monatsh. Chem. **107**, 1167 (1976).

[105] B. W. Roberts, J. Phys. Chem. Ref. Data **5**, 581 (1976).

[106] E. Revolinsky, G. A. Spiering, and D. J. Beerntsen, J. Phys. Chem. Solids **26**, 1029 (1965).

[107] F. Kadijk, R. Huisman, and F. Jellinek, Recl. Trav. Chim. Pays Bas **83**, 768 (1964).

[108] B. E. Brown and D. J. Beerntsen, Acta Cryst. **18**, 31 (1965).

[109] H. Barz, H. C. Ku, G. P. Meisner, Z. Fisk, and B. T. Matthias, Proc. Natl. Acad. Sci. USA **77**, 3132 (1980).

[110] G. P. Meisner and H. C. Ku, Appl. Phys. A **31**, 201 (1983).

[111] B. Morosin, Acta. Cryst. B **30**, 551 (1974).

[112] F. Hulliger, *Structure and Bonding*, volume 4, Springer-Verlag Gmbh, 1969.

[113] R. B. Somoano, V. Hadek, and A. Rembaum, J. Chem. Phys. **58**, 697 (1973).

[114] Y. Takeuchi and W. Nowacki, Schweiz. Mineral. Petrogr. Mitt. **44**, 105 (1964).

[115] G. V. S. Rao, M. W. Shafer, S. Kawarazaki, and A. M. Toxen, J. Solid State Chem. **9**, 323 (1974).

[116] W. Jeitschko, Acta Crystallogr. B **26**, 815 (1970).